TÉCNICO LISBOA

Converting microglia into induced neural stem cells

Toward a transdifferentiation system applicable *in vitro* and *in situ*

Miguel de Araújo Godinho Henriques Pereira

Thesis to obtain the Master of Science Degree in

Biotechnology

Supervisors: Prof. Dr. Oliver Brüstle &
Prof. Maria Margarida Fonseca Rodrigues Diogo

Examination Committee

Chairperson: Prof. Tiago Paulo Gonçalves Pinheiro Fernandes
Supervisor: Prof. Dr. Oliver Brüstle
Members of the Committee: Dr. Michael Peitz

November 2022

Preface

The work presented in this thesis was performed at AG Brüstle, Institute of Reconstructive Neurobiology, University Bonn Medical Faculty and University Hospital Bonn (Bonn, Germany), during the period February-August 2022. The project was supervised by Lea J. Berg and Prof. Dr. Oliver Brüstle, and financially supported by the EU's Horizon 2020 program (NSC-REC) as well as the ERASMUS+ program. The thesis was co-supervised at Instituto Superior Técnico by Prof. Margarida Diogo.

Declaration

I declare that this document is an original work of my own authorship and that it fulfills all the requirements of the Code of Conduct and Good Practices of the *Universidade de Lisboa*.

Acknowledgments

I would like to express my sincere gratitude and deepest thanks to Prof. Dr. Oliver Brüstle for letting me have this incredible opportunity to work in his laboratory and providing me with an enriching environment, both in terms of learning, through direct contact with pulsating scientists and wonderful experienced people at the forefront of innovation, as well as, on a personal level, by providing an environment surrounding responsibility and humanistic development, based on the values of prudence, consistency, and effort.

I would like to thank to my supervisor, Lea Berg, whom has the demeanor and essence of a genius, that since I arrived conveyed an excitement towards a spirit of stringency and persistence regarding research and science, a feeling that she tried to inject me, sometimes too rapidly, that a bubble of doubt flew from my brain. I know that I am not the most talkative and enthusiastically impressionable student, but nevertheless, she took me under her wing, always reminding me to persevere under adversity.

I would also like to point out a special thanks to the entire AG Brüstle, Life & Brain GmbH, IRN – Institute for Reconstructive Neurobiology, and University Hospital Bonn, for all the support in different areas.

To Prof. Margarida Diogo and Prof. José Santos, for being my faculty supervisor and mobility coordinator, respectively, who helped me during this astonishing process abroad. Furthermore, to all the professors and dedicated people within the university for all the help in trying to make me a good researcher and a good citizen, with a special mention to Prof. António Fialho.

To my friends, in the university and from all around the globe, for always supporting me and putting up with my self-doubts, pessimism and incontrollable perfectionism (in some regards).

Lastly, but not least important, to my magnificent family, for all the patience and unconditional support, for being an inspiration in terms of values like hard-work and sacrifice, and for always reciting meaningful sentences, as “Today, do what others do not want, so that tomorrow, you will have what others cannot.”.

Abstract

The progressive increase in human life expectancy and the associated increase in the prevalence of neurodegenerative diseases has fueled efforts to exploit the prospects of cellular programming in order to counteract the pathological degeneration of neural cells within the human brain. Several approaches have been investigated, including the neurotransplantation of *in vitro*-derived human cell types as well as neuronal cell fate conversion of brain-resident somatic cells *in situ*. For the latter, specifically microglia-to-neural stem cell (NSC) conversion represents an interesting alternative, combining the migratory and immunological characteristics of microglial starter cells with the merits of self-renewal and multipotent differentiation capacity exhibited by resulting NSCs.

In this project, we thus applied different microglia lineage tracing systems to monitor the cell fate of iPSC-derived microglia (iPSdMiG) after Sendai virus (SeV)-mediated overexpression of the two transcription factors SOX2 and cMYC. While we were not yet successful implementing a genetic tracing system that is based on the expression of the enhanced green fluorescent protein (EGFP) under the control of the integrin subunit alpha-M (*ITGAM*) gene promoter (ITGAMp; gene encoding the characteristic microglial marker CD11b), due to the inability of EGFP to be efficiently transcribed and translated from the inserted construct upon differentiation of AAVS1-edited ITGAMp-EGFP-iPSCs into iPSdMiG, and the failure of a nucleofection-based editing of mature iPSdMiG to circumvent a potential differentiation-associated epigenetic silencing affecting the ITGAMp-EGFP construct, we optimized semi-continuous cell tracking using the microglial marker Tomato Lectin. Our data overall suggest that SOX2-positive iNSC colonies, which start to appear from day 6 of conversion on, might indeed arise from marker-positive iPSdMiG. Thus, we next assessed whether doxycycline (DOX)-induced overexpression of SOX2 and cMYC in AAVS1-engineered iPSdMiG is able to trigger iNSC conversion, too. Although 14 day-long DOX treatment was able to induce transgene expression of SOX2 and cMYC and promote a significant downregulation of microglial markers such as *ITGAM* and *PU.1* in two transgenic iPSdMiG lines, NSC markers such as *endoSOX2*, *NES* and *PAX6* were not significantly induced on RNA and/or protein level. As an alternative to the inducible transdifferentiation of transgenic 'convertibles', we therefore worked toward the *in vivo* conversion of primary human microglia. As a first step on this route, we successfully implemented a protocol for the isolation and *ex vivo* cultivation of primary microglia from human brain tissue. Subsequent studies will now need to investigate whether isolated primary human microglia are principally amenable to SeV-mediated iNSC conversion. Overall, we expect this data to significantly contribute to our understanding of the potential prospects of microglia-to-iNSC conversion for future clinical therapy of neurodegenerative conditions.

Keywords: Neurodegenerative diseases; Regeneration; Transdifferentiation; Microglia; Neural stem cells.

Resumo

O aumento progressivo da esperança média de vida e o aumento associado da prevalência de doenças neurodegenerativas têm vindo a alimentar esforços para explorar as potencialidades da programação celular a fim de contrariar a degeneração patológica de células neurais no cérebro humano. Várias abordagens têm sido investigadas, incluindo a neurotransplantação de células humanas produzidas *in vitro* e a conversão *in situ* de células somáticas, residentes no cérebro, em células neuronais. Neste último caso, a conversão de células de micróglia em células estaminais neurais (NSCs), especificamente, representa uma alternativa bastante interessante ao combinar as características migratórias e imunológicas das células microgliais iniciais com as capacidades de autorrenovação e diferenciação multipotente exibidas pelas NSCs resultantes.

Neste projeto, começámos por aplicar diferentes sistemas de rastreamento de linhagem das células de micróglia para monitorizar o destino celular destas mesmas células derivadas de iPSC (iPSdMiG), após a sobreexpressão mediada pelo vírus Sendai (SeV) de dois fatores de transcrição, SOX2 e cMYC. Até agora não foi possível implementar com sucesso um sistema de rastreamento genético baseado na expressão da proteína fluorescente verde (EGFP), sob o controle do promotor do gene da subunidade alfa-M da integrina (ITGAMp; gene que codifica o marcador microglial CD11b). Isto deveu-se, por um lado à incapacidade de EGFP ser expresso eficientemente a partir da construção genética inserida mediante a diferenciação de ITGAMp-EGFP-iPSCs em iPSdMiG, bem como também devido à incapacidade de nucleofetar iPSdMiG e assim contornar um potencial silenciamento epigenético associado à diferenciação que afeta esta construção. No entanto, otimizámos o rastreamento celular semi-contínuo utilizando o marcador microglial Tomato Lectin (em inglês). Em geral, estes dados sugerem que as colónias de iNSC positivas para SOX2, que começam a surgir ao 6º dia de conversão, podem de facto advir de iPSdMiG positivas para este marcador. Assim, em seguida, avaliámos se a sobreexpressão de SOX2 e cMYC, induzida por doxiciclina (DOX), em iPSdMiG, seria também capaz de desencadear a conversão em iNSCs. Embora um tratamento de 14 dias com DOX tenha possibilitado induzir a expressão transgénica de SOX2 e cMYC e promover uma regulação negativa significativa de marcadores microgliais (*ITGAM* e *PU.1*) em duas linhagens de iPSdMiG transgénicas, marcadores característicos de NSCs (endoSOX2, NES e PAX6) não foram induzidos significativamente ao nível do RNA e/ou proteína. Como alternativa à transdiferenciação induzível de "convertíveis" transgénicos, trabalhámos também para a conversão *in vivo* de células de microglia humanas primárias, tendo dado os primeiros passos ao implementar com sucesso um protocolo para o isolamento e cultivo *ex vivo* de células primárias de microglia de tecido cerebral humano. Estudos subsequentes irão agora investigar se estas células de microglia humanas primárias isoladas são mais passíveis, ou não, à conversão em iNSCs mediada por SeV. Cremos que os dados obtidos, contribuirão significativamente para a compreensão das potencialidades da conversão de células da microglia em NSCs para uma futura aplicação em terapias clínicas associadas a condições neurodegenerativas.

Palavras-chave: Doenças neurodegenerativas; Regeneração; Transdiferenciação; Micróglia; Células estaminais neurais.

Table of Contents

List of Figures

List of Tables

List of Abbreviations

AAV	Adeno-associated virus
AAVS1	Adeno-associated virus integration site 1
AD	Alzheimer's disease
AIF1	Allograft Inflammatory Factor 1
APC	Allophycocyanin
Ascl1	Achaete-scute homologue 1
BBB	Blood-brain barrier
BDNF	Brain-derived neurotrophic factor
Brn2	Brain 2
CD11b	Cluster of differentiation molecule 11b
C1q	Complement component 1q
cMYC	Avian myelocytomatosis viral oncogene cellular homolog
CNS	Central nervous system
CNTF	Ciliary neurotrophic factor
CNV	Copy number variation
CSF1R	Colony-stimulating factor 1 receptor
CSPG	Chondroitin sulphate proteoglycan
DAPI	4', 6' diamidino-2-phenylindole
DOX	Doxycycline
EB	Embryoid body
ECM	Extracellular matrix
EDTA	Ethylenediaminetetraacetic acid
EGF	Epidermal growth factor
EGFP	Enhanced green fluorescent protein
ESC	Embryonic stem cell
FACS	Fluorescence-activated cell sorting
FCS	Fetal calf serum
FGF	Fibroblast growth factor
gDNA	Genomic DNA
GDNF	Glial cell-derived neurotrophic factor
GFP	Green fluorescent protein
HD	Huntington's disease
HEK	Human embryonic kidney
IBA1	Ionized calcium-binding adapter molecule 1
IFN-γ	Interferon-gamma
IGF1	Insulin-like growth factor 1
IL-1α	Interleukin-1 alpha
IL34	Interleukin 34

IL-6	Interleukin-6
iN	Induced neuron
iNSC	Induced neural stem cell
iPSC	Induced pluripotent stem cell
iPSdMiG	Induced pluripotent stem cell-derived microglial cell
ITGAM	Integrin subunit alpha-M
ITGAMp	Integrin subunit alpha-M promoter
KLF4	Krüppel-like factor 4
LAAP	L-ascorbic-acid-2-phosphate
LB	“Luria Bertani” or Luria Broth
LIF	Leukemia inhibitory factor
Lmx1α	LIM homeobox transcription factor 1 alpha
LV	Lentivirus
MHC	Major histocompatibility complex
Myod3	Myogenic differentiation 3
Myt1l	Myelin transcription factor 1-like protein
NES	Nestin
NeuroD1	Neurogenic differentiation protein 1
NG2	Neuron-glial antigen 2
NGF	Nerve growth factor
NGN2	Neurogenin 2
NOGO	Myelin-derived neurite outgrowth inhibitor
NURR1	Nuclear receptor-related 1 protein (or NR4A2)
NSC	Neural stem cell
NTN	Neurturin
OCT3/4	Octamer-binding transcription factor 3/4
Olig2	Oligodendrocyte transcription factor 2
Omgp	Oligodendrocyte myelin glycoprotein
PAX6	Paired box protein 6
PAULA	Personal AUtomated Lab Assistant
PBC	Peripheral blood cell
PCR	Polymerase chain reaction
PD	Parkinson’s disease
pDNA	Plasmid DNA
PE	Phycoerythrin
PerCP	Peridinin chlorophyll protein
PFA	Paraformaldehyde
PLL	Poly-L-lysine
PSC	Pluripotent stem cell
RE	Restriction enzyme

Rh	Recombinant human
RI	ROCK inhibitor Y-27632
ROS	Reactive oxygen species
SeV	Sendai virus
SOX2	Sex determining region Y-box 2
TF	Transcription factor
TL594	Tomato Lectin DyLight 594
TNF	Tumor necrosis factor
TRE3G	Tet-ON 3G
UHDRS	Unified Huntington's disease rating scale
UPDRS	Unified Parkinson's disease rating scale
VEGF	Vascular endothelial growth factor
WT	Wild-type

1. Introduction

1.1. The advent of cellular programming

Technological advances of the past century have enabled us to shed light on numerous mechanisms underlying distinct human pathological conditions. These research accomplishments were mainly achieved using one or more of the following biomedical approaches: (i) Use of human *post mortem* specimens to characterize the molecular correlates of a disease. (ii) Collection of surgical specimens (from individual patients) to perform *ex vivo* analysis of viable human cells (involving macroscopic (gross) and microscopic (histologic) tissue examinations), whereby the causes, mechanisms and/or extent of the disease can be examined. (iii) Employment of animal model systems to provide a living complex platform, biologically similar to humans, for identification of disease mechanisms that might be translatable to our species (Kim, J. *et al*., 2020). Notably, *post mortem* studies decreased in prevalence, due to ethical concerns (regarding respect for autonomy, beneficence and justice) and key methodological limitations such as immediate onset of autolysis, hindered interpretation of possible findings due to missing causation (*e.g.*, the deficit that patients display during their lifetime may not be connected to the deficits/malformations found in the tissue) and inappropriateness to study disease inception and/or progression (as *post mortem* tissue represents the end point of the disease; Drake, S.A. & Yu, E.T., 2016). Surgical specimens, on the other hand, are hardly accessible in larger quantities and also not available at all research sites. Accordingly, the mechanistic understanding of human diseases most significantly progressed with the implementation of animal models, which have meanwhile become a near universal tool in biomedical research. Notably though, some molecular and organismal features are not conserved even between genetically related species. Owing to this interspecies variability, extrapolating results from animal model systems to humans might not be the most straightforward method to generate knowledge, especially about human-specific diseases. Hence, there always has been a remarkable interest and need to investigate pathological conditions directly in human cell-based models (Kim, J. *et al*., 2020). To this end, ethically sourced primary human cells were found suitable to generate data of physiological relevance. Although the use of human primary cells for research purposes has thus proven valuable, this approach is not equally applicable to all fields. Organs or cell types that are not readily accessible for extraction, such as the heart or the central nervous system (CNS), represent a major bottleneck for the collection of sufficient primary material to address biomedical research questions.

Driven by the need to acquire hardly inaccessible cell types for biomedical research purposes such as disease modelling and regenerative cell therapy, scientists set out to develop methods to mimic embryonic *in vivo* development to derive human cell types *in vitro*. Firstly, methods to isolate embryonic stem cells (ESCs; Figure 1), initially from early mouse embryos (Evans, M. & Kaufman, M., 1981; Martin, G.R., 1981) and then from human embryos (Thomson, J.A., 1998), have been reported. ESCs are the cells composing the inner cell mass of the human blastocyst (an early embryonic stage that lasts from the 4^{th} to the 7^{th} day after fertilization) and are characterized by their ability to proliferate indefinitely while maintaining pluripotency, as well as to give rise to all the different somatic cell types of the body. In

1998, Thomson *et al.* achieved to derive and stably expand a human pluripotent ESC line *in vitro*, maintaining its developmental potential to give rise to derivatives of all three embryonic germ layers (Thomson, J.A., 1998). Accordingly, ESCs have become widely used as a platform to develop protocols for the *in vitro* differentiation of pluripotent stem cells (PSCs) into specific cell lineages and fates. However, ethical controversies, limitations in generating disease-specific ESCs and problems associated with tissue rejection following transplantation of ESC-derived cells in patients have – to some degree – restricted their use for more translational research (Evans, M. & Kaufman, M., 1981; Martin, G.R., 1981; Thomson, J.A., 1998).

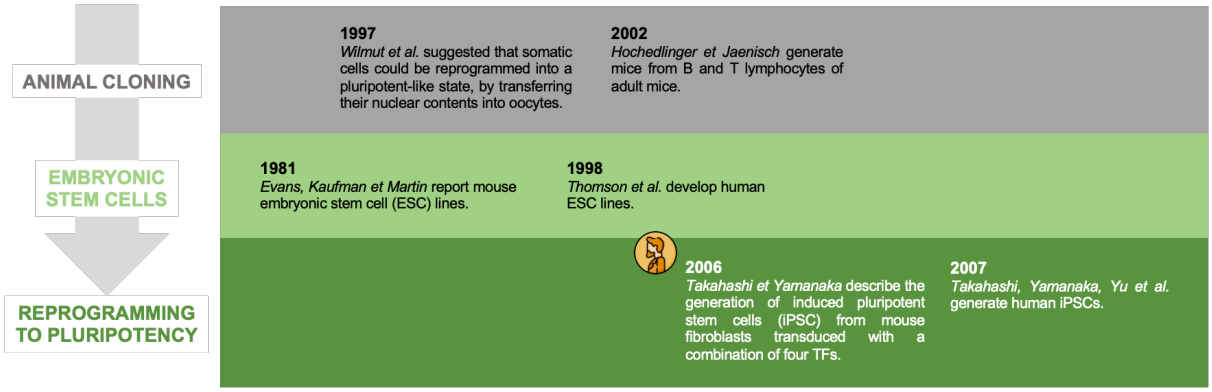

Figure 1 – Schematic illustration on the research endeavors that enabled the development of the iPSC reprogramming technique. Especially the valuable contribution from the Nobel prize-awarded discovery, portrayed by Takahashi and Yamanaka in 2006, paved the way for extended research on cellular programming. Adapted from Graf, T., 2011.

To circumvent the drawbacks associated with the use of ESCs, alternative strategies have next been devised allowing the generation of pluripotent cells directly from a patient's somatic cells, *i.e.,* methods to re-install a pluripotent state in already terminally differentiated cell types, enabling their consequent differentiation into alternative fates. Along this line, Wilmut *et al.* demonstrated as early as 1997 that somatic cells could be reprogrammed into a pluripotent-like state by transferring their nuclear contents into oocytes (Wilmut, I. *et al*., 1997), and Tada, M. *et al.* (2001) and Cowan, C.A. *et al.* (2005) likewise reported that reprogramming to pluripotency could alternatively be achieved by fusing somatic cells with ESCs. These two observations indicated that both unfertilized eggs and ESCs contain factors that could confer totipotency or pluripotency to somatic cells, suggesting a certain importance and significance of these factors for the programming/changing of a cell's fate.

In subsequent studies that gave important insights into the regulatory transcriptional network of stem cells and thus the molecular signature of 'stemness', several protein transcription factors (TFs), including octamer-binding TF 3/4 (Oct3/4; Nichols, J. *et al*., 1998; Niwa, H. *et al*., 2000), Sex determining region Y-box 2 (Sox2; Avilion, A.A. *et al*., 2003), and Nanog (Chambers, I. *et al*., 2003; Mitsui, K. *et al*., 2003), were identified as being crucial for self-renewal and the maintenance of pluripotency in both early embryos and cultured ESCs. Building on this knowledge, Kazutoshi Takahashi and Shinya Yamanaka (2006) finally made the ground-breaking discovery that retroviral overexpression of a combination of four of these TFs, namely Oct3/4, Sox2, Krüppel-like factor 4 (Klf4), and avian myelocytomatosis viral

oncogene cellular homolog (cMyc), could in fact induce pluripotency in mouse fibroblasts *in vitro*, thereby pioneering a new research field dedicated to the reprogramming of somatic cells into, so called, induced pluripotent stem cells (iPSCs; Takahashi, K. & Yamanaka, S., 2006). In the following years, it was similarly reported that also human fibroblasts can be converted into iPSCs using the same combination of TFs (Takahashi, K. *et al*., 2007). These newly devised iPSCs were ascertained to be very similar to ESCs, with long-term self-renewal capacity, clonogenicity (*i.e.*, can be cultivated indefinitely without differentiation, still retaining its reproductive ability to form identical cells or clones) and pluripotency (*i.e.*, the capability to differentiate into all mature cell types that are originated from the three primary germ layers, ectoderm, endoderm and mesoderm) even after *in vitro* long term culture (Murry, C.E. & Keller, G., 2008; Puri, M.C. & Nagy, A., 2012). Moreover, these cells appear to reproduce the major features of the ESC epigenome, including genome-wide methylation patterns, and in the establishment of bivalent histone hallmarks at specific *loci* (*e.g.*, H3K4me3 or H3K27me3 modifications). Apart from these similarities, iPSCs also have an equivalent possibility to acquire karyotypic abnormalities due to culture expansion and prolonged passages, and the ability to form aggressive teratomas in immunocompromised mice. However, some differences can be highlighted between these two types of PSCs: (i) Cellular origin – Contrarily to ESCs that are derived from the inner cell mass of pre-implantation blastocysts, iPSCs can theoretically be derived from any somatic cell. This fact enables iPSCs to overcome one of two major obstacles associated to ESCs with regards to ethical concerns, as these *in vitro*-derived cells presuppose the non-manipulation and non-destruction of embryos. (ii) Genetic expression of the pluripotent state – Although ESCs and iPSCs have some already mentioned similarities regarding the epigenome, in terms of gene expression some differences can be observed, specifically in early passage iPSCs. This evidence has led to the concept of an 'epigenetic memory' (attributable to the incomplete removal of somatic cell-specific DNA methylation at regions in proximity to CpG islands) that persists from the somatic cell of origin, and which confers a unique gene expression signature to iPSCs. (iii) Immunogenicity after transplantation – iPSCs can be derived from the patient's own cells thus creating patient-specific iPSCs for autologous transplantation without immune rejection, whereas ESCs, by being collected from different embryos and then allogeneically transplanted to different individuals, can result in graft-versus-host-associated detrimental effects (Puri, M.C. & Nagy, A., 2012).

In addition to providing a new cell source for biomedical research, the iPSC reprogramming technique introduced the more generally applicable concept that any change to a cell's identity requires a transition between epigenetic and subsequent transcriptional states (*i.e.*, inducing alterations in transcription that occur without a change in DNA sequence, but in DNA conformation and accessibility), which could be reached through a stepwise combination of genetically programmed cascades of TF-mediated protein expression patterns (see review by Mertens, J. *et al*., 2016). Through this, iPSC reprogramming paved the way to further develop more direct cell type conversion paradigms for various species and starting cell types, thus, overall, significantly advancing cellular programming – our toolbox for the modulation of transcriptional networks underlying cell identity, aiming at the conversion of one cell type into another.

1.2. iPSC reprogramming and its application for the derivation of neural cells

The successful conversion of somatic cells into tripotent iPSCs fueled attempts to subsequently differentiate iPSCs into virtually any cell type of the three different germ layers through the combination of transient expression of iPSC reprogramming TF cocktails in somatic cells, with controlled growth factor and small molecule exposure, to finally promote lineage commitment and terminal differentiation of arising iPSCs (Graf, T., 2011; Stadtfeld, M. & Hochedlinger, K., 2010). Currently, there are several protocols available to derive neural stem cells (NSCs), which are multipotent stem cells with the capacity for self-renewal and to give rise to functional neurons as well as glial cells, from iPSCs, arising from seminal works on animal models of neurodevelopment that identified key events in early mammalian neural specification and regionalization (Mertens, J. *et al*., 2016). These studies have shown that during *in vivo* neurogenesis (*i.e.*, the process by which *de novo* neuronal cells are produced; Figure 2), human ESCs from the blastocyst's inner cell mass differentiate into neuroepithelial stem cells forming the neural plate (Chambers, S.M. *et al*., 2009; Elkabetz, Y. *et al*., 2008). As a consequence of the intense proliferation of these cells and the presence of neurotrophic factors, neurulation occurs, resulting in a later stage NSC population called neural rosette NSCs that form the neural tube, as well as the generation of the first wave of neurons. Later, during fetal and adult neurogenesis, these rosette-type NSCs give rise to the latest stage of NSCs called radial glial cells, which will then produce most neurons and finally also the two types of glial cells, namely astrocytes and oligodendrocytes (Elkabetz, Y. *et al*., 2008; Farkas, L.M. & Huttner, W.B., 2008; Albert, K. *et al*., 2021). These latter cell types, differently from the messaging function of neuronal cells, will serve multiple physiological roles in the CNS, with astrocytes being responsible for tasks such as constitution and maintenance of the blood-brain barrier (BBB), regulation of ion density in the extracellular space, modulation of neuroinflammation, and synaptic formation and maturation, and oligodendrocytes, for functions related, for instance, to myelin production for improvement of neural conductivity, neurotrophic support for neuronal survival and stabilization of neuronal connectivity (Albert, K. *et al*., 2021; Wang, Y. *et al*., 2021).

Thus, during neural development, molecular programs advance in a concerted manner to generate distinct, highly specialized neural cell types in specific regions of the nervous system. Specifically, neurons are further subdivided in different neuronal subtypes based on several characteristics including their regional localization in the nervous system, their morphology, cellular marker and neurotransmitter expression, their connectivity as well as their electrophysiological properties. Due to this immense complexity, providing the right combination of cues is essential to differentiate PSCs into NSCs and safeguard their further differentiation into specialized terminal cell (sub)types (Mertens, J. *et al*., 2016). Yet, the *in vitro* differentiation of PSCs has been as much fine-tuned that it is by now possible to derive highly enriched cultures of specific neural cell types of clinical interest such as excitatory cortical neurons (Shi, Y. *et al*., 2012), dopaminergic neurons (Boyer, L.F. *et al*., 2012), motor neurons (Di Giorgio, F.P. *et al*., 2008; Dimos, J.T. *et al*., 2008), interneurons (Maroof, A.M. *et al*., 2013), and glial cells (Krencik, R. *et al*., 2011; Zhang, P.W. *et al*., 2016; Douvaras, P. & Fossati, V., 2015).

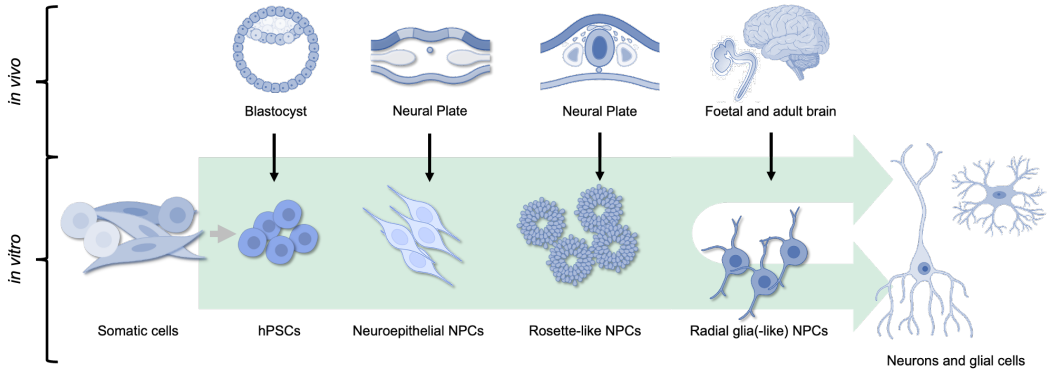

Figure 2 – Schematic illustration on the stages of neural differentiation in vivo and their in vitro equivalents. When human PSCs (comprising human ESCs and iPSCs) differentiate into neurons *in vitro* (lower row), they transit through defined cellular stages during which they resemble distinct NSC populations present during *in vivo* neurogenesis (upper row). PSCs resemble the inner cell mass of the blastocyst and are able to differentiate into neuroepithelial stem cells *in vitro*, corresponding to the neuroepithelial NSCs that form the neural plate *in vivo*. During *in vivo* neurulation, the neural tube closes for patterning to take place along the developmental axes and to give rise to the first wave of neurons. *In vitro*, the rosette-type NSCs that can also be derived from PSCs resemble this developmental stage. During fetal and adult neurogenesis, radial glia give rise to most of the postmitotic neurons. These correspond to the radial glia-like NSCs that can be generated from rosette-type NSCs *in vitro*. Adapted from Mertens, J. *et al.*, 2016, with graphical elements created in BioRender.com.

Notably, iPSC reprogramming does not come without limitations. On the one hand, the process of reprogramming somatic cells toward iPSCs and the subsequent differentiation of iPSCs into the cell type of interest is a very lengthy process that may require 4-6 months before the first neurons are generated, including up to 2 months just to generate and validate iPSC clones. Thus, this approach might not be the most appropriate if money and/or time restraints are decisive. On the other hand, once the entire process is accomplished, iPSCs represent stable intermediates that researchers can use over a prolonged period of time. Yet, it has to be considered that *in vitro*-expanded iPSCs can accumulate chromosomal abnormalities, genetic instabilities and copy number variations (CNVs) over time. These existing divergences are emergent concerns when subjecting new patient lines to cell programming, and in the case of iPSC reprogramming, these considerations are especially important owing to the clonal origin of iPSCs, as one iPSC clone typically represents only one single donor cell. Finally, in recent years, environmental, epigenetic, and age-related risks have become important determinants for disease inception (Mertens, J. *et al.*, 2016). Notably though, chromatin remodeling during iPSC reprogramming was shown to reset the epigenetic state of the cell, including its age-related signatures, to an embryonic-like state (Maherali, N. *et al.*, 2007). Moreover, competition within clonal growth of iPSC colonies as well as numerous rounds of cell division (or passages), may be selective forces for repair and dilution of macromolecular damages (Rando, T.A. & Chang, H.Y., 2012). These two processes result in the derivation of a completely rejuvenated cell after iPSC reprogramming, representing a major challenge for, *e.g.*, modelling late-onset diseases. Despite these limitations, iPSC-based neural cell models have valuably contributed to improve our understanding of autism spectrum disorders (Samaco, R.C. *et al.*, 2005; Marchetto, M.C.N. *et al.*, 2010), bipolar disorders (Mertens, J. *et al.*, 2015b), familial dysautonomia (Lee, G. *et al.*, 2009), and schizophrenia (Brennand, K.J. *et al.*, 2011), but also Alzheimer's disease (AD; Israel, M.A. *et al.*, 2012), Parkinson's disease (PD; Reinhardt, P. *et al.*, 2013)

and many more. Moreover, iPSC-derived cells turned out to be a strong candidate for neuroregenerative cell therapies attempting to tackle the consequences of such disorders (Stadtfeld, M. & Hochedlinger, K., 2010).

1.3. Direct cell fate conversion as an alternative to the iPSC route

Given the high demand for quick and easy to obtain human tissue-specific cell types, alternatives to iPSC-based technologies have been developed. One of the most implemented alternatives is direct cell fate conversion (also called transdifferentiation), in which a converted somatic cell directly arises from another differentiated somatic cell without requiring a transit through a pluripotent intermediate state (such as during iPSC reprogramming; Mertens, J. *et al*., 2016). The first reports describing the practicality and attainability of transdifferentiation were published as early as 1987, when Davis *et al.* reported that overexpression of Myod3 in a mouse fibroblast line converts fibroblasts into muscle cells (Davis, R.L. *et al*., 1987). In those days, cellular programming was considered to be restricted to the conversion of lineage-related cells of the same germ layer, but upon the introduction of the iPSC technology, this view changed dramatically (Graf, T., 2011; Mertens, J. *et al*., 2016). Bypassing most developmental stages and physiological lineage changes, attempts to attain somatic-to-somatic cell conversion across germ layers by the overexpression of lineage-specific TFs were undertaken. Over the years, this approach was adopted for different kinds of target cells (for a complete overview of all these attempts, see Horisawa, K. & Suzuki, A., 2020). Notably, by the end of 2018, neuronal lineage-related cells represented the most reported target cell population for direct conversion (Figure 3; Horisawa, K. & Suzuki, A., 2020).

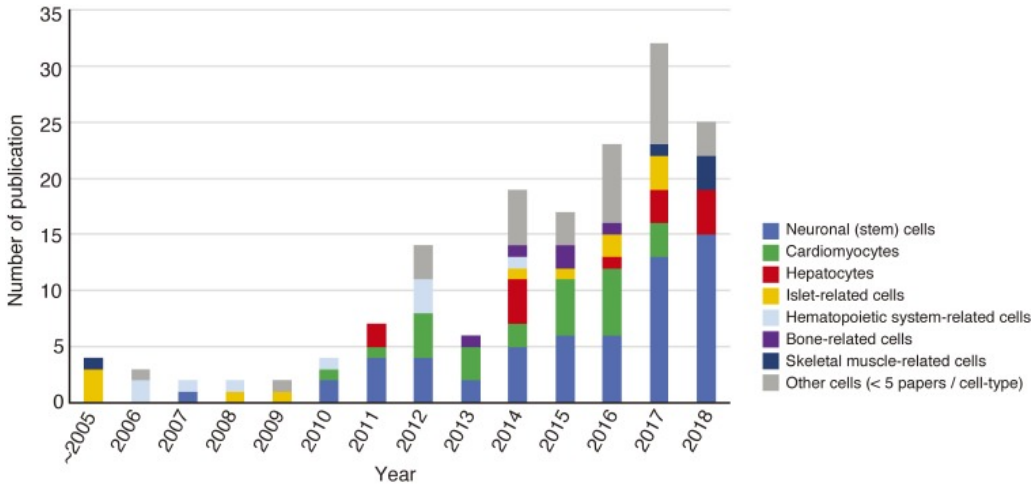

Figure 3 – Graph illustrating the number of publications related to direct conversion studies from mid 2005 to 2018. The numbers of publications regarding direct conversion into different target cell types are shown as a bar chart for the given time period. Each color refers to an individual target cell type. From these data, it is possible to deduce a trend for an increased interest in the derivation of neural cells by direct cell fate conversion. Published in Horisawa, K. & Suzuki, A., 2020.

Interestingly, one of the first attempts for direct trans-germ layer conversion was the Oct3/4, Sox2, Klf4, and cMyc-driven derivation of NSCs from mouse and human fibroblasts (Kim, J. *et al*., 2011; Thier, M.

et al., 2012) and human blood cells (Wang, T. *et al*., 2013). In these attempts, overexpression of the otherwise iPSC-instructing transgenes was combined, for example, with an exposure to key mitogens (proteins or chemical compounds that induce cell division by triggering mitosis) for NSC proliferation such as fibroblast growth factor 2 (FGF2), fibroblast growth factor 4 (FGF4), and/or epidermal growth factor (EGF; Tropepe, V *et al*., 1999; Kosaka, N. *et al*., 2006). However, in accordance with the transient expression of pluripotency-mediating TFs, this venture resulted in a 'partial' reprogramming, yielding mixed cultures of iPSCs and NSCs, thus, felling short on the promise of bypassing pluripotency (Bar-Nur, O. *et al*., 2015).

A major breakthrough with regards to directly converting somatic cells into neural cell types was achieved in 2010, when Vierbuchen *et al.* succeeded in converting mouse fibroblasts into induced neurons (iN) *in vitro* (Vierbuchen, T. *et al*., 2010). The overexpression of a combination of only three TFs – Brain-2 (Brn2, also known as Pou3f2), Achaete-scute homologue 1 (Ascl1) and myelin TF 1-like protein (Myt1l), collectively known as BAM – was reported to be sufficient to convert embryonic and adult mouse fibroblasts into mature iNs, which express multiple neuron-specific proteins and are further capable of generating action potentials and functional synapses (Vierbuchen, T. *et al*., 2010). After this seminal publication, several laboratories likewise reported protocols to convert human fibroblasts into iNs (Ambasudhan, R. *et al*., 2011; Pang, Z.P. *et al*., 2011; Pfisterer, U. *et al*., 2011). Furthermore, there is now encouraging data on fate conversion of non-neuronal, CNS-resident cells such as brain pericytes (Karow, M. *et al*., 2012) and yolk sac-born microglia (Matsuda, T. *et al*., 2019) toward a neuronal phenotype. Importantly, different from the derivation of neurons from iPSCs, functional human iNs can be generated from fibroblasts in a timeframe as short as 5-6 weeks until electrophysiological maturity has been achieved (Yang, N. *et al*., 2011). Moreover, iNs were shown to inherit age-associated phenotypes of their cell of origin, which can facilitate modelling age-related, late-onset diseases (Mertens, J. *et al*., 2016).

Directly generating terminally differentiated neurons can serve many purposes, including the provision of cells for disease modelling, drug discovery platforms and/or transplantation studies for cell therapy (Figure 4). However, clear limitations are associated with this procedure: (i) Since neurons are generally post-mitotic, *i.e.*, not being able to divide or self-regenerate, this approach might not be well suited for large-scale applications, considering the limited number of cells that can be generated. (ii) Provided that not all cells undergo successful transdifferentiation, additional strategies to eliminate non- or only partially converted cells need to be implemented. (iii) Resulting from the two aforementioned characteristics of direct cell fate conversion into iNs, each transdifferentiated neuron represents a singular conversion event, thus limiting the degree of standardization and quality control that can be reached with iN cultures (Mertens, J. *et al*., 2016). In light of these limitations, direct conversion of somatic cells into expandable NSCs deemed especially attractive and was successfully reported by several groups employing mouse (Lujan, E. *et al*., 2012; Tian, C. *et al*., 2012) and human (Ring, K.L. *et al*., 2012) fibroblasts as starter cells, and OCT4-free protocols overexpressing different NSC-enriched TFs or TF combinations to elicit transdifferentiation (Shahbazi, E. *et al*., 2016). This avenue has further

been explored for other conversion-amenable somatic cells, particularly easily accessible cell populations such as blood- (Sheng, C. *et al*., 2018) and urine-derived cells (Wang, L., *et al*., 2013). Nowadays, induced NSC (iNSC) derivation protocols are available for a variety of neonatal (Ring, K.L. *et al*., 2012) as well as adult human tissues (Mertens, J. *et al*., 2015a; Zou, Q. *et al*., 2014), featuring long-term self-renewal, clonogenicity, tripotency and responsiveness to lineage patterning cues.

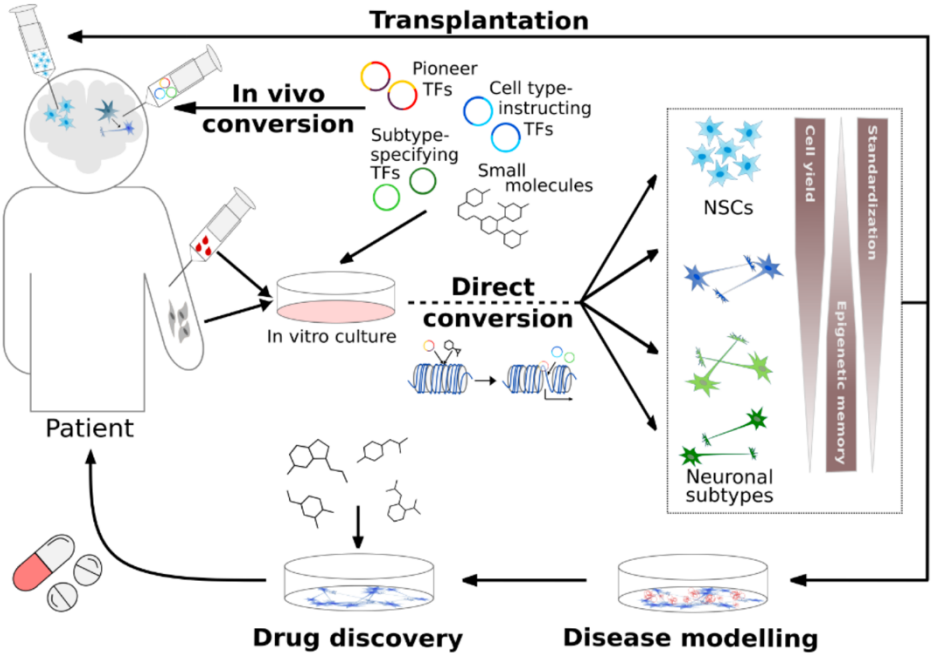

Figure 4 – Direct cell fate conversion strategies in the context of biomedical applications. Depending on the choice of programming factors, direct conversion can be tuned to derive different cell types and even distinct neuronal subtypes, as exemplified. These transdifferentiated cells could be useful in disease modelling, drug discovery and/or cell therapy (e.g., by neurotransplantation). Notably, direct cell fate conversion can not only be achieved in vitro, but also in vivo in order to promote a therapeutic effect from endogenous cell sources. Retrieved from Flitsch, L.J. & Brüstle, O., 2019.

In recent years, the cell programming toolbox has, thus, rapidly expanded, and the direct cell fate conversion technique has proven useful for several biomedical applications. However, and as summarized by Gascón, S. *et al*. (2017), several issues still remain to be addressed such as the impact of the target population on the conversion of different cell types, the numerous pathways underpinning direct cell fate conversion, the potential role of metabolic changes during the conversion process, and the influence and response of the microenvironment where the cells are located on the programming process (Gascón, S. *et al*., 2017).

1.4. Neurodegenerative diseases and paradigms for brain repair

Nowadays, neurodegenerative diseases represent a major threat to human health, equally posing a heavy social and economic burden on the world (Ray Dorsey, E. *et al*., 2018; Alzheimer's disease facts and figures, 2021). Partly because of the progressive extension in human lifespan (although other factors, such as genetic or environmental variables, are also considered to play a role in

neurodegeneration), the prevalence of neurodegenerative disorders is increasing, with AD and PD being the most common human neurodegenerative pathologies (Gitler, A.D. *et al*., 2017; Ray Dorsey, E. *et al*., 2018). Affecting together more than 60 million people worldwide and more than 200,000 just in Portugal, effective treatments for both diseases and other similar pathologies are desperately needed (Ray Dorsey, E. *et al*., 2018; A.D. International, 2020; Parkinsons.org, 2020). Nonetheless, there are still no effective therapies in place to prevent or at least slow down neuronal degeneration. However, to be able to treat rather the cause than the symptoms of neurodegenerative diseases, a deep understanding of the pathomechanisms underlying each specific disorder is required. Yet, since the molecular onset of the disease can be expected to be much earlier than the emergence of first symptoms, this knowledge might still not suffice to prevent neuronal loss in affected patients. Notably, unlike many other organs, the mammalian CNS has a very limited capacity for self-repair. While glial cells, such as astrocytes, can induce proliferation and cellular plasticity in response to some brain injuries and diseases (Kwon, H.S. & Koh, S.H., 2020), neurons are generally unable to self-regenerate (Chen, W. *et al*., 2019; Lei, W. *et al*., 2019). Therefore, neurons are not replaced upon neuronal damage or degeneration in the human adult brain, and there is even a strong debate about whether postnatal human brains are at all capable of endogenous neurogenesis (Frisén, J., 2016; Lei, W. *et al*., 2019).

Although neurodegenerative conditions can have several origins (*e.g.,* developmental, inherited or acquired) and occurrences (acute or chronic), with each one representing a different set of challenges, one constant in all of them is the noticeable degeneration of neurons. Accordingly, replenishing the neuronal population affected by a disease could potentially rescue the respective CNS function. Moreover, in both scenarios of acute and chronic neurodegenerative disorders there is also an inter-related macroglial and microglial/inflammatory reaction that may involve changes in the extracellular matrix (ECM) and/or alterations in the BBB, which can further promote damage and degeneration of neuronal cells (Bonneh-Barkay, D., & Wiley, C.A., 2009; Carvey, P.M. *et al*., 2009; George, N. & Geller, H.M., 2018). Hence, strategies that enable neuroprotection or circuit reconstitution can likewise be valuable approaches. Therefore, research endeavors have mainly focused on three approaches: First, applying trophic factors with cell rescue and putative-disease-modifying effects. Second, aiming at cell replacement using exogenously applied, *in vitro*-cultured cells. Third, promoting neural repair from within the brain by either mobilizing endogenous NSCs or employing strategies that involve the direct neuronal conversion of brain-resident cell types (Barker, R.A. *et al*., 2018).

1.4.1. Trophic factors with cell rescue and putative disease-modifying effects

On account of the discovery of the first trophic or neurotrophic factor, the nerve growth factor (NGF), in the 1950s (Levi-Montalcini, R. & Hamburger, V., 1951), a large number of research studies have pointed to the multiple functions of this group of molecules within an organisms' development and during its adulthood. As reviewed by Xiao, N. and Le, Q.T. (2016), most neurotrophic factors are indispensable during development and differentiation of the nervous system to allow neurons to develop and establish specific synaptic connections and neuronal circuits (Xiao, N. & Le, Q.T., 2016). Moreover, neurotrophic

factors' signaling can play an important role in the adult CNS by supporting, nourishing, and maintaining those connections for a normal brain function. The family of neurotrophic factors have long been extensively investigated for their abilities in supporting the survival, proliferation, and maturation of certain neurons (Xiao, N. & Le, Q.T., 2016), and recent works have reported that neurotrophic factors can be directly delivered to fight neurodegenerative conditions (Table 1; Weissmiller, A.M. & Wu, C., 2012).

Table 1 – Clinical trials using neurotrophic factors in patients with different neurodegenerative disorders. Abbreviations: NGF – Nerve growth factor; GDNF – Glial cell-derived neurotrophic factor; NTN – Neurturin; CNTF – Ciliary neurotrophic factor; BDNF – Brain-derived neurotrophic factor; IGF1 – Insulin-like growth factor 1. Adapted from Barker, R.A. *et al*., 2018.

Neurodegenerative disease	Use of neurotrophic factors in clinical trials
Alzheimer's disease (AD)	NGF
Parkinson's disease (PD)	GDNF/NTN
	NGF
Amyotrophic lateral sclerosis (ALS)	CNTF
	BDNF
	IGF1
Huntington's disease (HD)	CNTF

Although the results of initial studies assessing the effects of direct neurotrophic factor delivery in rodents were encouraging (Kromer, L.F., 1987; Mitsumoto, H. *et al*., 1994), clinical trials in humans did not prove to be effective, since the administered factors failed to reach their neuronal targets or were rapidly inactivated upon injection (Nutt, J.G. *et al*., 2003; Kordower, J.H. *et al*., 1999; Bartus, R.T., & Johnson, E.M., 2017a; Bartus, R.T., & Johnson, E.M., 2017b). Even further attempts with intraparenchymal delivery of glial cell-derived neurotrophic factor (GDNF) into the striatum of patients suffering from moderately advanced PD did not result in an improved motor Unified Parkinson's Disease Rating Scale (UPDRS; an evaluation scale used to longitudinally follow the progression of a patient's PD symptomatic) 6 months after growth factor administration, as compared to placebo-treated patients (Lang, A.E. *et al*., 2006). The reasons for these unfavorable results of human *in vivo* neurotrophic treatment trials were extensively discussed and might have been attributable to suboptimal dosing of the neurotrophic factor, inadequate delivery of the substances to the site of lesion and/or the disease pathology itself interfering with growth factor's function (Barker, R.A., 2006; Decressac, M. *et al*., 2012). Meanwhile, however, it has been more generally questioned whether neurotrophic factors might at all suffice to rescue normal brain function in a chronic and/or progressive disease setting. Once neurodegeneration advanced beyond a certain stage, attempts to repair neuronal circuits with trophic factors alone might not be viable, since, at this stage, the brain might already have lost a critical number of neurons. The fact that most neurodegenerative disorders are only diagnosed in later stages after extensive cell loss already occurred, would support this hypothesis.

Another strategy to aim at conveying neuroprotection would be to improve the surrounding tissue environment of affected neuronal populations to aid regenerative processes. This alternative could be achieved by modifying the response of glial cells and/or the ECM, both of which have been reported to produce signals that inhibit repair in the adult CNS (see reviews by Adams, K.L., & Gallo, V., 2018 and Fawcett, J.W., 2015). With regard to the former, it has been shown, for example, that microglia can induce astrocytes to become neurotoxic under CNS injury conditions, where high concentrations of microglia-secreted cytokines (*e.g.*, interleukin 1 alpha (IL-1α), tumor necrosis factor (TNF) and complement component 1q (C1q)) promote the loss in astrocytes' ability to promote neuronal survival, outgrowth, synaptogenesis and phagocytosis, and prompt them to cause the death of neurons and oligodendrocytes (Liddelow, S.A. *et al*., 2017). Additionally, it was reported that both astrocytes and oligodendrocytes can express cell surface molecules such as brevican from the lectican family of chondroitin sulphate proteoglycans (CSPGs; Siebert, J.R. *et al*., 2014) and oligodendrocyte myelin glycoprotein (Omgp; Wang, K.C. *et al*., 2002), respectively, that inhibit axonal regeneration, although the expression levels of these molecules seems to vary as a function of disease state, being greater in patients with acute traumatic injuries than those suffering from chronic neurodegenerative disorders (Barker, R.A. *et al*., 2018; Yiu, G. & He, Z., 2006). This observation inspired early clinical trials to try to block glial cell-produced inhibitory factors, for example using antibodies against the myelin-derived neurite outgrowth inhibitor (NOGO) molecule to treat patients with spinal cord injury. These trials revealed, however, very divergent results, with all patients experiencing at least one adverse event, while paraplegic/tetraplegic patients within the cohort still reported improvements of motor symptoms (Kucher, K. *et al*., 2018). Accordingly, the concept of glial cells being exclusively detrimental for CNS repair has been rejected, appreciating that glial responses may be even beneficial for repair. In amyotrophic lateral sclerosis, for example, transplanted glial cells have been used to buffer extracellular glutamate and thus protect motor neurons from cell death (Lepore, A.C. *et al*., 2008). Apart from targeting directly glial cells' response, a plethora of other studies grafting mesenchymal stem cells and even fibroblasts showed potential beneficial effects in a diseased CNS by enhancing neuritogenesis through the increased expression and consequent secretion of various neurotrophic and neuroprotective factors, including brain-derived neurotrophic factor (BDNF), leukemia inhibitory factor (LIF), osteopontin, and osteonectin, and the reduction of a pro-inflammatory immune response, given the decreased proinflammatory cytokine expression levels of interleukin-6 (IL-6), IL-1α, and interferon-gamma (IFN-γ; Mazzini, L. *et al*., 2010; Brick, R.M., *et al*., 2018; Cozene, B. *et al*., 2021).

The brain ECM, contrastingly, has been a matter of growing interest in recent years, revealing important aspects of its composition and function. The ECM is the macromolecular network in which neurons and glial cells are embedded, accounting for approximately 20 % of the total volume of the adult brain. This acellular structure has been shown to play a critical role in physiological conditions, including neurite outgrowth, synaptogenesis, and synaptic stabilization, as well as in pathological settings by regulating injury-related plasticity (as comprehensively summarized by Song, I. & Dityatev, A., 2018 and Burnside, E.R., & Bradbury, E.J., 2014). The latter was reported to be associated with the upregulation of certain CSPGs and other ECM molecules by reactive astrocytes after CNS injuries or during neuroinflammation

and degeneration, resulting in the formation of growth-impermissive environments and impaired synaptic plasticity of neurons. Notably though, as with glial cells, the ECM also seems to have neuroprotective effect under these conditions (Lam, D. *et al*., 2019).

1.4.2. Cell replacement therapies using exogenously derived and *in vitro*-cultured cells

Since a severe brain injury or a neurodegenerative disease is often associated with the loss of a critical number of neurons, the replacement of this cell type may become essential for functional improvement. Neurons can be replaced by intracerebral transplantation into single or multiple brain locations, aiming at recreating the disrupted neuronal circuitry, locally as well as over long distances. The very first cell transplantations into the brain were already reported in 1890, as Dr. W. G. Thompson was able to transplant cortical brain tissue between adult cats and dogs. However, the transplanted tissue was reported to have died relatively soon after surgery, since the transplants were performed between species in the absence of immunosuppression. Interestingly, Dr. Thompson wrote that his main objective with this operation was not to be able to restore the lost function but rather evaluate 'the vitality of the brain tissue' and the course of its degeneration (Thompson, W.G., 1890).

Due to the fact that PD and Huntington's disease (HD) are associated with a quite localized degeneration of predominantly one neuronal subtype (dopamine neurons of the midbrain in PD and medium spiny neurons of the striatum in HD; German, D.C. *et al*., 1989; Peschanski, M. *et al*., 1995), these disorders seem especially well-suited to target with cell-based approaches. Indeed, clinical transplantation trials using fetal tissue-derived cells have already been undertaken (Barker, R.A. *et al*., 2015). Notably, however, these transplantation efforts so far resulted in highly variable outcomes (Barker, R.A. *et al*., 2013a and 2013b). Although in some PD patients, motor improvement (Kefalopoulou, Z. *et al*., 2014) and complete graft survival (or extensive graft-derived dopaminergic innervation; Kefalopoulou, Z. *et al*., 2014; Li, W. *et al*., 2016) were observed, the cell grafts of several patients became affected by the disease process over time, manifesting in α-synuclein aggregation (Li, J.Y. *et al*., 2008). In addition, a fraction of patients experienced significant side effects after transplantation such as graft-induced dyskinesias (Politis, M. *et al*., 2010). Homotopically grafting fetal striatal tissue into the striatum of HD patients aiming at circuit reconstruction likewise showed only modest effects on improving the motor scale of the Unified Huntington's Disease Rating Scale (UHDRS) and exhibited overall poor graft survival and integration (Cisbani, G., & Cicchetti, F., 2014). This lack of consistently convincing outcomes across different transplantation studies might have been attributable to partially low numbers of disease-affected neuronal subtypes within the transplanted tissue preparations, high batch-to-batch variability arising from the need to dissect different fetuses for the preparation of donor cells and the risk of losing grafts as a consequence of immune rejection (Lindvall, O., 2015). In combination with ethical issues concerning the harvesting of human fetal tissue as well as the risk of possible deleterious adverse events (*e.g.*, transplantation-induced dyskinesias), these findings necessitated of more standardized ways to produce batches of donor cells with a defined composition.

The recent technological advancements in generating and differentiating human PSCs have made it possible to reliably, and robustly, generate large numbers of disease-relevant cell types amenable to cell replacement therapy (Barker, R.A. *et al*., 2017). Directly comparing the efficacy of transplanting human fetal ventral midbrain tissue and both human ESC- and iPSC-derived dopaminergic progenitors into rodent models of PD has revealed that human PSC-derived cells are able to survive neurotransplantation (Hargus, G. *et al*., 2010), appropriately innervate their anatomical target structures (Grealish, S. *et al*., 2014), integrate into host neuronal circuitry, produce effective neurotransmitters and finally even mediate functional recovery of 6-hydroxydopamine lesioned athymic adult rats in the amphetamine-induced rotation test after 16-18 weeks (Grealish, S. *et al*., 2015). Similarly, promising results have been reported for the transplantation of iPSC-derived medium spiny neurons in rodent models of striatal degeneration typically observed in HD (Reidling, J.C. *et al*., 2018). Moreover, Wang *et al.* reported in 2015 that autologous iPSC-derived dopamine neuron transplantation is able to improve the behavior and restore motor function in a non-human primate PD model (Wang, S. *et al*., 2015). Schweitzer, J.S. *et al.* (2020) even published a first-in-human case report about the implantation of patient autologous iPSC-derived midbrain dopaminergic progenitor cells in a patient with idiopathic PD, achieving improvement of the UPDRS score with concomitant evidence of graft survival and no observed dyskinesias or other adverse neurologic effects, thus, providing an important proof-of-principle for the potential power and safety of PSC-based cell therapies for neurodegenerative disorders (Schweitzer, J.S. *et al*., 2020).

Besides the advantage of being able to produce quite defined and highly quality controlled cell products, PSCs are amenable to genome editing strategies. Therefore, it can be envisioned that PSCs and their derivatives can be engineered to carry genetic modifications or corrections, making grafted cells more resistant or refractory to a certain disease pathology (Cox, D.B.T. *et al*., 2015). Furthermore, genetic alterations could be designed to enhance beneficial aspects of the cells' behavior, for instance, by enhancing the migratory capacity of grafted cells (Ladewig, J. *et al*., 2014). This could tackle one of the major obstacles of classical neural transplantation to date, that is the limited spread of grafted neural cells outside the transplantation site, where they commonly accumulate in a dense graft core (Fricker *et al*., 1999; Reidling, J.C. *et al*., 2018). Other challenges for the clinical application of human PSC-derived cells for neurotransplantation comprise the possible ethical debates and associated legal restrictions concerning the use of ESC-derived cell products, potential genomic instability of iPSCs and their derivatives, the risk of tumor formation if the final cell product is not devoid of undifferentiated iPSCs, and immunological considerations (Figure 5; Martin, U., 2017; Liu, X. *et al*., 2017). Thus, scientists have in parallel explored alternative routes to address neuroregeneration by exploiting brain-endogenous cell sources.

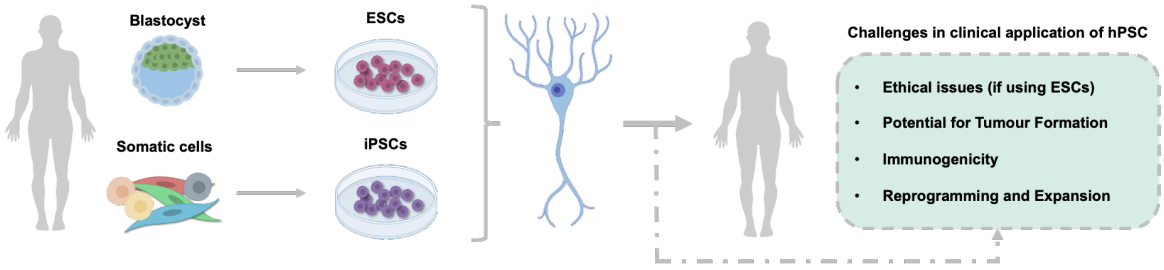

Figure 5 – Challenges associated with the clinical application of human PSC-derived neural cells for the treatment of neurodegenerative diseases. Adapted from Ford, E. *et al*., 2020, with graphical elements created in BioRender.com.

1.4.3. Strategies for neural repair from within the brain

Reports stating that exercise-based therapies and cognitive training can promote neurogenesis from endogenous NSCs in mice (van Praag, H. *et al*., 1999) and in humans (Griffin, É.W. *et al*., 2011; Erickson, K.I. *et al*., 2011) and induce local production of neurotrophins like BDNF in the brain (Griffin, É.W. *et al*., 2011; Chieffi, S. *et al*., 2017) have fueled efforts to exploit brain-resident cells for the restoration of neural function in a diseased context. Allowing neural cells to be born and develop in their natural *in vivo* environment could have the potential advantage to give rise to more authentic neuronal cell populations, which might be endowed with a more appropriate regional and/or neurotransmitter identity than *in vitro*-derived cells. In fact, Ichida, J.K. *et al.* compared primary mouse spinal motor neurons to ESC-derived, iPSC-derived, and directly converted motor neuron-like cells, revealing that all *in vitro*-derived neuronal populations expressed only about 55-86 % of the primary motor neuron transcriptome (Ichida, J.K. *et al*., 2018). This observation suggested fundamental limitations of *in vitro* systems to faithfully recapitulate *in vivo* development, which might present a challenge for neural regeneration by exogenous cell transplantation, since the authenticity of cellular phenotypes might be of importance to ultimately have an effective reconstruction of brain circuits and function.

Next to attempts to stimulate neurogenesis in the adult human brain (although limited and still heavily debated on; Lei, W. *et al*., 2019; Frisén, J., 2016) and to recruit new-born neurons or neuroblasts from active endogenous neurogenic niches to sites of neuronal injury (Arvidsson, A. *et al*., 2002), neural repair from within the brain could be achieved by applying the concept of direct cell fate conversion to brain-resident cells *in situ*. Considering the fact that glial cells and especially astrocytes (i) are lineage-related to neurons, (ii) are evenly distributed across the adult mammalian brain, (iii) constitute over half of the total brain-resident cells, and (iv) have an intrinsic capacity to proliferate, these cells represent an ideal candidate population for direct *in vivo* conversion into neurons to achieve neuroregeneration (Kwon, H.S. & Koh, S.H., 2020).

The concept of converting astrocytes into neurons was first tested *in vitro* in 2002, confirming that glial cells transdifferentiation into neurons could be achieved by the overexpression of the neurogenic TF paired box protein 6 (PAX6; Heins, N. *et al*., 2002). Three years later, in 2005, exciting proof-of-principle *in vivo* experiments in mice and littermates further revealed that astrocyte-to-neuron conversion could

also be elicited by the antagonization of the oligodendrocyte TF 2 (Olig2) after traumatic brain injury (Buffo, A. *et al*., 2005). Similarly, Kronenberg, G. *et al.* recapitulated this *in vivo* conversion, now after infliction of mild brain ischemia in mouse models, highlighting that through the combined inhibition of the repressor function of Olig2 and the overexpression of Pax6, resident astrocytic cells in the striatum could be reprogrammed toward functional neuronal differentiation, with reported capabilities of receiving synaptic input and generating action potentials (Kronenberg, G. *et al*., 2010). Single neurogenic TFs acting as potent fate determinants in development such as the transcriptional activator neuronal differentiation protein 1 (NeuroD1) and neuron-glial antigen 2 (NG2) were likewise shown to enable glial cells-to-neuron conversion in AD models (Guo, Z. *et al*., 2014) and in mouse ischemic injury (Chen, Y.C. *et al*., 2020). Even in adult non-human primates, *in situ* transdifferentiation of astrocytes into neurons was achieved (Zhang. X. *et al*., 2021), and it has also been successfully demonstrated that human glial cells can principally convert into neurons or neuroblasts at least *in vitro* (Rivetti Di Val Cervo, P. *et al*., 2017). Notably though, *in vitro* results not always translate to the respective *in vivo* scenario, as was noticed by Torper, O. *et al*. (2015) when developing an Adeno-associated virus (AAV)-based vector system for *in vivo* neural conversion of astrocytes (Torper, O. *et al*., 2015). While efficient in targeting and converting glial cells into neurons *in situ*, the vector system composed by a TF combination of Ascl1, Nurr1, and LIM homeobox TF 1 alpha (Lmx1α) which was found to elicit dopaminergic-like neurons from human PSCs (Theka, I. *et al*., 2013) and fibroblasts *in vitro* (Caiazzo, M. *et al*., 2011), promoted the generation of fast-spiking parvalbumin-containing interneurons when astrocytes were converted *in vivo*. This study thus emphasized the need to re-assess already described *in vitro* conversion protocols for their applicability *in vivo*.

In this context, it has to be noted that very recently, Wang, L.L. *et al.* reported that the presumed *in vivo* astrocyte-converted neurons previously described by several studies may indeed not originate from resident astrocytes but from vector-infected endogenous neurons (Wang, L.L. *et al*., 2021). In this article, the group thus refutes the claims of published studies depicting NeuroD1 AAV-based *in vivo* astrocyte-to-neuron conversions, arguing through the employment of multiple stringent lineage tracing strategies that virus-expressed reporters are prone to leakage, thus resulting in outcomes which are not more than mere artifacts (Wang, L.L. *et al*., 2021). These approaches have, thus, to be considered to be still in their infancy, and as such, there are some challenges and limitations that need to be overcome before this approach becomes suitable for biomedical application in the context of neurodegenerative diseases (Gascón, S. *et al*., 2017). First, local microenvironments in diseases such as AD or PD can be dominated by various deleterious factors, including excessive levels of reactive oxygen species (ROS) and inflammatory cytokines, which may affect the neuronal conversion efficiency, as well as the consequent *in vivo* survival and integration of the derived neurons (Singh, A. *et al*., 2019; Kwon, H.S. & Koh, S.H., 2020). For instance, Gascón, S. *et al.* demonstrated that by relying on the co-expression of the anti-apoptotic protein Bcl2 (or B-cell lymphoma 2 protein) with Ascl1 within astrocytes, a significant increase in neuronal conversion and an increase in the total number of surviving cells can be achieved through reduction of oxidative stress and ferroptosis (Gascón, S. *et al*., 2016). Second, *in vivo* conversion can be strongly context dependent (Gascón, S. *et al*., 2017). As an example, a study from Grande, A. *et al.*

described that Neurogenin 2 (NGN2)-mediated conversion of proliferating fibroblasts resulted in the emergence of GABAergic neurons in the mouse striatum but glutamatergic neurons in the neocortex (Grande, A. *et al*., 2013). Third, considering that neurodegenerative disorders as AD and PD tend to affect older people, age-related limitations to cell programming must be borne in mind, *e.g.*, astrocyte senescence that is observed in patients suffering from both these diseases (Bhat, R. *et al*., 2012; Chinta, S.J. *et al*., 2018). In addition, in circumstances where neurodegeneration is caused by gene mutations such as in familial neurodegenerative diseases (Wu, Z. *et al*., 2020; Zhang, T. *et al*., 2021), it might become relevant to account for gene mutations that are still present in brain-resident somatic cells before they are eventually enforced to convert into neurons, which would yet again be prone to degenerate as a consequence of the still persisting mutation. Fourth, the discovered fate-instructing factors and their delivery must be applicable in living humans. Here, regularly employed viral vector systems for gene therapy approaches may represent an auspicious solution. On the other hand, non-viral delivery strategies such as nucleic acids-protecting structures (*e.g.*, polyplexes/lipoplexes; Adler, A.F. *et al*., 2012), small molecules (*e.g.*, mannitol, to temporarily open the BBB and allow the penetration of larger molecules into the brain parenchyma; Wang, S. & Huang, R., 2019), or nanoparticles (*e.g.*, calcium phosphate or amino terminated organically modified silica nanoparticles; Corso, T.D. *et al*., 2005; Roy, I. *et al*., 2008) may also qualify for delivering the required cell programming cues *in vivo*, with the adjuvant characteristics of low safety concerns, great customizability and ease in manufacturing (see reviews by Tan, J.K.Y. *et al*., 2016 and Larouche, J. & Aguilar, C.A., 2019). Whatever delivery system is chosen, it must always enable factor distribution to the lesion site in a safe and preferentially non-invasive fashion. Fifth, considering the potential emergence of partially programmed cells deriving from the *in vivo* conversion process, their resultant somatic coding mutations, and the potential effect for tumorigenicity must be investigated as well as their impact on tissue homeostasis. Lastly, and as pointed out by Flitsch, L.J. & Brüstle, O. *et al.* in 2019, as *in vivo* conversion systems are continuously being improved and their efficiencies increased, detrimental effects as the depletion of the *in vivo* target cell population can become a serious issue, especially when talking about glial cells that serve particularly vital functions within tissue homeostasis and neuronal function. Given this circumstance, *in vivo* conversion into cells with residual self-renewal capacity such as NSCs, may be a promising course of action to further increase the potential of this method into neuronal conversion/regeneration (Flitsch, L.J. & Brüstle, O., 2019). Despite these issues that remain to be addressed in the context of *in vivo* direct cell fate conversion, this field seems to strive toward clinical translation. Since the mechanisms underlying *in vivo* cell programming are still not fully resolved, further research uncovering the mechanisms underpinning each conversion trajectory is essential to fully exploit the prospects of this approach (Flitsch, L.J. & Brüstle, O., 2019).

1.5. Microglia-to-NSC conversion: A potential strategy for *in vivo* and *in situ* neuronal replacement?

Most studies on the *in vivo* and *in situ* direct conversion of glial cells into neurons have been focused on macroglia, especially astrocytes, as starting cell type. Although astrocytes respond to injury or diseases

of the CNS by proliferation and accumulation, other glial cells are also importantly implicated in the tissue response to insults. Accounting for 0.5 % to 16.6 % of the total cell population in the human brain (Lawson, L.J. *et al*., 1992), microglia are the immunocompetent cells of the CNS parenchyma, being considered the resident tissue macrophages of this organ. Originating from yolk sac-born erythro-myeloid progenitors within the mesodermal branch of the hematopoietic lineage (Figure 6), microglia invade the CNS as early as week 4 of embryonic development before the closure of the BBB (Ginhoux, F. *et al*., 2010). Once in the brain, they rapidly divide, creating a pool of residual cells that are long-lived and have the ability to renew independently of the hematopoietic system. Afterwards, upon completion of the brain colonization process at week 24 of gestation, microglia disperse in a non-heterogeneous manner throughout the CNS. Like in mice, a higher relative number of microglial cells can be found in the human dentate gyrus of the hippocampus, the substantia nigra and parts of the basal ganglia, with the highest number of microglia being located in the olfactory telencephalon (Lawson, L.J. *et al*., 1990). By the end of the second postnatal week, microglia are fully matured and express an adult gene signature, which is governed by their ontogeny and function, but also their surrounding tissue environment (Bachiller, S. *et al*., 2018).

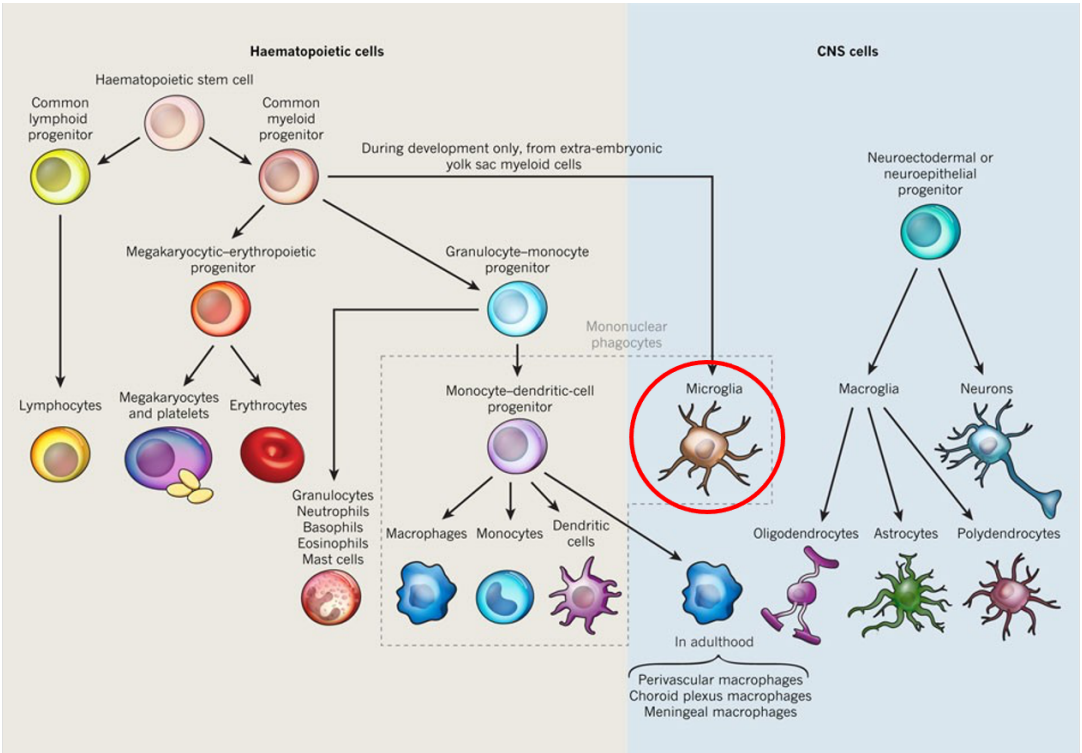

Figure 6 – Schematic illustration of the development of hematopoietic and neural lineage cells, with a particular focus on microglia (red circle). Microglia are the only cells of the hematopoietic lineage that are found in the parenchyma of the CNS. Cells of the hematopoietic system and CNS are depicted, with arrows indicating lineage relatedness. Adapted from Ransohoff, R. M. & Cardona, A.E., 2010.

Microglial cells are the first non-neuronal cell type to emerge in and interact within the developing CNS, regulating diverse processes including programmed cell death, synaptic maturation, and suppression, as well as elimination or pruning of dysfunctional synapses and myelin (Hughes, A.N. & Appel, B., 2020).

Even in the adult brain, microglia play a critical role in the modulation of neural circuit connectivity, especially in the adult cortex. For instance, it has been shown that depleting microglia in mice *in vivo*, by administering selective colony-stimulating factor 1 receptor (CSF1R) inhibitors, increases synaptic connectivity of both excitatory and inhibitory synapses to excitatory cortical neurons without altering their intrinsic electrophysiological properties (Liu, Y.J. *et al*., 2021). Recent reports further suggest that microglia are involved in memory retrieval (Wang, C. *et al*., 2020; Liu, Y.J. *et al*., 2021). In addition to maintaining neuronal circuit integrity, the prime functions of microglia are immunosurveillance and immunoresponse. To accomplish this, microglia are endowed with a sentinel ability as well as strong migratory capacity, being capable of eliciting defense mechanisms and immune responses within the entire CNS. As such, microglia are able to orchestrate a potent inflammatory response in any given location (Bachiller, S. *et al*., 2018). Even under physiological conditions, microglia are constantly motile, monitoring their surroundings. A recent study has shown, for example, that microglia migrate into regions with actively myelinating oligodendrocytes roughly every four hours in order to clear up myelin debris (Hughes, A.N. & Appel, B., 2020).

Under non-pathological conditions, microglia are morphologically characterized by having numerous branches spread across the tissue with the purpose of detecting the presence of any debris, pathogen, lesion, or disease process. Furthermore, under resting conditions, microglia do not possess phagocytic or endocytic properties, and express low levels of the major histocompatibility complex (MHC) antigens and other microglial activation markers (Tsuchiya, T. *et al*., 2005). However, these cellular properties are tightly controlled by the local microenvironment and by interactions between microglia and their surrounding cells. Upon an insult, for instance a neurodegenerative lesion, brain trauma, cerebral ischemia or infection, microglia become plastic and extremely mobile to quickly respond to their environment (Albert, K. *et al*., 2021). In addition to the insult itself, this response can be stimulated by the release of certain neurotransmitters such as glutamate and α-aminobutyric acid (Liu, H. *et al*., 2016; Czapski, G.A., & Strosznajder, J.B., 2021), which, in addition to initiating an excitotoxic cascade, can activate neighboring microglia by inciting structural changes and alterations in lysosome content (Majumdar, A. *et al*., 2007), membrane composition (Button, E.B. *et al*., 2014), electrophysiological properties (De Biase, L.M., *et al*., 2017) and gene transcriptome profiles (Hickman, S.E. *et al*., 2013). Since microglia are further chemotactically attracted toward the insult, they accumulate in great numbers at the lesion site, releasing chemokines as well as cytokines, and phagocyting, for instance, pathologically accumulating peptides such as α-synuclein in PD or amyloid-ß in AD (Bachiller, S. *et al*., 2018; Albert, K. *et al*., 2021). In addition, microglia produce neurotrophic factors such as GDNF, BDNF, FGF2 and VEGF, providing neurotrophic support to distressed neurons (Elkabes, S. *et al*., 1996; Narantuya, D. *et al*., 2010). Therefore, microglia strongly contribute to the elimination of the cause of injury, the restriction of tissue damage and the initiation of repair processes. Notably though, microglia-promoted inflammation can, apart from fighting pathogens, at the same time create a cytotoxic milieu and thus induce neurodegeneration (*e.g.*, as a consequence of continuous production of ROS; Simpson, D.S.A. & Oliver, P.L., 2020). Whether microglial activity is finally rather neuroprotective or detrimental, is therefore heavily depending on the multiple signaling cues active during a particular disease process.

Given their unique characteristics, microglia were hypothesized to be a very well suitable population to target for restoring lost neurons by direct conversion. Along this line, recent work by Matsuda, T. *et al.* (2019) successfully demonstrated the *in vitro* as well as *in vivo* transdifferentiation of primary mouse microglia into striatal projection neuron-like cells by employing the ectopic expression of the neurogenic TF NeuroD1, which crucially governs radial glia-to-neuron fate determination (Matsuda, T. *et al*., 2019). In the mouse brain, microglia-derived neurons were reported to be electrophysiologically active and able to form excitatory synapses with host neurons (Matsuda, T. *et al*., 2019). However, in a recent paper published by Rao, Y. *et al*., the feasibility of this conversion was challenged (Rao, Y. *et al*., 2021). The authors conducted comprehensive experiments to verify microglia-to-neuron lineage conversion, resorting to the protocol that was originally published by Matsuda, T. *et al.* (2019), but additionally implementing high-purity primary microglial cell culture, live cell imaging, microglial depletion procedures and *in vivo* lineage tracing experiments. By doing so, Rao, Y. *et al*. concluded that the ectopic expression of NeuroD1 can neither convert microglia into neurons *in vitro* nor in *in vivo*. Instead, the authors reported that NeuroD1 expression actually induces microglial cell death (Rao, Y. *et al*., 2021). Thus, controversial conclusions have emerged from different laboratories on whether astrocyte- and microglia-to-neuron transdifferentiation is indeed possible or might have been falsely concluded from leakage of high-dosed viral vectors and/or other experimental artifacts (Chen, Y.C. *et al*., 2020; Wang, L.L. *et al*., 2021).

Although future studies need to address and resolve these discrepant observations, converting microglia into neurons still represents, at least theoretically, a promising therapeutic approach for replenishing neurons in the CNS. However, microglia-to-neuron conversion might endow some shortcomings that need to be considered from a translational perspective. As the extent of neurodegeneration and the number of neurons lost due to a given disease might be quite extensive, it would be advisable to rely on a comparatively high number of converted cells to elicit a significant therapeutic effect. However, neurons are postmitotic, precluding further expansion of the target cell, and thus limiting the number of effective neurons in place to the number of successfully converted microglia. In conjunction with potentially low conversion efficiencies, it could be possible that the number of neurons available for disease amelioration after conversion is too low to be effective. Moreover, although some disease might cause the degeneration of only one specific neuronal cell subtype, for wider therapeutic application, it would be preferable to have the ability to produce different types of cells by microglia transdifferentiation to adjust for the requirements of specific conditions. Finally, yet importantly, emerging evidence indicates that iNs, in contrast to ESC- and iPSC-derived neurons, largely retain age-associated transcriptomic and epigenetic signatures (Mertens, J. *et al*., 2015a), which, although representing an asset to model age-related disorders, may pose severe limitations for clinical translation. Consequently, an approach to convert microglia into neural cells with the ability for self-renewal, exhibiting multipotent differentiation capacity and lack of age-related hallmarks, such as iNSCs derived from peripheral blood (Sheng, C. *et al*., 2018), could potentially be better suited for clinical application.

2. Objectives

Confidential data from Oliver Brüstle's laboratory suggest the feasibility of converting iPSC-derived microglia (iPSdMiG) into iNSCs by resorting to the overexpression of the two TFs SOX2 and cMYC (Berg *et al*., in preparation); a transdifferentiation system that was based on a published protocol for the conversion of adult peripheral blood cells (PBCs) into iNSCs (Sheng, C. *et al*., 2018). Although this finding holds great prospects for a potential future clinical translation, as it combines the migratory and immunological characteristics of microglial starting cells with the ability of self-renewal and multipotent differentiation exhibited by the NSC target cells, several prerequisites have to be addressed in order to make this system prospectively translatable to the clinics.

First, considering the recent publication challenging the feasibility of microglia-to-neuron conversion (Rao, Y. *et al*., 2021), we will set out to implement a microglia lineage reporter system for monitoring the suggested microglia-to-iNSC cell fate transition induced by Sendai virus (SeV)-mediated overexpression of the TFs SOX2 and cMYC. Such a system would enable the specific verification of the ontogeny of arising NSCs. Driving microglia-to-iNSC conversion toward a future clinical application, we will further explore two different methodological approaches for microglia-to-NSC conversion *in situ* or *in vivo*. Similarly to Torper, O. *et al*. (2013), we will explore an inducible conversion system that could prospectively be applied for the *in situ* conversion of already SOX2/cMYC-equipped iPSdMiG into iNSCs upon an inducing stimulus. On the other hand, endorsing a future *in vivo* conversion strategy targeting brain-resident primary cells, we will here explore whether a kit-based isolation protocol, which was optimized for the extraction of mouse primary microglia, allows efficient isolation and subsequent propagation of microglial cells from human primary brain tissue *ex vivo*.

Thus, this thesis aims at providing a collection of proof-of-principle experiments that will hopefully allow us to deeply characterize and further develop the prospects of microglia-to-iNSC transdifferentiation in the context of future biomedical applications.

3. Materials and Methods

3.1. Cell culture

3.1.1. IPSC culture and differentiation toward iPSdMiG

IPSCs were thawed in a 37 ºC water bath for 1 minute, diluted 1:10 with pre-heated DMEM/F12 medium (Gibco, Thermo Fischer Scientific), centrifuged at 800 rpm for 5 minutes and subsequently cultured on 6-well tissue culture plates coated with vitronectin (1:200; Thermo Fischer Scientific) in StemMACS™ iPSbrew media (Miltenyi Biotech), supplemented with 10 µM ROCK inhibitor Y-27632 (RI, Cell Guidance Systems) only until the following medium change. Upon reaching ~90 % confluency, iPSCs were dissociated by incubation with StemPro Accutase (Thermo Fischer Scientific) at 37 ºC for ~10 minutes, diluted 1:3-1:4 with pre-warmed DMEM/F12 medium, centrifuged at 1,300 rpm for 4 minutes and seeded in 6-well tissue culture plates coated with vitronectin, in a cell concentration of $5x10^5$ cells per 6-well in StemMACS™ iPSbrew media supplemented with 10 µM RI. For routine expansion of iPSCs, cells were washed once with 0.5 mM ethylenediaminetetraacetic acid (EDTA) in 1xDPBS (Gibco, Thermo Fischer Scientific), dissociated by incubation with 0.5 mM EDTA in 1xDPBS at room temperature for ~5 minutes and by a washing step with StemMACS™ iPSbrew media, and seeded in 6-well tissue culture plates, coated with vitronectin, in typical splitting rates of 1:2-1:6, in StemMACS™ iPSbrew media.

For assessing transgene induction levels in SOX2/cMYC-transgenic iPSC lines (for details on the cell lines used in this thesis see Attachment 1), StemMACS™ iPSbrew medium was supplemented with 2 µg/ml doxycycline (DOX; Stem Cell Technologies) the day after cell seeding. Two days after DOX induction, iPSCs were lysed for subsequent RNA extraction (see chapter ‘3.2.2 RNA extraction, cDNA synthesis and quantitative RT-PCR (qPCR)).

For analysis of microglia, iPSCs were differentiated into iPSdMiG by Michaela Segschneider or Mona Mathews-Ajendra according to a proprietary protocol from LIFE and BRAIN GmbH (patent application n. º EP20162230), which is detailly described elsewhere (Mathews, M. *et al.*, 2022).

3.1.2. IPSdMiG-to-iNSC conversion

3.1.2.1. SeV-mediated overexpression of SOX2 and cMYC

For SeV-mediated iNSC conversion, $4x10^6$ wild-type (WT) iPSdMiG were retrieved from the supernatant of differentiation flasks by Michaela Segschneider or Mona Mathews-Ajendra. As seeding controls, a fraction of the harvested cells was directly seeded in 96-well or 24-well imaging plates (Ibidi) at a cell density of 2,679 cells/cm^2 and 64,935 cells/cm^2, respectively. For seeding, cells were centrifuged at 1,500 rpm for 5 minutes, resuspended in N2 medium (DMEM/F12 with HEPES, 1xN2 supplement and

2 mM Glutamax (all from Gibco, Thermo Fischer Scientific)) supplemented with 100 ng/ml recombinant human interleukin 34 (rhIL34; Peprotech), and distributed to Matrigel-coated (1:45; Corning Inc.) plates as described. Remaining suspension cells were then stained for CD11b by incubation on ice for 1 hour of 1:50 CD11b-Phycoerythrin (PE) antibody (Miltenyi Biotech). Afterwards, CD11b-positive cells were sorted out using a BD FACS Aria Fusion or BD FACS Aria III by Peter Wurst or David Kühne from the Flow Cytometry Core Facility of the University Bonn, Medical Faculty. After sorting, two aliquots of $1.5x10^5$ CD11b-purified microglia were prepared. Cells were centrifuged at 1,500 rpm for 5 min, cell pellets were resuspended in culture medium (as described below) after supernatants have been discarded, and aliquots were then transferred to a S2 laboratory. In a S2 laboratory, both aliquots were centrifuged at 1,500 rcf and 32 ºC for 30 minutes. To one cell aliquot, SeVs coding for SOX2 and cMYC (ID Pharma) were added at a multiplicity of infection of 5. After spin-infection, cells were either directly plated in the Matrigel-coated 96-well or 24-well imaging plates at a cell density of 10,714 cells/cm^2 or 21,429 cells/cm^2 and 64,935 cells/cm^2, respectively, or first seeded in uncoated 4-wells at a density of 78,947 cells/cm^2. All plate formats were cultivated overnight in S2 under normoxic conditions (37 °C, 21 % O_2). Following the latter procedure, cells were detached using a cell scraper at day 1, washed with 1xDPBS, scraped again to ensure full detachment of cells, and collected in individual tubes for a subsequent centrifugation at 1,500 rpm for 5 minutes. Resulting supernatants were discarded in a S2 laboratory and cell pellets were resuspended in the respective medium back in a S1 laboratory. From spin-infection on, SeV-infected cells and uninfected controls were resuspended and cultured in iNSC conversion medium (advanced DMEM/F12:Neurobasal (1:1; both from Life Technologies), 1xN2 (GE Healthcare), 1xB27 (without vitamin-A; Thermo Fisher Scientific), 2 mM L-glutamine (Thermo Fisher Scientific)), 3 µM CHIR99021 (Miltenyi Biotec), 1 µM purmorphamine (Miltenyi Biotec), 0.5 µM A83-01 (Tocris), 10 ng/ml human Leukemia Inhibitory Factor (hLIF; Novoprotein), 64 µg/ml L-ascorbic-acid-2-phosphate (LAAP; Sigma Aldrich), 1 µg/ml laminin (Sigma Aldrich; only present in the first 10 days), and 5 µM tranylcypromine (Enzo Life Sciences; only present in the first 10 days)), while seeding controls were cultured in N2 medium supplemented with 100 ng/ml rhIL34. Medium changes were performed every other day.

At day 2, cells were stained with Tomato Lectin DyLight 594 (TL594; 10 µg/ml; Vector Labs or Thermo Fisher Scientific) for 1 hour at 37 ºC, except one well of the seeding control from each plate format serving as negative control for the TL594 staining. Re-staining with TL594 was performed at day 7 of cultivation in all corresponding wells. After incubation of TL594, wells were washed two times with 1xDPBS (Thermo Fisher Scientific) before adding fresh medium to the wells. After TL594 staining at day 2, imaging plates were transferred back to a S1 laboratory and maintained under hypoxic conditions (37 °C, 5 % O_2) up until day 14 of conversion. All S2 cell culture work was performed by Lea Berg.

From D2-D14, plates were daily imaged with a GE IN Cell Analyzer 2200 (GE Healthcare) using the following settings: 6x6 fields of view without spaces in-between pictures, 10x objective for 24-well and 20x objective for 96-well plates, phase contrast and Cy3 channels. Images were post-processed using Microsoft Office PowerPoint™, CellProfiler™ analysis software or Image J v1.8.0_172 image analysis

software. At day 14, cells were fixed in 4 % paraformaldehyde (PFA, Sigma Aldrich) and 24-well plates were subsequently stained for microglial and NSC markers (see chapter '3.14. Immunocytochemical Analyses).

3.1.2.2. DOX-mediated conversion of iPSdMiG into iNSCs

For evaluating whether DOX-induced overexpression of SOX2 and cMYC from the AAVS1 safe harbor locus of human iPSdMiG would suffice to transdifferentiate microglial cells into iNSCs, $3.75x10^4$ SOX2/cMYC-transgenic iPSdMiG were seeded per Matrigel-coated (1:60) 6 cm cell culture dish in iNSC conversion medium supplemented with DOX concentrations varying from 0-2 µg/ml. Cells were maintained under hypoxic conditions (37 °C, 5 % O_2), and medium changes were performed every other day. At day 14 of conversion, cells from all conditions were dissociated with StemPro Accutase as described and pelleted for subsequent cell lysis.

3.1.3. Nucleofection of iPSdMiG

Nucleofection experiments were performed with a 4D-Nucleofector (Lonza) in 100 µl nucleofection cuvettes using the P3 Primary Cell Line 4D-Nucleofector X-Kit L (Lonza) according to the manufacturer's instructions. In short, $7x10^5$ and $2x10^5$ WT iPSdMiG were harvested from the supernatant of an iPSdMiG differentiation per nucleofection reaction later subjected to the programs EN-158 and CM-158, respectively. Cells were centrifuged at 1500 rpm for 5 minutes, and consequently resuspended in 100 µl nucleofection buffer consisting of 82 µl kit solution and 18 µl supplement per reaction. Seeding controls ($4\text{-}7x10^5$ cells) were alternatively directly resuspended in 1 µl STEMdiff™ APEL™ 2 medium (Stem Cell Technologies) supplemented with 100 ng/ml rhIL34, and subsequently seeded into one well of an uncoated or poly-L-lysine (PLL)-coated (5 µg/ml; Sigma Aldrich) 12-well plate. To some nucleofection reactions, 2 µg and 0.4 µg pMAX-GFP were added before nucleofection with the programs EN-158 or CM-158, respectively, as specified in the respective text sections. After nucleofection, cells were likewise seeded into one well of an uncoated or PLL-coated 12-well plate per reaction in 1 µl STEMdiff™ APEL™ 2 medium supplemented with 100 ng/ml rhIL34. Cells were cultured for two days under normoxic conditions (37 °C, 21 % O_2) after nucleofection.

For optimization of cell viability during and after nucleofection of mature iPSdMiG, cells were further exposed to three anti-apoptotic compounds, before and after nucleofection, using the program EN-158. Specifically, iPSdMiG in suspension were treated with 10 µM RI (Cell Guidance Systems), 50 nM chroman 1 (MedChem Express) mixed with 1.5 µM Emricasan (Selleckchem), 1:1000 polyamine supplement (Sigma Aldrich) and 0.7 µM trans-ISRIB (Tocris; altogether referred to as 'CEPT'; Chen, Y. *et al*., 2021), or 5 µM muristerone (Biotechne), 1 hour prior to nucleofection. In addition, anti-apoptotic treatments were added in the concentrations specified to the seeding medium post nucleofection. Nucleofection was otherwise performed as described.

Nucleofection efficiency and cell viability were documented daily by live cell imaging using a Personal AUtomated Lab Assistant (PAULA; Leica Microsystems). At day 2 post nucleofection, cells were detached using a cell scraper, washed with 1xDPBS, scraped again to ensure full detachment of cells, and collected in individual Eppendorf tubes, which were then centrifuged at 500 rcf for 5 minutes. After centrifugation, cell pellets were resuspended in 1xDPBS for subsequent flow cytometry analysis. Flow cytometry analysis was performed using an Accuri™ C6 Plus Personal Flow Cytometer (BD) and in which samples were measured twice, one with the presence of 1 µl propidium iodide (Thermo Fisher Scientific) and another without this live/dead stain. Flow cytometry data were processed with FlowJo 10.5.3 software (BD).

3.1.4. Lentiviral expression of ITGAMp-EGFP in iPSdMiG

3.1.4.1. Cloning of the lentiviral plasmid pLenti-ITGAMp-EGFP

Two different plasmids were used as cloning templates to acquire the transgenic insert of interest and the lentiviral backbone, namely pAAVS1-ITGAMp-EGFP (provided by Lea Berg) and pLenti-EF1α-core-fGFP (provided by Christina Au Yeung), respectively. For backbone extraction, the pLenti-EF1α-core-fGFP plasmid was digested with the restriction enzymes (REs) SalI-HF and PspXI (both New England Biolabs) for 2 hours at 37 ºC. Afterwards, 1 µl of Antarctic Phosphatase (New England Biolabs) was added to prevent re-ligation of linearized plasmid DNA (pDNA) and the sample was left to incubate for 1 hour at the same temperature. The resultant digested sample (20 µl) was run along with a 1 kb DNA Ladder (PeqLabs) and an undigested sample (without RE) as a control, on a 1 % agarose (Carl Roth) gel in 1xTAE buffer (40 mM Tris-acetate (Sigma Aldrich) and 1 mM EDTA (Sigma Aldrich) dissolved in UltraPure Milli-Q® water (Merck Millipore)) for 2 hours at 100 V before detection using Bio-rad Gel Doc XR+ Imaging System (Bio-rad). After gel electrophoresis, the identified backbone band was excised and stored at 4 ºC until further gel extraction. DNA was subsequently extracted from these gel piece using the QIAquick Gel Extraction kit (Qiagen), according to the manufacturer's instructions.

The ITGAM promoter region and the EGFP sequence within pAAVS1-ITGAMp-EGFP plasmid were amplified by polymerase chain reaction (PCR) with appropriate overhangs for cloning using the following primers: forward primer, 5′-TAT CGA TCA CGA GAC TAG CCT CGA GTG CGT TTT TTT TTT TTT TTA GAG ATA AGA GTC-3′ and reverse primer, 5′-TGT AAT CCA GAG GTT GAT TGT CGA CTT ACA CCC ACT CGT GCA G-3′. Specifically, using the Q5® High-Fidelity DNA Polymerase kit (New England Biolabs), each PCR reaction contained 1000 ng pDNA, diluted in a total volume of 25 µl ddH_2O with 1xQ5® reaction buffer (New England Biolabs), 10 mM of each dNTP (dATP, dGTP, dCTP and dTTP; all from Thermo Fisher Scientific), 0.5 U Q5® DNA Polymerase (New England Biolabs) and 2 µl primer mix. PCR was run on a Biometra T3 Thermoblock (Analytik Jena) using the following cycling conditions: 5 minutes at 98 °C; 35 cycles of 30 seconds at 98 °C, 30 seconds at 52 °C, 54 ºC or 56 °C and 150 seconds at 72 °C, followed by 5 minutes at 72 °C before cooling down to 10 °C. Products were then separated by gel electrophoresis in which 25 µl PCR product or 7 µl 1 kb DNA Ladder were loaded on

a 1 % agarose gel and ran in 1xTAE buffer for 2 hours at 100 V before detection using Bio-rad Gel Doc XR+ Imaging System. Bands of the expected sizes were excised, and the contained DNA was extracted from the collected gel pieces using the QIAquick gel extraction kit, according to the manufacturer's instructions.

Afterwards, Gibson Assembly was performed using the 2xHiFi Gibson Assembly Master Mix (New England Biolabs). Specifically, 125.5 ng of amplified insert of interest and 100 ng of lentiviral backbone were assembled into a circular pDNA in a 3:1 ratio by PCR using the following conditions: 60 minutes at 50 ºC and 30 minutes at 45 ºC.

The 5-α strain of *E. coli* High Efficiency bacteria from the Gibson Assembly kit (New England Biolabs) was used for transformation of the assembled pDNA. 25 µl of a competent bacterial suspension were thawed on ice and subsequently gently mixed with 2.5 µl of pDNA for 30 minutes over ice. Following this mixture, bacteria were heated at 42 ˚C for exactly 45 seconds before being cooled down on ice for exactly 2 minutes. SOC buffer (New England Biolabs) was added to the mixture and an incubation of 1 hour was performed in a shaking incubator, set to 37 ºC and at 200 rpm. 150 µl of bacteria suspension were then distributed in a Luria Bertani (LB)-agar (Carl Roth) medium-filled plate, supplemented with ampicillin (Qiagen), and left to dry for 15 minutes with the agar side down. Afterwards, plates were incubated overnight at 37 ºC. From the incubation period, 7 bacterial ampicillin-resistant clones were pick up with an individual 10 µl pipette tip and inoculation of tubes containing LB medium (Applichem) supplemented with ampicillin (1:1000) was performed for consequent bacterial expansion towards Miniprep. Inoculated tubes were maintained in a shaking incubator for 48 hours at 37 ºC and 200 rpm, given that bacterial deposition was possible to observe at this timepoint. Tubes were centrifuged at full speed (4,700 g) for 5 minutes and then, Plasmid PureLink™ Quick Miniprep kit (Invitrogen, Thermo Fisher Scientific) was used for pDNA isolation according to the manufacturer's instructions. pDNA concentrations were determined using a NanoDrop 2000 spectrophotometer (Thermo Fisher Scientific) and plasmids were stored at -20 °C until further use.

After Miniprep, the DNA of all extracted clones was assessed for the presence of backbone and insert sequences by performing restriction digestion and insert amplification PCR, followed by gel electrophoresis, as described. Afterwards, two positively tested clones were randomly selected for 24 h-long inoculation at 37 °C and 200 rpm in a 500 ml conical flask within a shaking incubator. Bacteria were pelleted by centrifuging 10 minutes at 4,000 rcf, followed by Maxiprep using the PureLink™ HiPure Plasmid Filter Maxiprep kit (Invitrogen, Thermo Fisher Scientific) according to the manufacturer's instructions. Resulting DNA concentrations were measured using a NanoDrop 2000 spectrophotometer, before 1200 ng DNA were diluted in 12 µl TE buffer (Invitrogen, Thermo Fisher Scientific) per sample, which were subsequently send to Microsynth Seqlab (Bonn, Germany) for Sanger sequencing using the primers Seq_F1. 5'-GATAGTAGGAGGCTTGGTAG-3', Seq_F2. 5'-GCACAATCTCTGCTCACTGC-3', Seq_F3. 5'-GCTGAGGAAGGAGGATCAC-3', Seq_F4. 5'-GCAGTGGCATTATTGAGGC-3', Seq_F5. 5'-GCAGGCTAAGTCTATTCAGC-3', Seq_F6. 5'-GCAACATCCTGTTCGGCA-3' and Seq_R1. 5'-

CGCCACGTTGCCTGACAACG-3'. ApE ("A plasmid Editor") v3.0.9 and/or SnapGene® 6.1 software (Insightful Science; available at snapgene.com) were used for analyzing Sanger sequencing data.

3.1.4.2. ITGAMp-EGFP-lentivirus production and lentiviral infection of iPSdMiG

For production of ITGAMp-EGFP-lentivirus (LV), human embryonic kidney (HEK293FT) cells were thawed and seeded as described on Poly-L-Ornithine-coated (5 µg/ml; Sigma Aldrich) 10 cm dishes (Corning Inc.) in HEK medium (consisting of 1x Advanced DMEM (Thermo Fisher Scientific) and 2 mM L-glutamine (Thermo Fisher Scientific)) plus 10 % fetal calf serum (FCS; Gibco, Thermo Fischer Scientific). HEK293FT cells were cultured under normoxic conditions (37 °C, 21 % O_2) until reaching ~70 % confluency.

Afterwards, plasmid transfection and LV production were performed by Lea Berg in S2. In short, medium was changed to HEK medium supplemented with 2 % FCS and 25 µM chloroquine (Sigma Aldrich). Afterwards, lipofection was performed by drop-wise addition of a mixture of 440 µl OptiMEM (Thermo Fisher Scientific) and 60 µl Lipofectamine 2000 (Thermo Fisher Scientific) that was beforehand incubated with 10 µg pLenti-ITGAMp-EGFP, as well as 5 µg of each of the packaging plasmids psPAX2 and pMD2G, for 5 minutes at room temperature. Six hours after lipofection, culture medium was changed to HEK medium containing 5 % FCS. The next day, FCS concentration was increased to 10 %. At days 2 and 3 after lipofection, supernatants were harvested during medium change. Harvested supernatants were then pooled and filtered through a 0.45 µm pore-sized acetate filter membrane (Corning Inc.), before ¼ volume of Lenti-X™ concentrator (Clontech Laboratories) was added to the solution. Following 24 hours of incubation at 4 °C, viral particles were concentrated by centrifugation at 1,500 rpm and 4 °C for 45 minutes. The supernatant was discarded, and the virus-containing pellet was resuspended in Neurobasal medium (Thermo Fisher Scientific). LV was stored at -80 °C until further use.

For lentiviral infection, $5x10^5$ WT iPSdMiG were seeded per well of a PLL-coated 12-well plate in N2 medium (DMEM/F12 with HEPES supplemented with 1xN2 supplement and 2 mM Glutamax (all from Gibco, Thermo Fischer Scientific)) plus with 100 ng/ml rhIL34, by Michaela Segnschneider. The next day, iPSdMiG were transferred to a S2 laboratory and infected with ITGAMp-EGFP LV in a 1:50 dilution in N2 medium supplemented with rhIL34. Cells were transferred back to S1 after three medium changes/washes. All S2 work was performed by Lea Berg. Specifically, medium was changed on days 2 and 4. On days 2, 4 and 6, GFP fluorescence of uninfected and LV-infected iPSdMiG was documented by live cell imaging with PAULA. After PAULA imaging on day 6, iPSdMiG were detached using a cell scraper, washed with 1xDPBS, scraped again to ensure full detachment of cells, and collected in individual Eppendorf tubes, which were centrifuged at 500 rcf for 5 minutes. Then, cell pellets were resuspended in 50 µl 1xDPBS supplemented with 1:50 CD11b-PE antibody (Miltenyi Biotech) and/or 1:1000 Allophycocyanin (APC) far red fluorescent reactive dye (LIVE/DEAD™ Fixable Far Red Dead Cell Stain for 633 or 635 nm excitation; Thermo Fischer Scientific), which were incubated for 1 hour at

room temperature. Antibodies/dyes were washed out following addition of 1xDPBS and consequent incubation for ~10 minutes at room temperature with vortexing once in a while. After another centrifugation at 500 rcf for 5 minutes, cell pellets were finally resuspended in 1xDPBS for subsequent flow cytometry analysis using a Accuri™ C6 Plus Personal Flow Cytometer (BD). Data analysis was performed using FlowJo 10.5.3 software (BD).

3.1.5. Isolation of primary human microglia

For isolating primary human microglia (PhMiG) from a brain tissue sample collected by the neurosurgical department of the University Hospital Bonn (ethics approval nr.179/21), a protocol developed by the laboratory of Dr. Annette Halle (German Center for Neurodegenerative Diseases, Bonn) for the isolation of primary microglia from adult mouse brains was applied. This protocol was adapted from the manufacturer's instructions for the 'Adult Brain Dissociation Kit, mouse and rat' (Miltenyi Biotec™). In short, upon receiving the brain tissue sample, 8 sagittal cuts were performed, and the resulting pieces were transferred to a gentleMACS™ OctoDissociator C tube (Miltenyi Biotec), which was prefilled with an enzyme mix containing 50 µl Enzyme P, 1.9 ml Buffer Z, 10 µl Enzyme A and 20 µl Buffer Y. Mechanical dissociation and enzymatic incubation of the tissue pieces occurred at 37 ºC for 30 minutes by using the machine's ABDK program. After tissue dissociation and extracellular matrix digestion, myelin as well as cell debris and erythrocytes were removed using the kit's Debris and Red Blood Cell Removal Solutions, respectively. The described cell isolation procedure was manually performed by Vanessa Frickel (LIFE & BRAIN GmbH, Bonn).

After cell isolation, the resulting cell suspension was then stained for the microglial marker CD11b as described with minor modifications. Compared to the CD11b staining protocol previously provided, 1:50 CD11b-PE antibody was herein immediately added to the cell suspension and allowed to incubate for 10 minutes on ice and in the dark. After addition of 1xDPBS to the cell suspension to dilute the antibody, cells were centrifuged at 500 rcf for 5 minutes. The consequent supernatant was discarded, cell pellets were resuspended in 1 ml 0.1 % Bovine Serum Albumin (BSA; Gibco, Thermo Fischer Scientific) in 1xDPBS and 1:200 DNase (Sigma Aldrich) and cells were passed-through a 40 µm cell strainer (BD) to remove cell clumps and to help with cell individualization.

Based on CD11b expression, microglial cells were purified using a FACSMelody instrument (BD) by Lea Berg. After Fluorescence-activated cell sorting (FACS), PhMiG were manually counted using a Neubauer counting chamber and subsequently seeded at a density of $1.6x10^4$ cells per well of a 96-well imaging plate in Adult Microglia L929 medium (consisting of DMEM high glucose medium, 10 % fetal bovine serum, 0.1 % penicillin/streptomycin, 0.1 % sodium pyruvate, L-Glutamine (all Gibco, Thermo Fischer Scientific) and 20 % L929 conditioned medium (kindly provided by Tambe Bertrand Agbor, German Center for Neurodegenerative Diseases)). Medium was changed every other day. After 7 days of *ex vivo* culture, cells were fixed for subsequent immunocytochemical characterization.

3.2. Molecular biology techniques

3.2.1. DNA extraction and RT-PCRs

Genomic DNA (gDNA) was extracted using the DNeasy Blood & Tissue kit (Qiagen) from frozen cell pellets according to the manufacturer's instructions. DNA concentrations were determined using a NanoDrop 2000 spectrophotometer (Thermo Fisher Scientific) and gDNA was stored at -80 °C.

Subsequently, gDNA was used for genotyping of the AAVS1 locus by PCR using the Q5® High-Fidelity DNA Polymerase (New England Biolabs). Each reaction contained 500 ng gDNA, diluted in a total volume of 25 µl ddH_2O with 1xQ5® reaction buffer (New England Biolabs), 1xQ5® High GC enhancer (New England Biolabs), 1 mM of each dNTP (dATP, dGTP, dCTP and dTTP; all from Thermo Fisher Scientific), 0.5 U Q5® DNA Polymerase (New England Biolabs) and 1.25 µl primer mix. Primer mixes were tailored for the AAVS1 WT sequence (primer mix '2P-WT': 5 µM AAVS1-F and 5 µM AAVS1-R_WT), the AAVS1 sequence containing the transgenic construct (primer mix '2P-INS': 5 µM AAVS1-F and 5 µM AAVS1-R_INS) or both in parallel (primer mix '3P': 10 µM AAVS1-F, 5 µM AAVS1-R_WT and 5 µM AAVS1-R_INS). Primer sequences were as follows: AAVS1-F 5'-ACC AAC GCC GAC GGT ATC AG-3', AAVS1-R_WT 5'-CAC CAG GAT CAG TGA AAC GC-3' and AAVS1-R_INS 5'-CAG ACC CTT GCC CTG GTG GT-3' (all primers from IDT). PCR was run on a Mastercycler X50a (Eppendorf) using the following cycling conditions: 4 minutes at 98 °C; 5 cycles of 30 s at 98 °C, 30 s at 68 °C and 8 minutes at 72 °C; 40 cycles of 30 s at 98 °C, 30 s at 63 °C and 8 minutes at 72 °C; and finally, 5 minutes at 72 °C, before cooling down to 10 °C. PCR products were size separated by gel electrophoresis. Specifically, 25 µl PCR product or 7 µl 1 kb DNA Ladder (PeqLabs) were loaded on a 1 % agarose (Carl Roth) gel, which was then run in 1xTAE buffer (40 mM Tris-acetate (Sigma Aldrich) and 1 mM EDTA (Sigma Aldrich) dissolved in UltraPure Milli-Q® water (Merck Millipore)) for 2 hours at 120 V before detection using Bio-rad Gel Doc XR+ Imaging System (Bio-rad). The same protocol was also employed for verifying the presence of the NGN2 transgenic insert within the AAVS1 safe harbor locus of the corresponding genetically modified iPSC line.

In addition, gDNA was also used for specifically genotyping the inserted transgene cassette by PCR using the Q5® High-Fidelity DNA Polymerase kit. In this instance, each reaction contained 100 ng or 500 ng gDNA, diluted in a total volume of 25 µl ddH_2O with 1xQ5® reaction buffer, 10 mM of each dNTP (dATP, dGTP, dCTP and dTTP), 0.5 U Q5® DNA Polymerase and 2 µl primer mix. Primer mix was specific for the inserted EGFP sequence and was composed of 5 µM F1 forward primer 5'-TCT TCA TCC AGA GCT TCC CC-3' and 5 µM R1 reverse primer 5'-CGT CGT TCA TGT ACA CCA CC-3'. PCR was run on a Biometra T3 Thermoblock (Analytik Jena) using the following cycling conditions: 3 minutes at 94 °C; 35 cycles of 30 s at 94 °C, 30 s at 60 °C and 1 minute at 72 °C, followed by 5 minutes at 72 °C before cooling down to 10 °C. PCR products were size separated by gel electrophoresis being 25 µl PCR product or 7 µl 1 kb DNA Ladder loaded on a 1.5 % agarose gel, which was then run in 1xTAE buffer for 30 minutes at 100 V before detection using Bio-rad Gel Doc XR+ Imaging System.

Furthermore, prior to Sanger sequencing, we attempted to amplify the genomic sequence of interest by PCR. In this case, each reaction contained 100 ng or 500 ng gDNA, diluted in a total volume of 25 µl ddH_2O with 1xQ5® reaction buffer, 10 mM of each dNTP (dATP, dGTP, dCTP and dTTP), 0.5 U Q5® DNA Polymerase and 2 µl primer mix. Primer mix was composed of 5 µM F2 forward primer 5'-CCA TCT GTT GTT TGC CCC TC-3' and 5 µM R2 reverse primer 5'-TAA GGA ATG GAC AGC AGG GG-3'. PCRs were run on a Mastercycler X50a or on a Biometra T3 Thermoblock. For the former, cycling conditions were 4 minutes at 98 °C; 5 cycles of 30 s at 98 °C, 30 s at 54.9 ºC, 55.3 ºC, 56.2 ºC, 57.7 ºC, 59.6 ºC, 61.6 ºC, 63.4 ºC, 65.4 ºC, 67.4 ºC, 68.9 ºC, 69.8 ºC or 70.2 ºC, depending on each slot, and 8 minutes at 72 °C; 40 cycles of 30 s at 98 °C, 30 s at 54.9 ºC, 55.3 ºC, 56.2 ºC, 57.7 ºC, 59.6 ºC, 61.6 ºC, 63.4 ºC, 65.4 ºC, 67.4 ºC, 68.9 ºC, 69.8 ºC or 70.2 ºC, depending on each slot, and 8 minutes at 72 °C, followed by 5 minutes at 72 °C before cooling down to 4 °C. For the latter, the PCR program comprised 1 minute at 98 °C, 5 minutes at 98 °C; 35 cycles of 30 s at 98 °C, 30 s at 68.5 ºC and 1 minute at 72 °C, followed by 5 minutes at 72 °C before cooling down to 10 °C. Depending on the expected product sizes, bands were size-separated on a 1 % agarose gel in which 25 µl PCR product or 7 µl 1 kb DNA Ladder were loaded and run in 1xTAE buffer for 2 hours at 120 V. Detection of gel bands was likewise performed using Bio-rad Gel Doc XR+ Imaging System. As indicated in the main text, some bands of interest were excised after gel electrophoresis. DNA was subsequently extracted from these gel pieces using the QIAquick Gel Extraction kit (Qiagen). For Sanger sequencing, 18 ng DNA per 100 bp of the respective PCR product were diluted in a total volume of 12 µl TE buffer (Invitrogen, Thermo Fisher Scientific). Sanger sequencing was performed by Microsynth Seqlab (Bonn, Germany) using the primer F2_Sanger Seq., 5'- GCA TTG TCT GAG TAG GTG TC-3'.

3.2.2. RNA extraction, cDNA synthesis and quantitative RT-PCR (qPCR)

For RNA extraction, cells were lysed in RLT buffer (Qiagen) supplemented with β-mercaptoethanol (1:100; Sigma Aldrich). Subsequently, RNA was isolated using the RNeasy Mini kit (Qiagen) following the manufacturer's instructions. Isolated RNA was reverse transcribed using the qScript cDNA Synthesis kit (Quanta Biosciences) in which each reaction contained 1000 ng RNA diluted in a total volume of 20 µl (15 µl of sample, 4 µl 5x qScript reaction mix (Quanta Biosciences) and 1 µl qScript reverse transcriptase (Quanta Biosciences)). In situations when low concentrations of RNA were obtained, total RNA to be used in 15 µl of solution was calculated based on the sample with the lowest concentration and the resulting qScript mixes were adjusted accordingly to the value of RNA with nuclease-free H_2O (Quanta Biosciences). qScript PCR was run on a Biometra T3 Thermoblock using the following cycling conditions: 5 minutes at 22 °C, 30 minutes at 42 °C, followed by 5 minutes at 85 °C before cooling down to 4 °C. RNA and cDNA concentrations were quantified using a NanoDrop 2000 spectrophotometer. Per qPCR reaction, approximately 300 ng cDNA were diluted in a total volume of 19 µl qPCR master mix, consisting of ddH_2O with 200 µM of each dATP, dGTP, dCTP and dTTP, 10 nM fluorescin calibration dye (Thermo Fisher Scientific), 0.75x SyBr Green (Thermo Fisher Scientific), 4 % DMSO (Sigma Aldrich), 1x PCR Reaction buffer (Thermo Fisher Scientific), 3 mM MgCl2 (Thermo Fisher Scientific) and 0.6 U Taq polymerase (Thermo Fisher Scientific), and supplemented with 1 µl

primer mix consisting of 5 µM forward and reverse primers (all from IDT). Primer sequences were as follows: *18S* F: 5'-TTC CTT GGA CCG GCG CAA G-3', R: 5'-GCC GCA TCG CCG GTC GG-3'; *AAVS1-SOX2* F: 5'-TGA GAG CCC TGC ACA TGA AG-3', R: 5'-TGT AGC TGC CAT TGG ACC AG-3'; *AAVS1-cMYC* F: 5'-TGC GGC AGA TCT CCA ACA AT-3', R: 5'-CCT TAG GGG CCT TCT CGT TG-3'; Allograft Inflammatory Factor 1 (*AIF1*) F: 5'-GCG CTT ATC CCT TCT GCT CT-3', R: 5'-TCT CTC CTC TCC CAC TTC CG-3'; *endoSOX2* F: 5'-GTA TCA GGA GTT GTC AAG GCA GAG-3', R: 5'-TCC TAG TCT TAA AGA GGC AGC AAA C-3'; *ITGAM* F: 5'-ACA CAG CAG CTT CTC TCC AC-3', R: 5'-AGT GGG CAT CTT TAT TGG GCA-3'; NES F: 5'-GGA GAA GGA CCA AGA ACT G-3', R: 5'-ACC TCC TCT GTG GCA TTC-3'; *PAX6* 5'-AAT AAC CTG CCT ATG CAA CCC-3', R: 5'-AAC TTG AAC TGG AAC TGA CAC AC-3'; *PU.1* F: 5'-TCC AGT ACC CAT CCC TGT CC-3', R: 5'-TCT TCT TGC TGC CTG TCT CC-3'; *P2RY12* F: 5'-CGA GGG GTG TAG GTA AAG TCC-3', R: 5'-GGG TTT GGC TCA GGG TGT AA-3'. QPCRs were run on a Mastercycler RealPlex^2 epGradient S (Eppendorf) in 96-well format using the following cycling conditions: 3 minutes at 95 °C; 40 cycles of 15 s at 95 °C, 20 s at 60 °C and 30 s at 72 °C; 1 minute at 95 °C and 15 s at 55 °C, followed by a temperature gradient to 95 °C over the course of 20 minutes, and finally 15 s at 95 °C before cooling down to 4 °C. QPCR products were assessed by melting curve inspection. Cycle threshold values of the genes of interest were exported to Microsoft Office Excel™, normalized to the house-keeping gene *18S,* and transformed to mean fold changes using the $2^{-\Delta\Delta Ct}$ method (Livak, K.J. & Schmittgen, T.D., 2001).

3.2.3. Immunocytochemical analyses

Cells were fixed in 4 % PFA (Sigma Aldrich) for 10 minutes at room temperature. Subsequently, cells were blocked and permeabilized with 10 % FCS and 0.5 % Triton X-100 (Sigma Aldrich) in 1xDPBS for 1 hour, except for staining of PhMiG whose blocking and permeabilization was achieved with 10 % FCS in 1xDPBS for extracellular and 10 % FCS plus 0.3 % Triton X-100 in 1xDPBS for intracellular antibody dyes. Samples were incubated with primary antibodies overnight at 4 °C in primary antibody solution composed of 5 % FCS and 0.3 % Triton X-100 in 1xDPBS. Primary antibodies included mouse anti-CD14 (2.5 µg/ml; BD Biosciences Pharmingen™), APC-conjugated mouse anti-CD45 (10 µg/ml; BD Biosciences Pharmingen™), rabbit anti-ionized calcium-binding adapter molecule 1 (IBA1; 1 µg/ml; FujiFilm), rabbit anti-PU.1 (10 µg/ml, Cell Signaling Technology), mouse anti-SOX2 (5 µg/ml; R&D Systems), mouse anti-Nestin (NES; 2.5 µg/ml; Biolegend) and chicken anti-GFP (10 µg/ml; Abcam). Following washing in 1xDPBS with 0.3 % Triton-X, specimens were incubated with the corresponding secondary antibodies, Alexa Fluor 488 anti-mouse IgG, Alexa Fluor 488 anti-rabbit IgG, Alexa Fluor 488 anti-chicken IgY, Alexa Fluor 555 anti-mouse IgM, Alexa Fluor 555 anti-rabbit IgG or Alexa Fluor 647 anti-rabbit IgG (all 1 µg/ml and all from Thermo Fischer Scientific), for 2 hours at room temperature in secondary antibody solution composed of 5 % FCS and 0.3 % Triton-X in 1xDPBS. Finally, cells' nuclei were counterstained with 2 µg/ml 4', 6' diamidino-2-phenylindole (DAPI; Sigma Aldrich) or Hoechst solution (Thermo Fischer Scientific) for 5 minutes at room temperature. Specimens were washed with 1xDPBS with 0.3 % Triton-X before imaging. Images were acquired with a Leica fluorescence

microscope DMI 6000B (Leica Microsystems) with image acquisition software LAS X Life Science Microscope Core Module, and post-processed using Image J v1.8.0_172 analysis software.

3.3. Statistical analyses

All experimental data was first tested for the requirements of linear models, *i.e.*, normal distribution and homogeneity of variances, using the Shapiro-Wilk and linear regression fit of $r^2 > 0.7$, and Brown-Forsythe tests, respectively. If these assumptions were met, parametric paired Student's t-test, parametric unpaired independent t-test with Welch's correction, one-way ANOVA, or two-way ANOVA with Tukey and Šídák's post-hoc multiple comparisons tests were performed as indicated. If these assumptions were not met, non-parametric equivalents such as the Wilcoxon matched-pairs signed rank test, the Kruskal-Wallis test with Dunn's correction or the Mann-Whitney U test were performed. Statistical significance was assumed for $p < 0.05$. All statistical analyses were performed using GraphPad Prism v9.4.1 (GraphPad software Inc.). Data are depicted as mean ± standard deviation.

4. Results and Discussion

4.1. Microglia lineage tracing

4.1.1. *ITGAM* promoter-driven EGFP expression from the human AAVS1 safe harbor locus does not efficiently label iPSdMiG

Previous data of the Institute of Reconstructive Neurobiology suggest that SeV-based overexpression of the two TFs SOX2 and cMYC converts iPSdMiG into iNSCs (Berg, L.J. *et al.*, unpublished). In this approach, iPSdMiG arise from multi-lineage embryoid bodies (EBs), which can be harvested from the supernatant of the mixed differentiation cultures with purities around 25-40 % (Figure 7A; Mathews, M. *et al*., 2022). Thus, a genetic microglia lineage reporter system, based on the expression of a fluorescent reporter gene under the control of a cell type-specific promoter, had been devised in order to exclude that iNSCs arise from the small number of non-microglial cells contained in iPSdMiG harvests. Specifically, a lineage tracing cassette that is composed of the integrin subunit alpha-M (*ITGAM*) gene promoter (ITGAMp; gene encoding the characteristic microglial marker cluster of differentiation molecule 11B (CD11b)) followed by a sequence encoding the enhanced green fluorescent protein (EGFP) was introduced into the AAVS1 safe harbor locus of human iPSCs (Figure 7B). In theory, upon differentiation into microglial cells, cells derived from this transgenic iPSC line should induce expression of EGFP upon induction of *ITGAM*, thus marking the point of differentiation when cells acquire a microglial cell identity. In the context of iNSC conversion, EGFP-positive cells should then be traced by daily imaging after infection with SeV-SOX2 and SeV-cMYC, expecting that a progressive downregulation of EGFP expression and consequent cell growth into neuroepithelial colonies could be observed in case of successful iPSdMiG-to-iNSC transdifferentiation.

To ensure that the transgenic ITGAMp-EGFP cassette had been successfully inserted into the AAVS1 safe harbor locus of iPSCs and their differentiated progeny (genome editing and subsequent differentiation were performed before the start of this thesis project), iPSCs and iPSdMiG were first genotyped using multiple primer combinations (Figure 7B) being either specific to the AAVS1 locus (Figure 7C) or the inserted transgene cassette (Figure 7D). While the transgenic iPSC line might have represented a mosaic line still containing a fraction of non-edited and/or heterozygous iPSCs, the PCR's result confirmed that the derived iPSdMiG were homozygously edited in the AAVS1 locus (Figure 7C). In addition, gDNA from both, iPSCs and iPSdMiG, contained the inserted EGFP sequence, as the expected band of 219 bp in size appeared in all tested gDNA samples as well as in the original donor pDNA, which served as positive control for the PCR. Notably, however, immunocytochemical analysis revealed that ITGAMp-EGFP-iPSdMiG did not express detectable levels of EGFP on protein level, although the microglial identity of iPSdMiG was confirmed by expression of IBA1 (Figure 7E). Thus, although an EGFP sequence could be detected by PCR amplification, EGFP was not efficiently transcribed and translated from the inserted construct, making the proposed lineage tracing system non-operational.

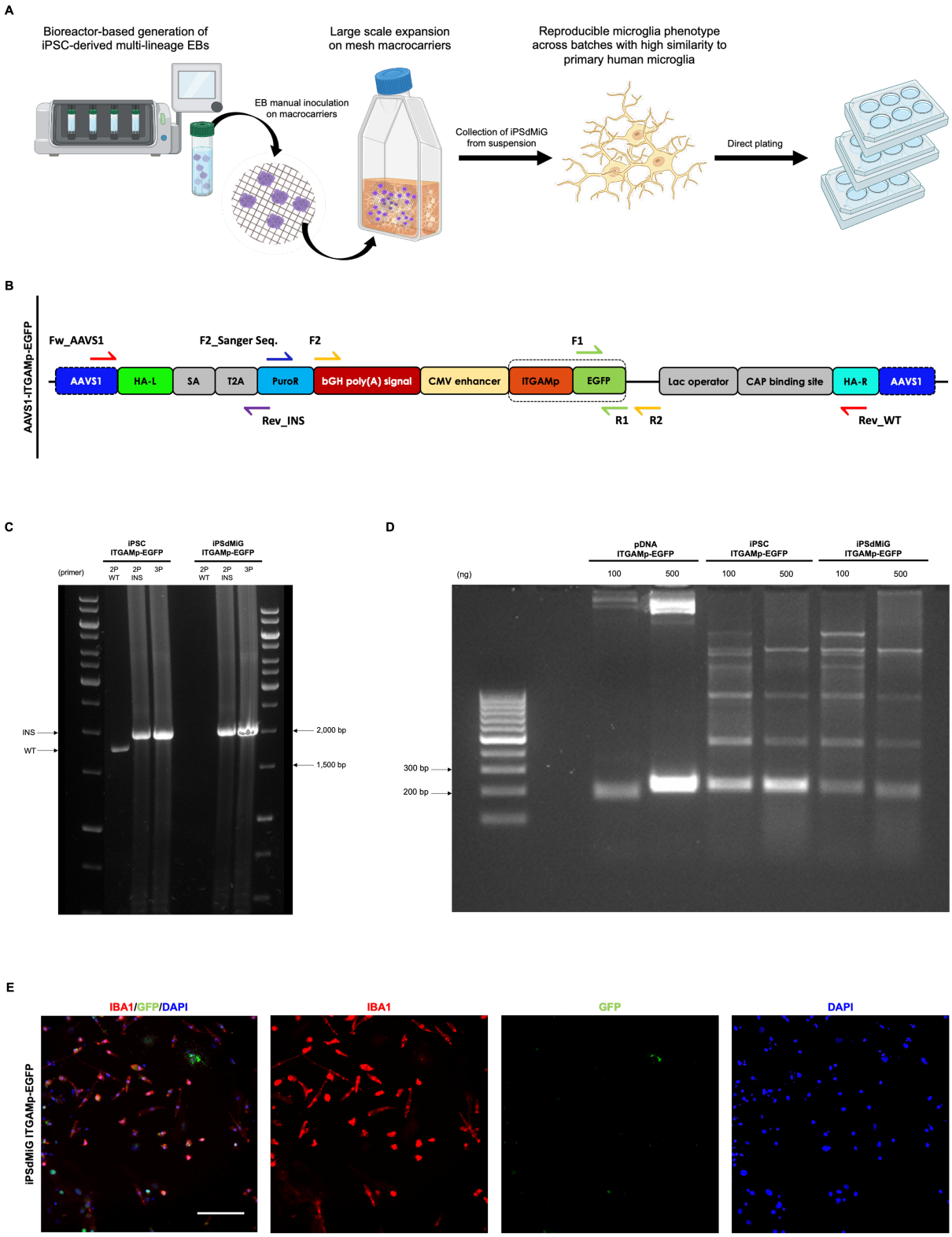

Figure 7 – Despite the successful integration of an ITGAMp-EGFP lineage tracing construct into the AAVS1 locus of a human iPSC line and the iPSdMiG derived thereof, functional GFP expression was not observed. A. Schematic illustration depicting the differentiation of iPSdMiG from iPSCs via the production of multi-lineage EBs that are subsequently propagated on mesh macrocarriers after manual inoculation. In the end of the expansion period, iPSdMiG can be harvested from the cell suspension for subsequent platting in 2D culture to be used for further experiments. Figure panel in analogy to Mathews, M. *et al.*, 2022). Graphical elements created with BioRender.com. **B.** Schematic illustration of the different PCR primers employed in the context of Figures 7 and 8 and their respective binding sites within the edited AAVS1 locus. Primers: Fw_AAVS1 (red

arrow)/Rev_INS (purple arrow)/Rev_WT (red arrow) – primers to test the absence or presence of transgenic inserts within the AAVS1 safe harbor locus in the context of Figure 7C; F1/R1 (green arrows) – amplification of EGFP sequence in the context of Figure 7D; F2/R2 (yellow arrows) – amplification of sequence of interest for subsequent Sanger sequencing in the context of Figures 8A-D; F2_Sanger Seq. (blue arrow) – primer used for Sanger sequencing in the context of Figure 8E. **C.** Gel electrophoresis of a genotyping PCR specific to the AAVS1 locus. For both cell types, iPSC and iPSdMiG, three different reactions were performed: 2P WT, containing a forward and a reverse primer for the WT AAVS1 sequence (expected band size: 1,800 bp); 2P INS, containing a forward primer for the WT sequence and a reverse primer targeting the PuroR gene of an inserted transgene cassette (expected band size: 2,040 bp); and 3P, containing the forward and reverse primers for the WT sequence as well as the reverse primer targeting the PuroR gene to evaluate the sample's zygosity. **D.** Gel electrophoresis of a PCR amplifying the transgenic EGFP sequence in ITGAMp-EGFP pDNA, ITGAMp-EGFP iPSC gDNA and ITGAMp-EGFP iPSdMiG gDNA samples. Expected band size: 219 bp. **E.** Representative immunofluorescent pictures of ITGAMp-EGFP iPSdMiG after immunocytochemical staining against the microglial marker IBA1 (red) and GFP (green). Cell nuclei were counterstained with DAPI (blue). Scale bar = 100 µm. Abbreviations: AAVS1 limiters – indicative of the start and end of the WT AAVS1 sequence; bGH poly(A) signal – bovine growth hormone polyadenylation signal; CAP binding site – Catabolite activator protein binding site; CMV enhancer – human cytomegalovirus immediate-early enhancer; HA-L – left homology arm; HA-R – right homology arm; PuroR – puromycin resistance gene; SA - splice acceptor; T2A - 2A self-cleaving peptides' element.

Thus, we next aimed at verifying that the inserted EGFP sequence was devoid of point mutations precluding the transcription of a functional mRNA, which might have occurred in the process of genome editing and would have remained uncovered by the performed genotyping PCRs. To this end, we first performed a gradient PCR using the ITGAMp-EGFP pDNA as template to ascertain which annealing temperature would be best suited to amplify the region of interest for subsequent Sanger sequencing. Annealing temperatures were varied from 55-70 ºC, since the optimal annealing temperature for the primers used (F2/R2 in Figure 7B) was predicted by NEB Tm Calculator (https://tmcalculator.neb.com; New England Biolabs) to be in-between 65-70 ºC. Interestingly, despite this prediction, all tested temperatures resulted in intense and clear bands with the expected size of ~3,090 bp using the ITGAMp-EGFP pDNA (Figure 8A).

We next performed a conventional PCR with 68.5 ºC as annealing temperature including the following samples: (i) ITGAMp-EGFP pDNA serving as a positive control for the specific construct under investigation (expected band size ~3,090 bp), (ii) iPSC ITGAMp-EGFP and iPSdMiG ITGAMp-EGFP as gDNA samples of interest, (iii) ITGAMp-EGFP construct-negative, wild-type control gDNA (iPSC WT; no band expected) and (iv) a gDNA positive control derived from a quality-controlled iPSC line overexpressing the TF NGN2 from the AAVS1 locus (iPSC NGN2; expected band size ~2,780 bp; see also Attachment 2). Following gel electrophoresis, however, only a single band of ~3,090 bp in size was detected for the pDNA sample (Figure 8B).

Considering that the PCR even failed for the gDNA positive control, we next tested whether this included gDNA might be more sensitive to the chosen annealing temperature than the original pDNA that was used for setting up the PCR system. We thus performed a gradient PCR on gDNA from the iPSC NGN2 sample, including a single genotyping-PCR reaction with a verified annealing temperature of 63.4 ºC (please see Peitz, M. *et al*., 2020 for details on NGN2 genotyping) as gDNA PCR control. This gradient PCR revealed that only annealing temperatures around and below 59.6 ºC would allow this sample's sequence of interest to be reasonably amplified (Figure 8C). In addition, the genotyping-PCR performed

at 63.4 ºC resulted in an intense and clear band with the expected size of ~2,040 bp, which confirmed the presence of a successfully homozygously inserted NGN2 sequence within the AAVS1 safe harbor locus of these iPSCs and thus, that the zygosity of the AAVS1 editing would not be the cause of the unseen expected band in the previous PCR.

Accordingly, we next performed a touchdown PCR with an annealing temperature of 56 ºC including all previously tested pDNA and gDNA samples. The result depicted in Figure 8D shows that next to the previously detected band of ~3,090 bp in the pDNA sample, gDNA samples of iPSdMiG ITGAMp-EGFP, iPSC WT and iPSC NGN2 now all displayed bands of a similar size in-between 2,500-3,000 bp (Figure 8D). Notably, although this band size was indeed expected for iPSC NGN2, the band size of iPSdMiG ITGAMp-EGFP would have been expected to be more similar to the respective pDNA sample than that of the iPSC NGN2 gDNA. Therefore, those three bands were excised from the gel. DNA was extracted from the respective gel pieces and subsequently sent to Microsynth Seqlab (Bonn, Germany) for Sanger sequencing (using the primer F2_Sanger Seq. from Figure 7B). According to the results of the Sanger sequencing (Figure 8E), only the PCR product from the ITGAMp-EGFP pDNA contained the expected transgenic sequence, while the PCR products of the two different gDNA samples did not give rise to interpretable sequencing data. Thus, it was neither possible to confirm nor to exclude the occurrence of point mutations within the transgenic ITGAMp-EGFP cell lines.

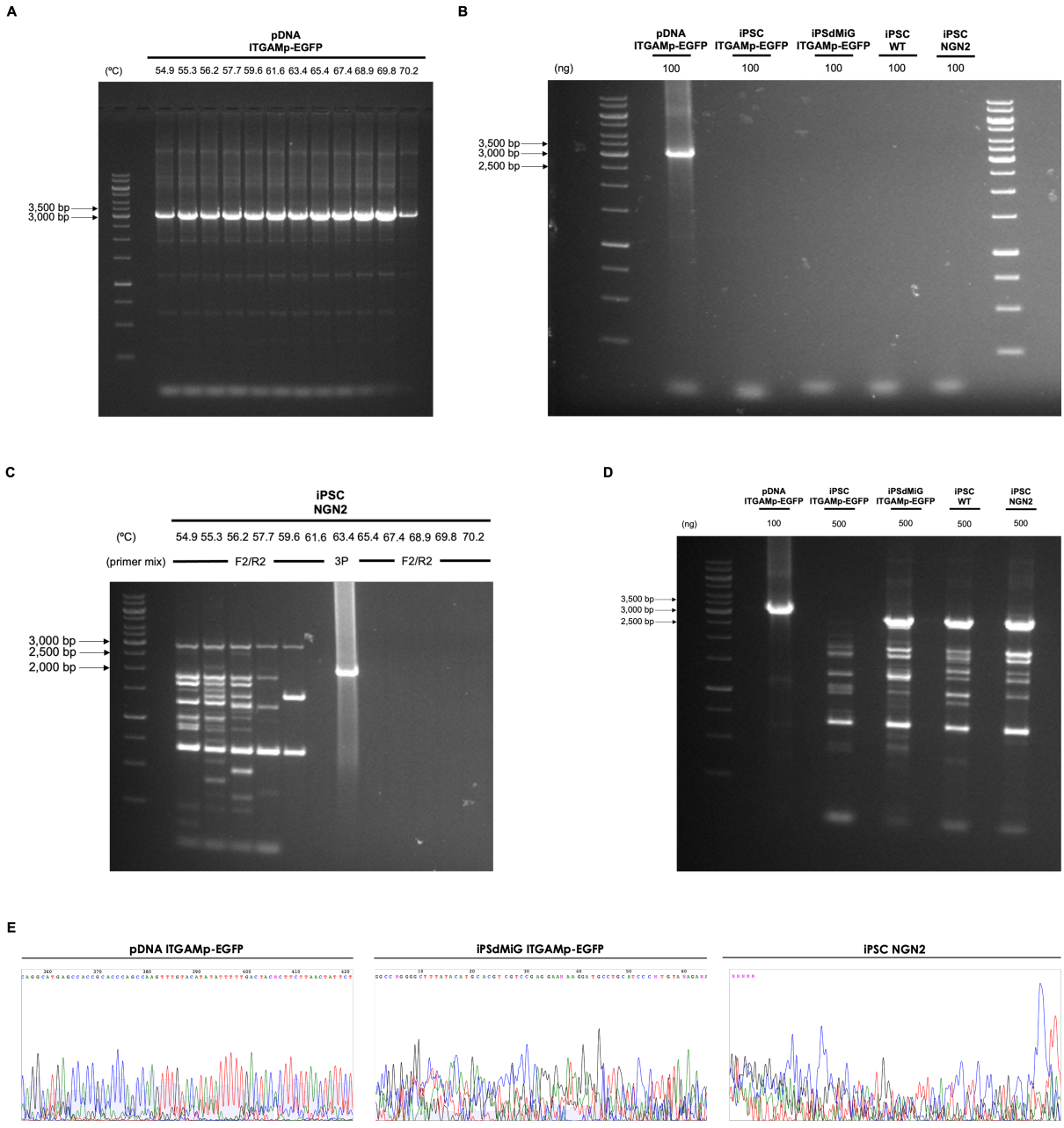

Figure 8 – Optimization of PCR conditions for amplification of the ITGAMp-EGFP construct and Sanger Sequencing analysis fail to exclude the occurrence of point mutations in iPSCs and iPSdMiG of the ITGAMp-EGFP cell line. A. Gel electrophoresis of a gradient PCR (annealing temperatures from 55-70 ºC) on ITGAMp-EGFP pDNA. Expected band size: 3,090 bp. **B.** Gel electrophoresis of a conventional PCR with 68.5 ºC annealing temperature. Expected band sizes: 3,090 bp for ITGAMp-EGFP samples, 2,776 bp for iPSC NGN2. **C.** Gel electrophoresis of a gradient PCR (annealing temperatures from 55-70 ºC) on iPSC NGN2 sample. Expected band sizes: 2,776 bp for iPSC NGN2, 2,040 bp for the presence of AAVS1-NGN2. **D.** Gel electrophoresis of a touchdown PCR with 56.0 ºC annealing temperature. For pDNA and gDNA, 100 ng and 500 ng DNA were used to perform the PCR, respectively. Expected band sizes: 3,090 bp for ITGAMp-EGFP samples, 2,776 bp for iPSC NGN2. **E.** Sanger sequencing chromatogram results of extracted gel bands from samples pDNA ITGAMp-EGFP, iPSdMiG ITGAMp-EGFP and iPSC NGN2. Samples with evenly spaced, clear peaks and unambiguous base calling represent samples with higher sequencing quality.

4.1.2. Nucleofection of iPSdMiG fails to circumvent potential differentiation-associated epigenetic silencing affecting the ITGAMp-EGFP construct

Although alternative reporter gene systems could be envisioned, for instance, based on the Cre-LoxP recombination mechanism (Branda, C.S. & Dymecki, S.M., 2004), the use of a simplistic fluorescent reporter of gene expression and its stable insertion into the AAVS1 safe harbor locus would provide three major advantages: (i) Real-time observation of reporter gene expression – Fluorophore accumulation can be directly observed in living eukaryotic cells prior to quantitative terminal analysis, which allows a reasonable approximation of the expression level of the marker of interest. Moreover, expression levels of the fluorescent protein can be easily monitored using a fluorescent microscope with relative sensitivity and accuracy or, instead, using flow cytometry that is approximately ten times more sensitive than conventional microscopy (Soboleski, M.R. *et al*., 2005). (ii) Measurement of protein expression on a cell-by-cell basis – By implementing techniques that allow us to visualize and/or measure fluorescence in individual cells, a more accurate picture of promoter activity in the whole, potentially heterogenous cell population can be generated than by employing reporter strategies that merely provide an average result of promoter activity across the entire population (Soboleski, M.R. *et al*., 2005). (iii) Security of expression – By inserting the transgenic construct within an AAVS1 safe harbor locus, the properties presented by this site are thought to enable the lineage tracing system to increase its overall effectiveness by inciting a continuous expression of the transgenic sequences. Safe harbor loci are associated with a limited disruption of endogenous genes, low proximity to oncogenes, low risk of insertional mutagenesis in the host genome and a chromatin structure that is reported to not be prone to epigenetic silencing. Furthermore, it was originally thought that within safe harbor loci, transgenic constructs remain protected from deleterious genetic effects that can preclude expression (Ogata, T. *et al*., 2003).

Importantly though, in recent years, the claim that transgene expression from safe harbor loci is robust and persistent throughout differentiation has been questioned in several publications. For instance, Bhagwan, J.R. *et al*. reported in 2020 that transgene expression from the AAVS1 locus of human iPSCs varies between individual iPSC clones, and is silenced during subsequent differentiation toward both hematopoietic cells and cardiomyocytes (Bhagwan, J.R. *et al*., 2020). Similarly, Klatt, D. *et al*. (2020) found that promoter silencing can occur in the AAVS1 safe harbor locus of human iPSC-derived myeloid cells and proposed that a comparison of different promoters driving the inserted transgenic cassettes could be necessary to achieve stable transgene expression within a specific cell type (Klatt, D. *et al*., 2020).

Altogether, these reports suggest that even in the AAVS1 locus, the inserted ITGAMp-EGFP construct might have undergone epigenetic silencing in the course of iPSC-to-iPSdMiG differentiation. One possible strategy to circumvent differentiation-associated epigenetic silencing could thus be to directly engineer the AAVS1 locus of mature iPSdMiG instead of immature iPSCs. To this end, we first set out to test whether mature iPSdMiG are principally amenable to nucleofection; a prerequisite for AAVS1

engineering. Although nucleofection of PhMiG or human iPSdMiG has not yet been reported, several recent papers have addressed nucleofection of immortalized microglia-like cell lines. Accordingly, we employed the two most efficient nucleofection programs reported to date, namely programs EN-158, which nucleofects immortalized human microglial SV40 cells with an efficiency of 75-99 % (Pajarskienė, J. *et al*., 2021), and CM-158, which yielded nucleofection efficiencies of 60-70 % in mouse BV2 (Sui, Z. *et al*., 2007) and human CHME3 cells (Malikov, V. *et al*., 2022), to nucleofect human WT iPSdMiG with a small pMAX-GFP vector control plasmid from Lonza. Phase contrast and fluorescent live cell images were captured daily (Figure 9A) until flow cytometry analysis of iPSdMiG cells was performed 2 days after nucleofection (Figure 9B). Morphologically, iPSdMiG looked way healthier and more similar to the non-nucleofected seeding control after being subjected to the CM-158 nucleofection program (Figure 9A), which was largely in line with the flow cytometry analysis, revealing that the program EN-158 tended to induce more cell death (24.03 % ± 7.97 > 17.68 % ± 5.38; Figure 9C) and yield a lower nucleofection efficiency (2.41 % ± 1.10 < 4.15 % ± 4.47; Figure 9D) than the program CM-158. However, for both programs, there was no difference in the percentage of GFP-positive cells within the living population whether or not the pMAX-GFP plasmid was added to the nucleofection cocktail, and nucleofection efficiencies overall significantly deviated from what was previously reported in literature (Figure 9D; Pajarskienė, J. *et al*., 2021, Sui, Z. *et al*., 2007, Malikov, V. *et al*., 2022).

Since the captured fluorescent live images suggested that at least for the program EN-158, GFP signal seemed indeed to be expressed but primarily in unhealthy and/or apoptotic cells (Figure 9A), we next investigated whether the application of anti-apoptotic treatments, before and after nucleofection, could rescue this program's nucleofection efficiency, preventing cell death after plasmid nucleofection. Specifically, we tested three different treatments that were reported to counteract apoptosis, namely ROCK inhibitor Y-27632 (RI), a Rho-associated protein kinase inhibitor reported to be able to markedly diminish apoptosis in marmoset iPSCs by suppressing the expression and activity of caspase 3 (Watanabe, K. *et al*., 2007), CEPT, a small-molecule cocktail (chroman 1, emricasan, polyamines, and trans-ISRIB, collectively known as CEPT) described to improve viability of PSCs by simultaneously blocking several stress mechanisms that can compromise cell structure and function (*e.g.*, replication stress or DNA damage mechanisms, stress associated with ultralow cell densities, integrated stress response and electroporation, to name a few; Chen, Y. *et al*., 2021), and Muristerone, an ecdysteroid reported to be able to prompt a strong antiapoptotic effect in human colon carcinoma cell line RKO by inhibition of Fas ligand- and TNF-related apoptosis-inducing ligand-induced apoptosis and abrogation of caspase activation (Oehme, I. *et al*., 2006), as well as in iPSdMiG in a post-freeze-thaw recovery situation (Mathews, M. *et al*., 2022). However, none of these treatments was able to significantly reduce toxicity (Figures 10A & 10B) and thus increase nucleofection efficiency in iPSdMiG (Figures 10A & 10C). This fact might be due to the existence of hardly any publications evaluating the effects of these drugs in iPSdMiG or microglial-like cells and that the effects of these drugs within the modulation of apoptosis were mainly evaluated in immortalized or PSC lines rather than in this cell type. Although in 2021, Chen, Y. *et al*. were able to state that CEPT supports cell survival after an electroporation procedure in PSCs, here today we also could confirm that the same cannot be said for microglial cells as it seems that this

and the other anti-apoptotic drugs are not able to counteract the deleterious effects of the nucleofection procedure.

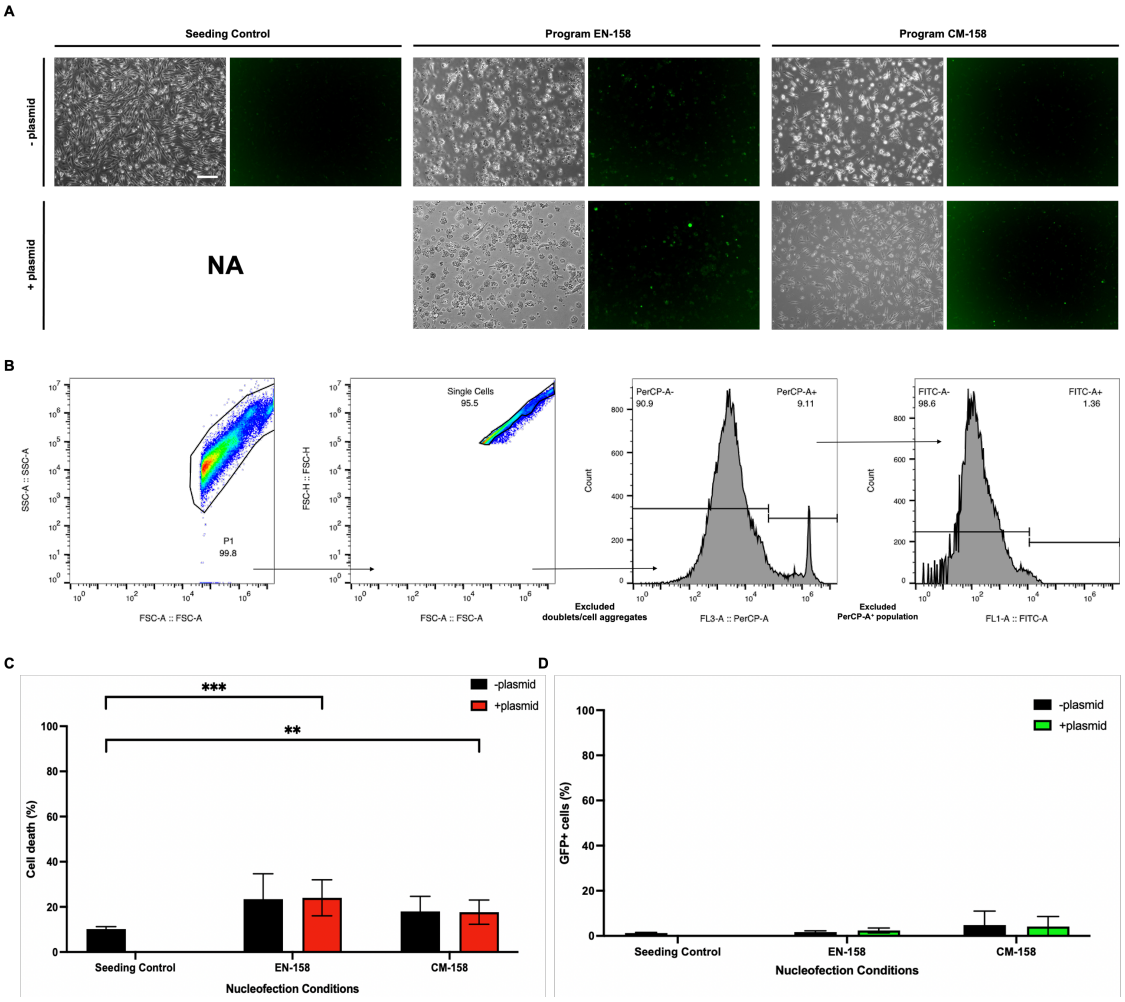

Figure 9 – Mature iPSdMiG are not amenable to plasmid nucleofection programs employed for immortalized microglia-like cell lines. A. Phase contrast and GFP channel live images of iPSdMiG in five different conditions (Seeding control, as well as programs EN-158 and CM-158, each ± pMAX-GFP plasmid). Scale bar = 100 µm. **B.** Representative workflow depicting the gating strategy during flow cytometry analysis. Doublets and/or cell aggregates were excluded from all detected events matching SSC-A and FSC-A thresholds. Afterwards, singlets were divided based on a Peridinin chlorophyll protein (PerCP) expression threshold. Only PerCP-A-negative, *i.e.*, living cells were assessed for their GFP positivity (thresholded in FITC channel). **C.** Percentage of dead cells (*i.e.*, PerCP-A-positive singlets) in each evaluated condition. N = 3 independent experiments, mean ± SD, ** $p < 0.01$, *** $p < 0.001$ as determined by two-way independent ANOVA followed by Tukey and Šídák's post-hoc multiple comparisons tests. **D.** Percentage of GFP-positive cells in each evaluated condition, representing nucleofection efficiency. N = 3 independent experiments, mean ± SD, all conditions *n.s.* as determined by two-way independent ANOVA followed by Tukey and Šídák's post-hoc multiple comparisons tests.

In fact, it appears that the treatment of cells with these drugs doesn't significantly influence in any way the cell death of iPSdMiG associated to this procedure. Furthermore, the use of a nucleofection-based program primarily designed and optimized for immortalized microglial lines in iPSdMiG can also explain this deviation from the literature, as not only it uses higher voltages than a simple electroporation technique in order to permeabilize the cells' nuclei, but it also relies on the premise that different cell

types require different nucleofection conditions, such as voltage, number of pulses, time of each pulse, amount of genetic material to be transfected, etc. Thus, it is safe to say that by recapitulating here the administration of anti-apoptotic drugs that were assessed to work mainly in immortalized or PSC lines, we took the first steps in testing their applicability within the modulation of apoptosis in iPSdMiG and within a nucleofection setting. However, further optimization is evidently additionally needed as no specific nucleofection conditions nor the way the three anti-apoptotic drugs work on iPSdMiG are currently understood.

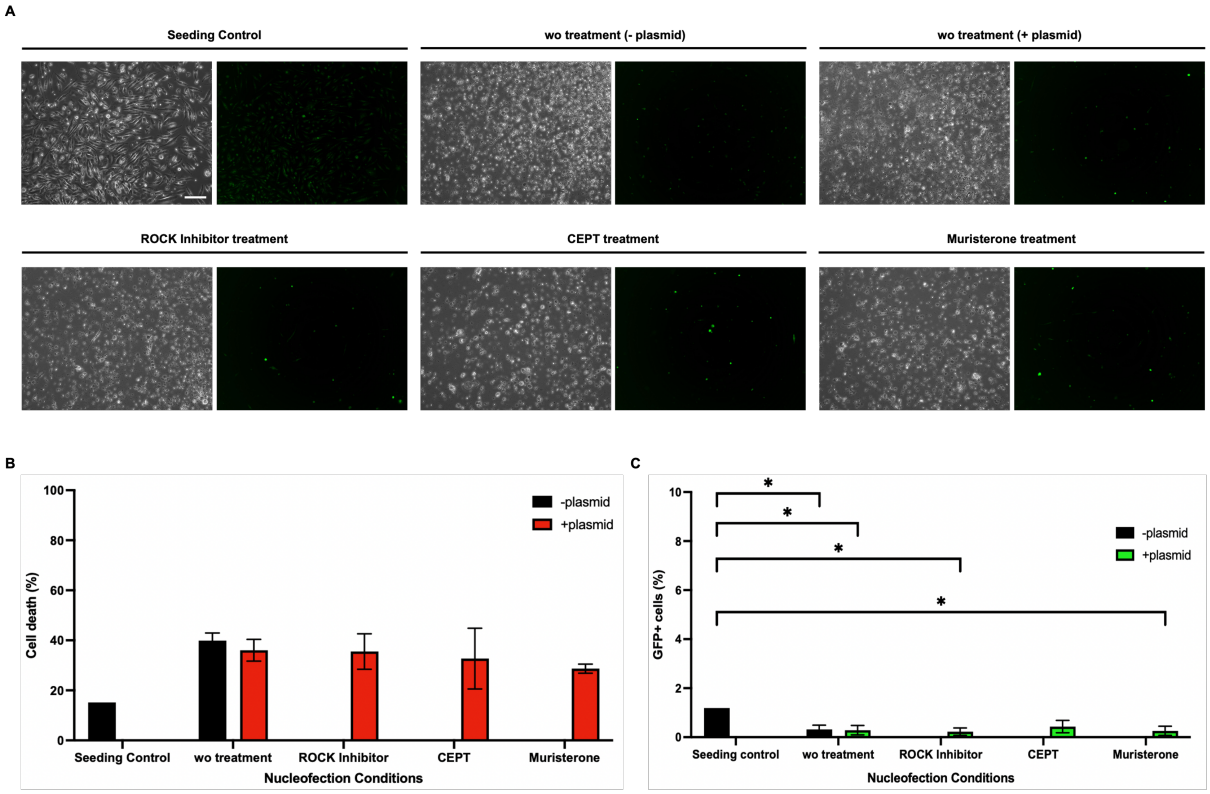

Figure 10 – Application of anti-apoptotic treatments were unable to rescue EN-158 program's nucleofection efficiency and prevent cell death after plasmid nucleofection. A. Phase contrast and GFP channel live images of iPSdMiG in six different conditions (Seeding control, wo treatment (-plasmid), wo treatment (+plasmid), with ROCK Inhibitor treatment, with CEPT treatment and with Muristerone treatment). Scale bar = 100 µm. **B.** Percentage of dead cells (*i.e.*, PerCP-A-positive singlets) in each evaluated condition. N = 3 independent experiments, mean ± S*D*, all conditions *n.s.* as determined by one-way independent ANOVA followed by Tukey's post-hoc multiple comparisons test. **C.** Percentage of GFP-positive cells in each evaluated condition, representing nucleofection efficiency. N = 3 independent experiments, mean ± S*D*, * $p < 0.05$ as determined by Kruskal-Wallis test with Dunn's correction and subsequent multiple comparisons test.

4.1.3. Lentiviral-based strategy falls short on viability for microglia lineage tracing

Since neither the differentiation of AAVS1-edited ITGAMp-EGFP-iPSCs into iPSdMiG, nor the nucleofection-based editing of mature iPSdMiG appeared to be viable strategies for microglia lineage tracing, we next designed and cloned a lentiviral plasmid expressing EGFP under the control of the *ITGAM* promoter (see Attachment 3; Figure 11A). This construct was based on two different source plasmids, namely pAAVS1-ITGAMp-EGFP to be used as a template to amplify the transgenic insert of

interest and pLenti-EF1α-core-fGFP for retrieving the lentiviral backbone. Specifically, the pLenti-EF1α-core-fGFP plasmid was enzymatically digested with PspXI and Sal1 REs, and the ITGAMp-EGFP sequence was amplified from its AAVS1 source plasmid by PCR, producing overhangs suited for subsequent Gibson Assembly with the extracted backbone (Figure 11B). The latter PCR was performed at three different annealing temperatures, specifically at 52 ºC, 54 ºC, and 56 ºC, to evaluate which one could satisfy an effective amplification of the ITGAMp-EGFP sequence. However, this amplification revealed no difference between annealing temperatures as it conveyed intense and clear gel bands from all tested temperatures (Figure 11B). Therefore, all three gel pieces were extracted and pooled together for DNA extraction. After Gibson assembly, DNA was transformed into *E. coli* bacteria for plasmid amplification. Transformed bacteria were plated on LB-agar plates supplemented with ampicillin to only allow isolated bacterial clones expressing the respective resistance gene to grow. The surviving 7 clones were manually separated, and a fraction of the bacterial suspension was then lysed to isolate pDNA. The pDNA was quality controlled by cloning PCR with 54 ºC as annealing temperature and enzymatic plasmid digestion with PspXI and Sal1 REs, revealing that the DNA of all 7 clones seemed to contain the employed backbone and ITGAMp-EGFP fragments (Figure 11C). Based on these results, 2 bacterial clones were randomly selected for further bacterial expansion, followed by isolation of highly concentrated pDNA by Maxiprep procedure. The resulting pDNA preparations were finally subjected to Sanger sequencing. Since this analysis demonstrated that only the nucleotide sequence of clone 2 was devoid of point mutations, mismatches, or deletions (Figure 11D), the pDNA of this clone was subsequently used for LV production in HEK cells (Figure 11A; performed by Lea Berg).

To assess the functionality of the newly established LV-based reporter system, WT iPSdMiG were infected with concentrated ITGAMp-EGFP LV (performed by Lea Berg). As expected, only LV-infected cells expressed GFP 6 days after infection (Figure 12A). Co-expression of CD11b, which is encoded by the endogenous ITGAM gene, and GFP, which is driven by the lentivirally inserted *ITGAM* promoter sequence, was evaluated by flow cytometry at day 6 after infection (Figure 12B). This analysis revealed that while CD11b was equally expressed in non-infected and infected iPSdMiG, 7.09 % and 26.80 % of all cells expressed GFP, respectively. However, this difference was not statistically significant. Importantly though, all GFP-expressing cells seemed to co-express CD11b. Taken together, this data suggest that the produced ITGAMp-EGFP LV specifically labels CD11b-positive microglial cells. Yet, the efficiency of lentiviral infection was comparably low in our experiment. To improve this associated efficiency, perhaps it would be advantageous to rely on additional optimized viral-based gene delivery strategies developed in recent years (as comprehensively summarized by Gouvarchin Ghaleh, H.E. *et al.*, 2020), for example, by adding intracellular shuttling enhancers, (*e.g.*, dexamethasone, that increases cytoplasmic importin-α levels to facilitate the transport of the lentiviral pre-integration complex to the nucleus) or intracellular barriers' inhibitors (*e.g.*, cyclosporine A and H that inhibit Interferon-induced transmembrane 3, an immune barrier against LV transduction present in all cells). Furthermore, the development of microfluidics in the field of gene delivery also could bring an auspicious prospect for improving efficiency of this LV-infection process as they have the potential to mimic *in vivo* environments, provide a controlled micro-scaled surrounding that improves the interaction of LVs with

target cells, and due to the limited half-life of LV particles, allow the LVs to reach their targets while still being sustained in culture media.

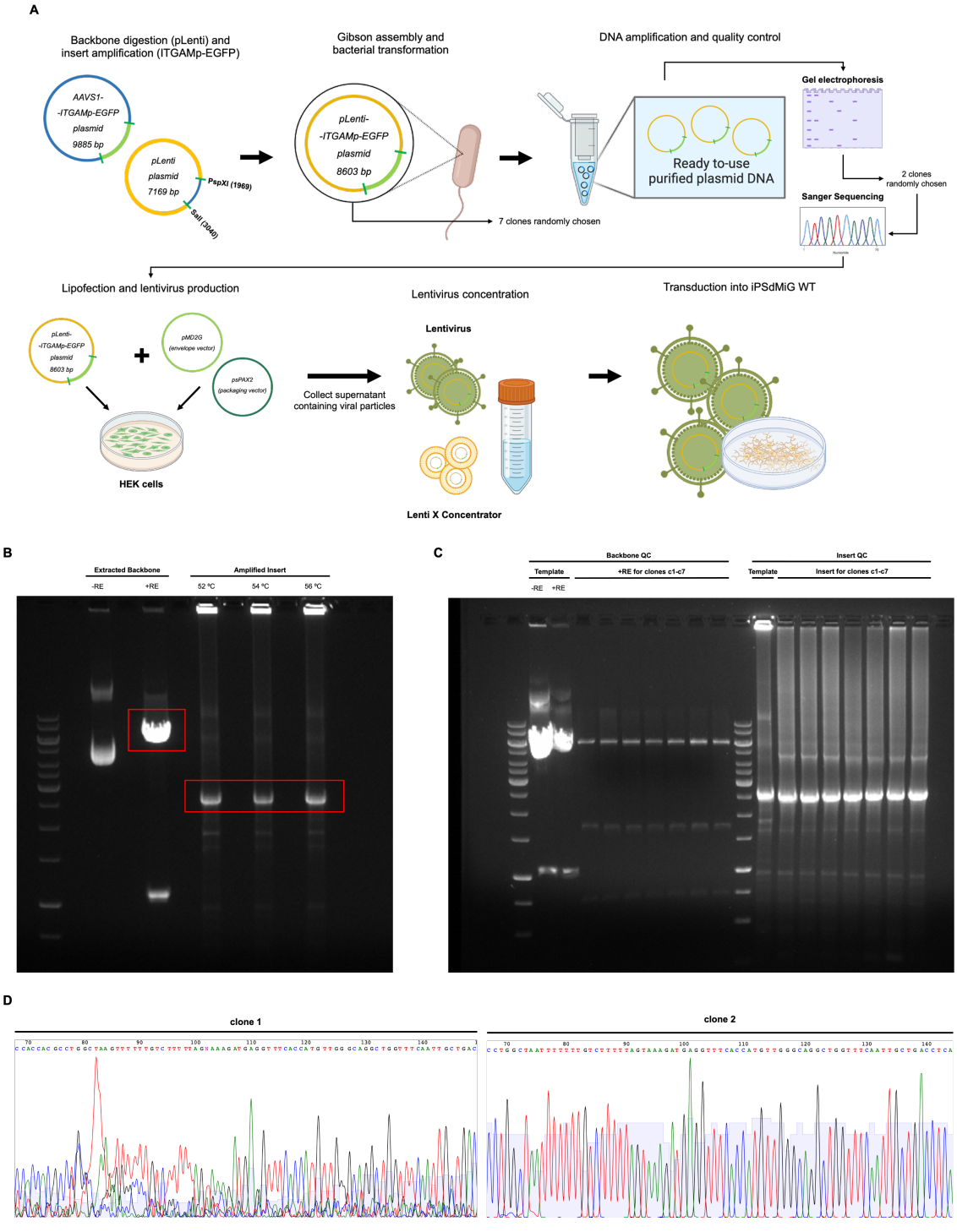

Figure 11 – Lenti-ITGAMp-EGFP lentiviruses' production reveals successful. A. Schematic illustration of the procedure followed for pLenti-ITGAMp-EGFP cloning and respective LV production. Graphical elements created with BioRender.com. **B.** Gel electrophoresis of products resulting from (i) pLenti-EF1α-core-fGFP digestion with the REs PspXI and SalI for backbone extraction and (ii) PCR amplification of the ITGAMp-EGFP sequence of interest from the source plasmid pAAVS1-ITGAMp-EGFP. For the latter, different annealing temperatures ranging from 52-56 ºC were assessed. Expected band sizes for backbone and insert were 6,094 bp and 2,510 bp, respectively. Gel bands of matching sizes (red squares) were excised from the gel for

subsequent DNA isolation. **C.** Gel electrophoresis depicting the results of the performed quality control on 7 different transformed bacterial pLenti-ITGAMp-EGFP clones. Expected band sizes for backbone and insert were 6,094 bp and 2,510 bp, respectively. **D.** Representative Sanger sequencing chromatogram of two clones that were randomly selected for Maxiprep. Sample with evenly spaced, clear peaks and unambiguous base calling represents a sample with higher sequencing quality.

Thus, and while this data seemed to emphasize a certain applicability of this system for microglia lineage tracing, given the runtime of this thesis, the explored lineage tracing approach was discarded and the reasonable plausibility of this system to be employed was not possible to be confirmed. Notwithstanding, future projects should carry on in evaluating this system's appropriateness for monitoring iPSdMiG-to-iNSC conversion as it has the potential to be a valuable genetically driven process to demonstrate, in real-time, the transdifferentiation of one cell type into another.

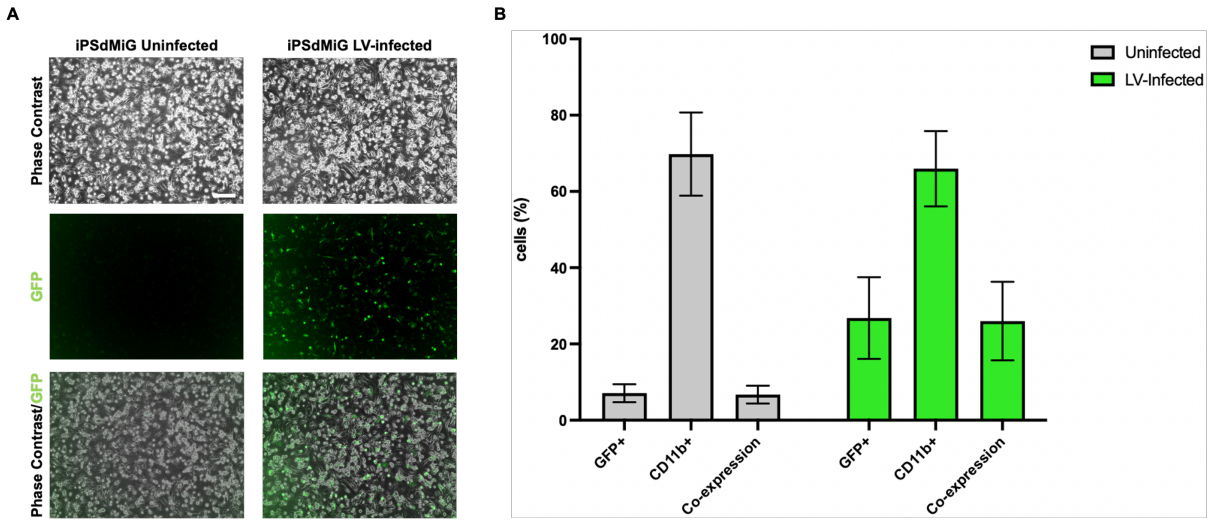

Figure 12 – GFP and CD11b expressions seem to display a positive linear correlation in LV-infected iPSdMiG. A. Phase contrast and GFP channel live images of iPSdMiG in two different conditions: Uninfected and LV-infected. Scale bar = 100 µm. **B.** Graph depicting the percentage of GFP- and/or CD11b-positive cells within the two conditions evaluated. N = 3 independent experiments, mean ± S*D*. Not significant (ns) as determined by parametric unpaired independent t-test with Welch's correction.

4.1.4. TL594-based lineage tracing system succeeds in confirming iPSdMiG-to-iNSC conversion

An alternative to the implementation of genetic lineage tracing systems represents the use of stainable markers. A major limitation of this approach, however, is that markers need to be suitable for live cell staining and imaging. Moreover, markers used for lineage tracing should be sufficiently specific to the cell type of interest and stably expressed/stained even after day-long cultivation *in vitro*. Several labels have already successfully been used for the visualization and monitoring of microglia, both *in vitro* (Leong, C. *et al*., 2014) and *in vivo* (Eme-Scolan, E. & Dando, S.J., 2020), but staining with lectin proteins that show affinity for carbohydrate groups, which play numerous roles in biological recognition phenomena and are expressed on the surface of microglia, has proven to be especially well suited for monitoring individual microglial cells and their interactions with their surrounding (Villarreal, A. *et al*.,

2021; Brawek, B. *et al*., 2019). Thus, we next set out to implement a staining strategy with a lectin protein obtained from *Lycopersicon esculentum*, which has a specific affinity for poly-N-acetyl lactosamine sugar residues that are found on the plasma membrane and in the cytoplasm of microglial cells (Villacampa, N. *et al*., 2013), for monitoring iPSdMiG-to-iNSC conversion.

To first determine the specificity and stability of this staining approach, iPSdMiG and established iNSCs were stained with TL594 (tomato lectin directly coupled to a red-emitting fluorophore; obtained from Vector Labs or Thermo Fisher Scientific) and cultured for 14 days *in vitro* with imaging of TL594 fluorescence every other day. This pre-experiment confirmed that TL594 expression in iPSdMiG was stable for roughly 7 days, and that iNSCs were not labelled by TL594 (data not shown). Considering the requirements for several medium changes within the time frame of 14 days in which iPSdMiG-to-iNSC conversion is expected to happen, a semi-continuous imaging setup based on an automated microscopy platform, the GE IN Cell Analyzer 2200 (GE Healthcare, Chicago, Illinois, USA), was chosen since it would allow daily picture acquisition in the same position of the cell culture plate. The complete experimental setup, which was based on our published iNSC conversion protocol (Sheng, C. *et al*., 2018) but adopted to iPSdMiG and the technical requirements of the IN Cell Analyzer platform, was thus as follows (Figure 13A): (i) Plating of freshly retrieved cells, harvested from the supernatant of iPSdMiG differentiation cultures, in 96-well imaging plates (*i.e.*, serving as seeding control). (ii) Purification of iPSdMiG harvests by FACS for the microglial marker CD11b. (iii) Spin infection of FACS-purified iPSdMiG ± SeVs expressing SOX2 and cMYC (+SeV condition and uninfected control, marking day 0 of conversion). (iv) Overnight culturing of the resulting infected and uninfected conditions in a small cell culture volume and surface format. (v) Replating of spin-infected cells in 96 well imaging plates at a density of 2,679 cells/cm^2. (vi) Daily imaging with IN Cell Analyzer until day 14 of conversion. Medium changes were performed every other day and TL594 staining was performed on days 2 and 7 of conversion. Notably, following this procedure, cells looked very stressed at day 2 of conversion, as they were morphologically roundish and did not adopt their characteristic ramified morphology. Moreover, already by day 4, imaging fields were mostly devoid of TL594-positive cells (Figure 13A), possibly due to cell death or loose attachment resulting in cell loss during medium changes. Thus, attempting to decrease the procedure-imposed cell stress, cells were next seeded into imaging plates right after spin infection, omitting the replating step at day 1 of conversion (Figure 13B). In addition, two imaging plate formats and three seeding densities were tested: 10,714 cells/cm^2 or 21,429 cells/cm^2 per well of a 96-well imaging plate or 64,935 cells/cm^2 per well of a 24-well imaging plate. With this procedural alteration, cells indeed appeared less roundish at day 2 in all conditions, displaying ramifications characteristic of microglia in homeostasis, and were still attached at day 4 of conversion (Figure 13B).

From day 6 of conversion onwards, we observed the formation of neuroepithelial-like colonies, which seemed characteristic for arising iNSCs (Figure 14A & 14B; for the complete timeline see Attachments 4 and 5). Notably though, comparably stable colony placement was only observed from around day 10 of conversion onwards. Single cells and smaller cell aggregates seemed highly dynamic and/or migratory before that time point, significantly impeding the identification of potential colony-founding

cells by proximity interference. Nevertheless, based on a similar morphology and closeness to the location where iNSC colonies finally grew out (black outlines), potential pairs of starting cell and arising cell aggregate were identified in images captured on consecutive days (Figure 14A & 14B, blue and green arrow and outlines).

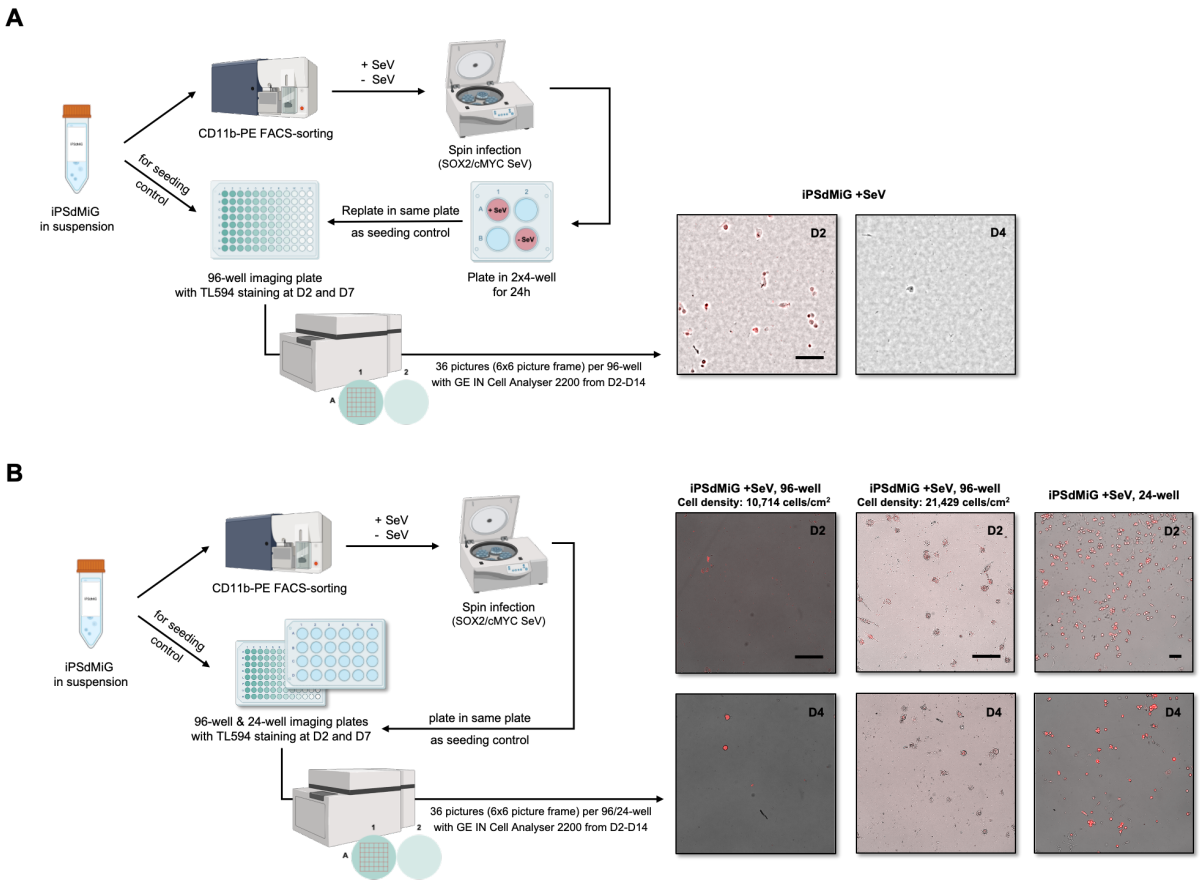

Figure 13 – Experimental strategy development for ontogeny tracing of iNSCs using a Tomato Lectin (TL594) microglial marker and IN Cell Analyzer-based semi-continuous live cell imaging. A. Schematic illustration of the original conversion and lineage tracing strategy. Representative overlay images (phase contrast and Cy3 channel) of SeV-infected and TL594-stained iPSdMiG at days 2 and 4 of conversion are presented on the right. Graphical elements created with BioRender.com. **B.** Schematic illustration of the modified conversion and lineage tracing strategy, now employing both 96-well and 24-well imaging plate formats. Representative overlay images (phase contrast and Cy3 channel) of SeV-infected and TL594-stained iPSdMiG at days 2 and 4 of conversion are again presented on the right. Graphical elements created with BioRender.com.

However, for none of these examples, the identification of colony origin was indisputable. This especially applied to conditions with higher starting densities, which increased the number of potential candidates for founding cells (*e.g.*, in 24-well format; data not shown). Thus, while immunocytochemical analysis at day 14 of conversion confirmed that colonies arising after SeV infection of iPSdMiG expressed the NSC marker SOX2 but neither TL594 nor the microglial marker IBA1 (Figure 15), semi-continuous live cell imaging yielded data that encouraged but could not ultimately manifest that TL594-positive microglia transdifferentiated into iNSCs.

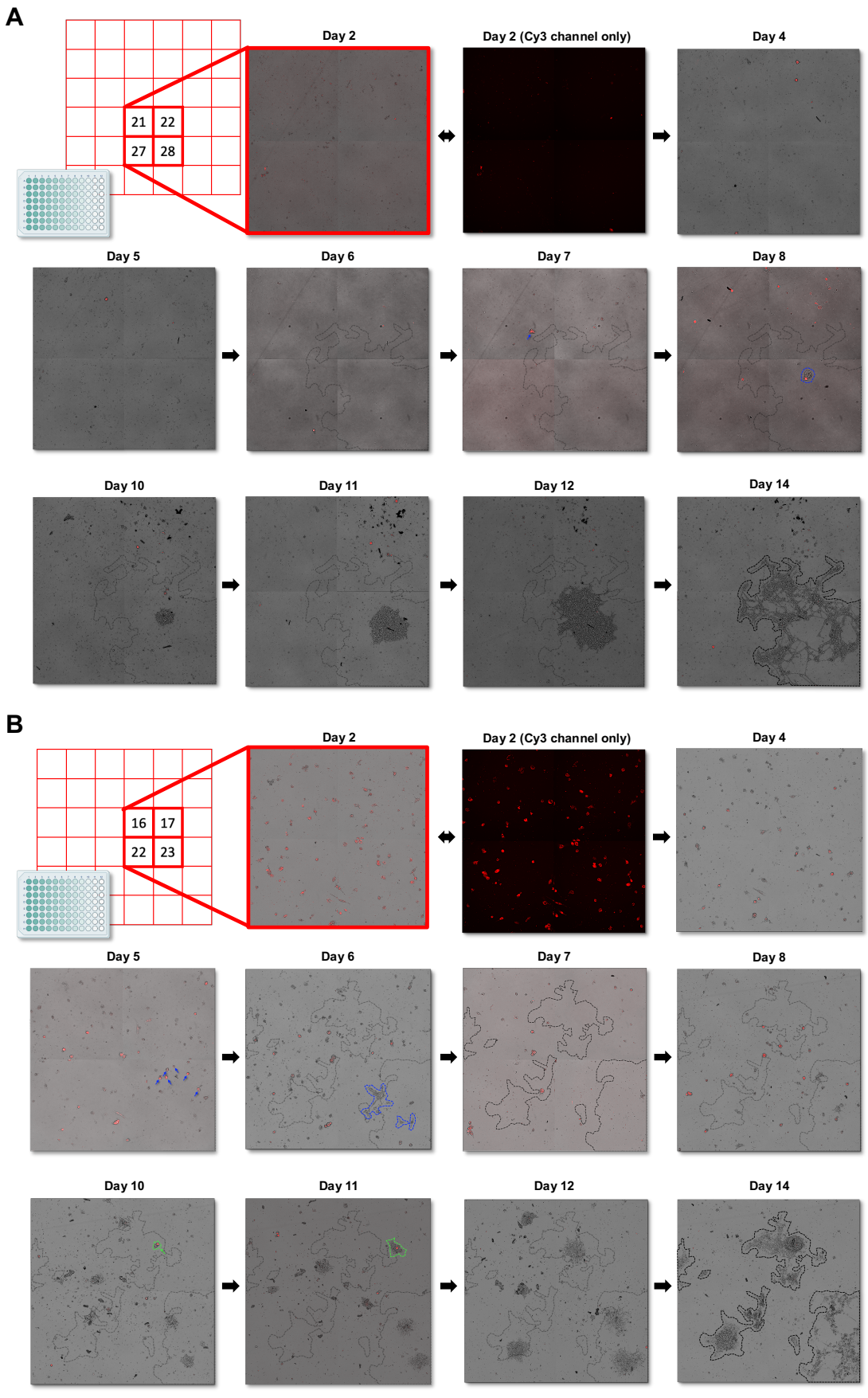

Figure 14 – Semi-continuous lineage tracing during iNSC conversion is impeded by substantial cell displacement during early stages of transdifferentiation, yet indicates that neuroepithelial-like colonies might arise from TL594-positive

iPSdMiG. A. Chronological follow-up of iPSdMiG-to-iNSC conversion in a 96-well imaging plate seeded with 10,714 cells/cm^2. Merged 2x2 tiles of phase contrast and Cy3 channel INCell pictures (composed of fields 21, 22, 27 and 28). For day 2 of conversion, the Cy3 single channel image is displayed, too. Potential TL594-positive founding cells of a colony that was observed the following day are highlighted by a blue arrow (day 7) and outline (day 8), respectively. **B.** Chronological follow-up of iPSdMiG-to-iNSC conversion in a 96-well imaging plate seeded with 21,429 cells/cm^2. Merged 2x2 tiles of phase contrast and Cy3 channel INCell pictures (composed of fields 16, 17, 22 and 23). For day 2 of conversion, the Cy3 single channel image is displayed, too. Potential TL594-positive founding cells of a colony that was observed the following day are highlighted by a blue (day 5/6) or green (day 10/11) arrow and outline, respectively. Graphical elements were created with BioRender.com.

As a consequence, future experiments should combine low starting cell densities around 10,000 iPSdMiG/cm^2 with continuous video-based, large-field live cell imaging to monitor SeV-mediated iNSC conversion using this marker-based tracing system. Despite the limitations associated with our current imaging setting, the obtained overall data encourage the assumption that TL594-stained microglia are the starting cell for iNSC conversion. Specifically, this is suggested by several examples where TL594-positive cells seemed related to subsequently arising neuroepithelial-like cell aggregates. Moreover, at least within the tiles generated from 96-well plate format, less than 5 % of all cells seem to be TL594-negative, implying that the probability of this conversion to happen is quite high, as this small percentage can be assumed within a normal associated error related to counting and a conservative threshold on the TL-594 positivity of cells.

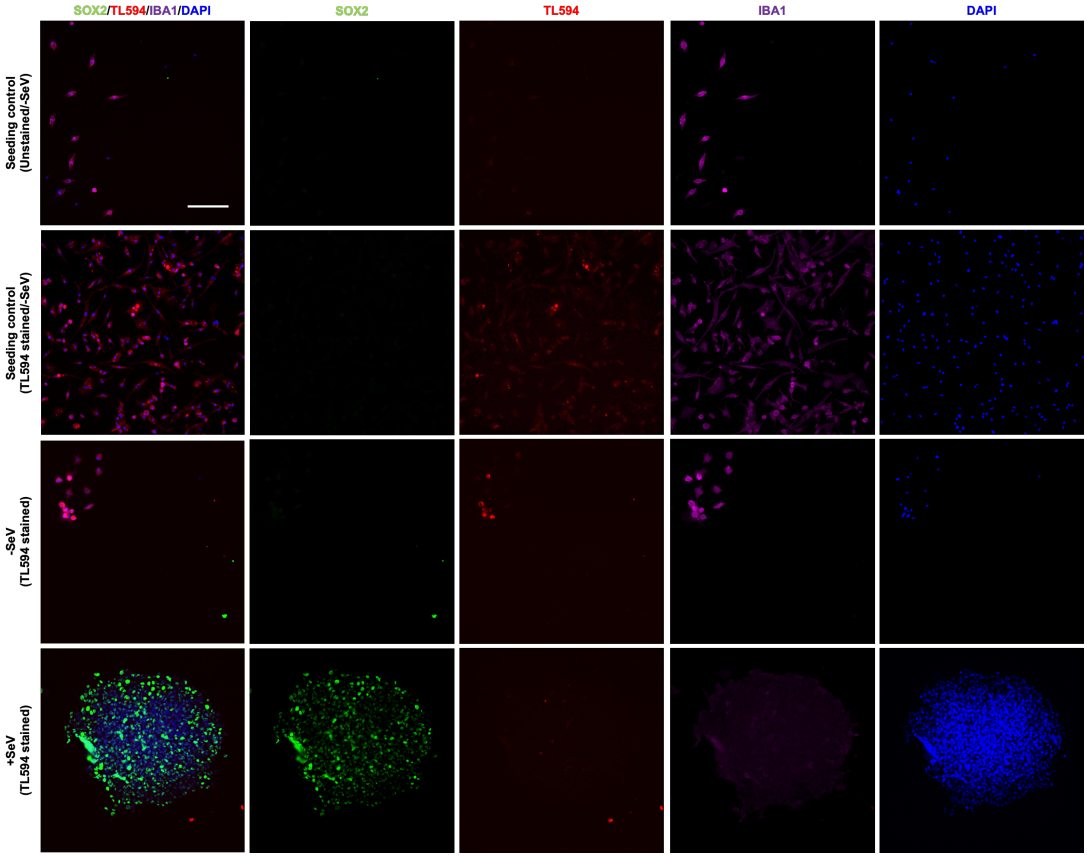

Figure 15 – Immunocytochemical analysis performed at day 14 of conversion in 24-well imaging plates-seeded cells highlights a successful iPSdMiG-to-iNSC conversion process. Analysis was performed on cells from the seeding control, uninfected (-SeV) and SeV-infected (+SeV) conditions cultured in 24-well imaging plates. Cells were stained with TL594 (red) at days 2 and 7 of the conversion process, and were finally fixed and stained for the microglial marker IBA1 (purple) and the NSC marker SOX2 (green) at day 14 of conversion. Nuclei were counterstained with DAPI (blue). Scale bar = 100 µm.

4.2. Inducible microglia conversion

Since the clinical applicability of SeVs could be limited, for instance, by their immunogenicity for patients (Gurumoorthy, N. *et al*., 2022), alternative strategies for the delivery of conversion-inducing TFs need to be explored. We specifically addressed whether genomic integration of an inducible TF expression cassette could prospectively allow us to induce iNSC conversion *in situ*, a similar strategy as the one conceived by Torper, O. *et al*. in 2013. The *in situ* conversion approach would be based on the transplantation of transgenic 'convertibles', being iPSdMiG already equipped with inducible SOX2 and cMYC transgenes and thus amenable to an *in situ* conversion upon a respective stimulus. Analogously to our original lineage tracing strategy, lab members had previously integrated a transgenic expression cassette into the AAVS1 genomic safe harbor locus of human iPSCs, allowing inducible expression of SOX2 and cMYC upon application of DOX (Figure 16A). Due to its straightforward usability and user-friendly layout, DOX-controlled operator systems represent highly attractive tools to be employed for research purposes. DOX-controlled systems are further considered to be comparably tight, precise, and safe for *in vivo* applications – since DOX is a clinically relevant drug, approved to be used in human beings, and can be easily administered to a potential patient *per os* – and, thus, appear suitable for a future pharmacological *in situ* gene induction strategy (Das, A.T. *et al*., 2016).

However, considering that our previous experiments pointed toward a potential mechanism resulting in epigenetic silencing of the AAVS1 locus upon iPSC-to-iPSdMiG differentiation, the ability of DOX to induce sufficient expression of transgenic SOX2 and cMYC in order to trigger conversion of iPSdMiG into iNSCs had to be investigated. Therefore, we first assessed transgene induction levels after two day-long DOX-treatment in all available SOX2/cMYC-transgenic iPSC clones by RT-qPCR analysis with transgene-specific primers. Notably, although *SOX2* and *cMYC* was specifically induced in the presence of DOX in all analyzed clones, expression levels varied substantially between individual clones (Figure 16B). Future experiments need to address whether the extend of variation merely resulted from the zygosity of AAVS1 editing, or whether additional mechanisms might have contributed to heterogenous transgene expression levels.

We next chose three clones with different transgene induction levels, namely c2, the clone with the highest induction of SOX2 and cMYC, c1, a clone with intermediate cMYC but comparatively low SOX2 expression levels, and c7, a clone with induction levels of SOX2 and cMYC in-between c1 and c2, for iPSdMiG differentiation. In accordance with our hypothesis of epigenetic silencing affecting transgene expression from the AAVS1 locus in human iPSdMiG, expression levels were lower in iPSdMiG after 14 days of DOX treatment than in the respective parental iPSC clone after 2 days of DOX induction (Figure 17). Nevertheless, comparing the induction levels of different clones to each other within one cell type, it seemed like the same trends could be observed in iPSCs and iPSdMiG. Interestingly, and although the presence of DOX was proven to induce transgene expression of SOX2 and cMYC also in the case of iPSdMiG, the use of different DOX concentrations in this experiment revealed that despite the

increase in DOX, the effect of this change would not necessarily mean a higher induction of these TFs (Figure 17).

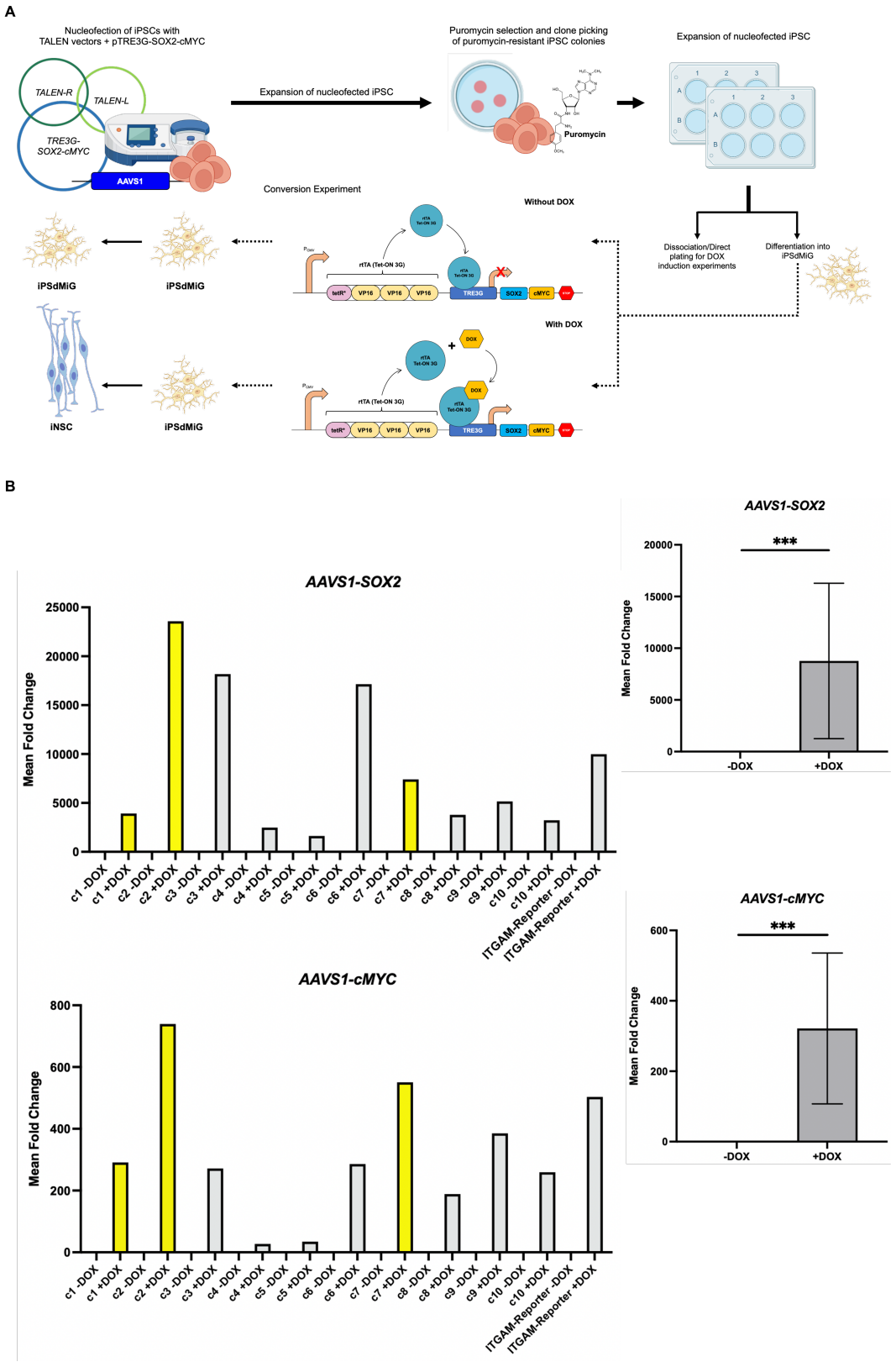

Figure 16 – Although expression of transgenic *SOX2* and *cMYC* is induced in the presence of DOX, transgene induction levels after DOX-treatment are different depending on the individual iPSC clone analyzed. A. Schematic illustration of the

experimental strategy for the creation and application of a DOX-inducible iPSdMiG-to-iNSC conversion system. Transgenic single colony-derived iPSC lines were previously derived by institute members by TALEN-mediated insertion of a Tet-ON 3G (TRE3G)-SOX2-cMYC expression cassette, additionally harboring a puromycin resistance gene, into the AAVS1 safe harbor locus. IPSC clones as well as iPSdMiG derived from a selection of clones were employed for assessing transgene inducibility upon DOX treatment. DOX binds to the reverse tetracycline-controlled transactivator protein allowing binding to and subsequent activation of the TRE3G element, which in turn drives expression of the downstream positioned TFs SOX2 and cMYC. Overexpression of SOX2 and cMYC in iPSdMiG is expected to drive transdifferentiation toward iNSC identity. Graphical elements created with BioRender.com. **B.** Expression of the transgenic TFs SOX2 and cMYC was evaluated by RT-qPCR in iPSCs after 2 day-long culture in the presence or absence of 2.0 µg/ml DOX. Left side of each graph: N = 1 per clone. For statistical analysis, data of all clones were pooled (right side of each graph): Mean ± SD, *** $p < 0.001$ as determined by Wilcoxon matched-pairs signed rank test for AAVS1-SOX2 and paired t-test for cMYC. Clones marked in yellow were chosen for further experiments.

In fact, it seemed to indicate that transgene expression using this inducible system might display a threshold response, perhaps dependent on the abundance of the transactivator protein (seen in Figure 16A), given that with high concentrations of this drug, iPSdMiG SOX2 and cMYC mean fold change would remain roughly unaltered in certain situations. Thus, this potential dependence of induced gene expression on the cellular abundance of this transgenic transactivator might provide important evidence to help understand the necessary requirements for a successful conversion process. However, future experiments need to address whether this hypothesis is true and if by changing the concentration of this protein, DOX-inducible transgene induction can achieve higher expression levels with the same DOX concentration.

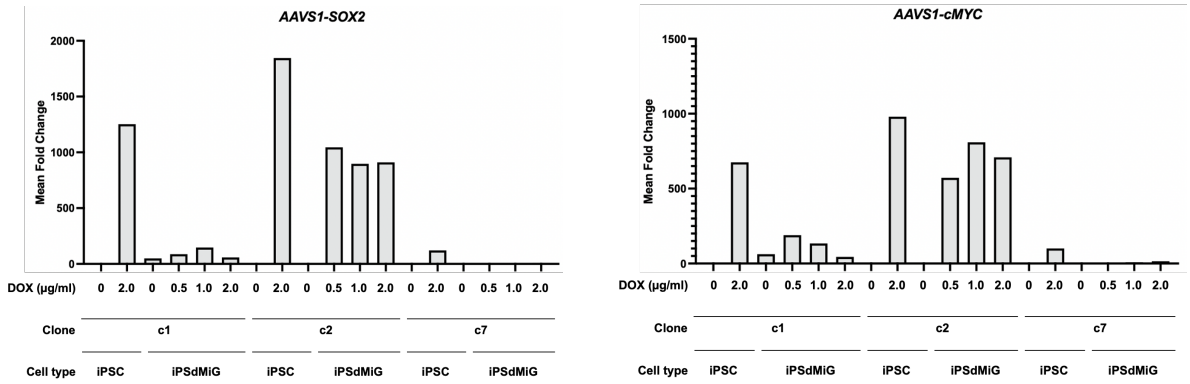

Figure 17 – DOX treatment enables a higher induction level of SOX2 and cMYC in iPSCs than in the differentiated progeny (iPSdMiG). Expression of the transgenic TFs SOX2 and cMYC was evaluated by RT-qPCR in the presence or absence of varying concentrations of DOX in iPSCs and iPSdMiG of the clones c1, c2 and c7. N=1.

Based on the *SOX2* and *cMYC* expression levels in iPSdMiG, clones c2 and c7 were chosen for further characterization. To this end, iPSdMiG from both clones were cultured in the presence or absence of DOX for 14 days in iNSC conversion medium. On day 13 of conversion, cultures were dissociated, and a fraction of the cells was re-plated in imaging plates for subsequent fixation and immunocytochemical staining, whilst remaining cells were pelleted for RNA extraction, followed by cDNA synthesis and RT-qPCR analysis for microglial and NSC markers. The latter analysis revealed that the expression of all four assessed microglial marker genes, namely *ITGAM*, *AIF1*, *PU.1* and *P2RY12*, tended to decrease upon DOX application, a trend that reached statistical significance for the markers *ITGAM* and *PU.1*

(Figure 18A). Interestingly though, NSC makers such as *endoSOX2*, *NES* and *PAX6* failed to be induced by DOX addition, and expression levels were very different from NSC marker expression in iPSdMiG-derived iNSCs converted by SeV-mediated overexpression of SOX2 and cMYC (Figure 18B).

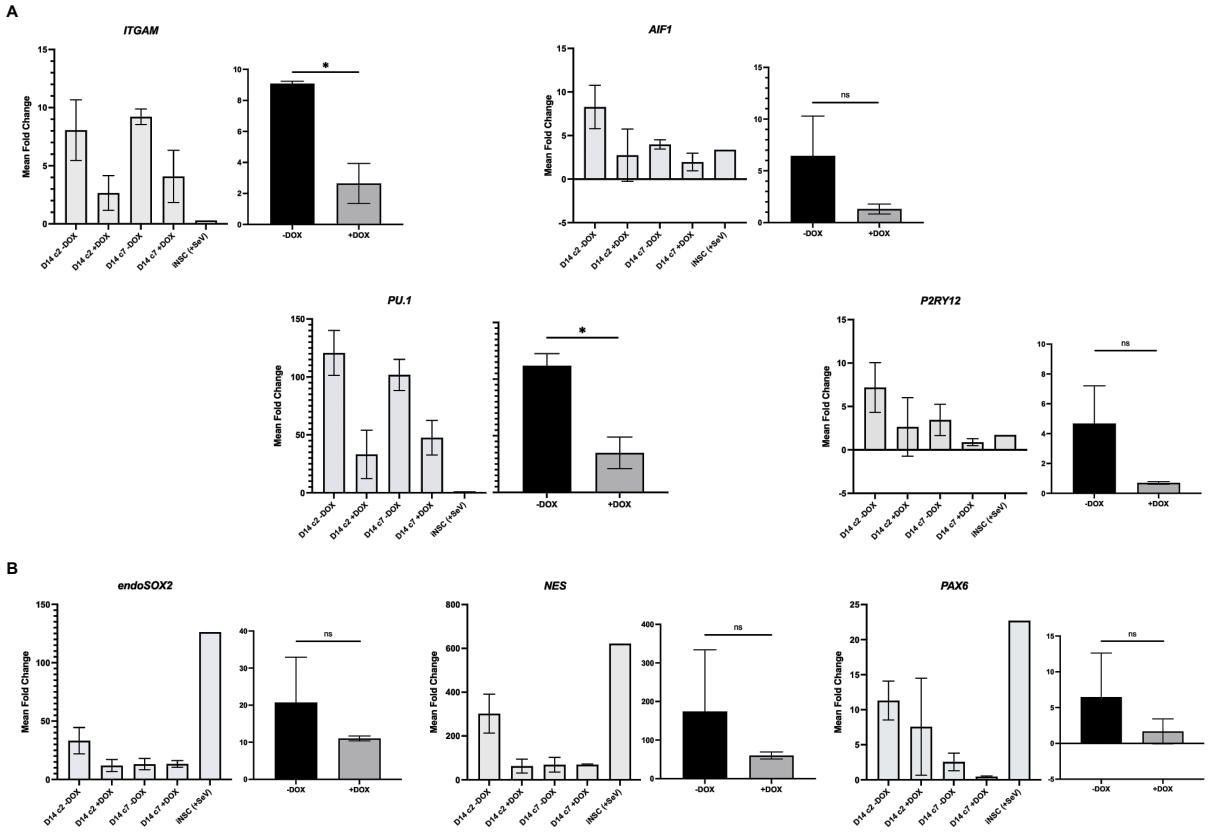

Figure 18 – RT-qPCR analysis for microglial and NSC markers reveals failure of DOX in inducing iPSdMiG-to-iNSC conversion in iPSdMiG clones c2 and c7. Expression of microglial (**A**) and NSC markers (**B**) was evaluated by RT-qPCR after 14 day-long cultivation of iPSdMiG derived from SOX2/cMYC-transgenic iPSC clones c2 and c7 in the presence or absence of DOX. RNA of established iPSdMiG-derived iNSCs converted via SeV-mediated overexpression of SOX2 and cMYC (iNSC (+SeV)) was used as positive control for iNSC conversion. Left side of each graph: N = 3 independent experiments per clone, mean ± *SD*. For statistical analysis, data of both clones were pooled (right side of each graph): Mean ± *SD*. * $p < 0.05$ as determined by a non-paired, non-parametric Mann-Whitney U test.

While DOX-induced cultures seemed to contain neuroepithelial-like colonies prior to dissociation (Figure 19A), immunocytochemical staining post replating confirmed that DOX-induced cultures still contained PU.1- and IBA1-expressing microglia-like cells, and were largely devoid of NES- or even SOX2-expressing NSC-like cells (Figure 19B; for more information about the cell markers used, please see Attachment 6). Altogether, these results indicate that although DOX-mediated overexpression of SOX2 and cMYC might have been able to initiate the process of conversion by enabling the decrease in expression of microglial genetic hallmarks, the expression of these two TFs was not enough to effectively manipulate the expression levels of iNSC lineage-instructing TFs and endogenous phenotype-provider markers, and thus, to distinctly transdifferentiate *in vitro* cultured microglia to *bona fide* iNSCs through this DOX-inducible ectopic transgene expression system.

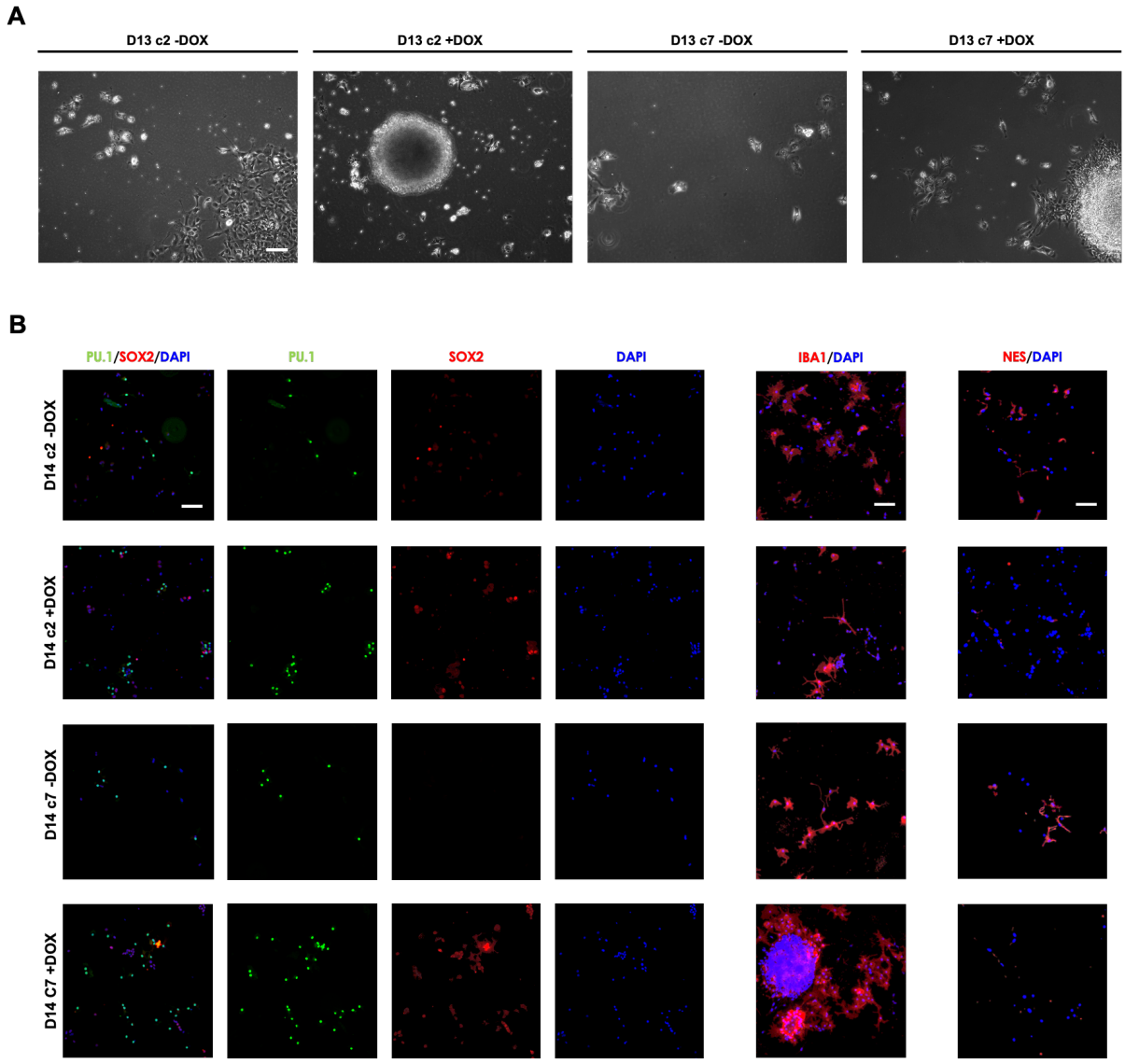

Figure 19 – Despite the presence of neuroepithelial-like colonies prior to dissociation, immunocytochemical staining post replating demonstrated that DOX-induced cultures still contained microglia-like cells and were largely devoid of NSC-like cells. **A.** Phase contrast pictures of day 13 cultures, prior to dissociation, of iPSdMiG SOX2/cMYC clone c2 and c7, in conditions without DOX (-DOX; 0 µg/ml) or with DOX (+DOX; 1.0 µg/ml). Scale bar = 100 µm. **B.** Cells were stained for specific microglial (PU.1 and IBA1) and NSC markers (SOX2 and NES). Nuclei were stained with DAPI. Scale bars = 100 µm.

The inability of this approach to work might have been due to the induction level of SOX2 and cMYC not be able to perhaps reach a given value or threshold inclined for the full conversion of cells into iNSCs, possibly owing to the DOX concentrations used. In addition, also the observance of neuroepithelial-like colonies at day 13 but not during immunocytochemical analysis at day 14, might suggest that cells may have been lost or died during this re-seeding step, which should be accounted on a future experiment. However, a more plausible explanation might be given by the potential AAVS1 locus epigenetic silencing mechanism that might be affecting this transgenic construct in iPSdMiG. As a future prospective, one can perhaps rely on other gene editing tools and use for instance, a piggyBac-like system to insert the DOX-inducible SOX2/cMYC expression construct in a random, but less epigenetically influenced region of the genome. Furthermore, and given the difficulty in understanding the required levels of SOX2 and

cMYC induction for *bona fide* conversion, other inducible genetic systems can perhaps also be explored such as a Cre/loxP recombinase system (Branda, C.S. & Dymecki, S.M., 2004). This system could be composed of a construct with a loxP-flanked stop codon that is followed by a constitutive promoter driving the expression of SOX2 and cMYC, and in which transgene expression under non-induced conditions would render this system to be always off and upon addition of Cre recombinase to the cell culture medium, to excise the stop codon and express both iPSdMiG-to-iNSC conversion-inducing transgenes. The major advantage of using a system like this would be perhaps the straight-forward ability of an enzyme to turn on the continuous expression of SOX2 and cMYC without necessarily depending on the concentration of a given substrate to do so.

4.3. Toward primary microglia conversion

Next to the inducible *in situ* conversion of 'convertibles', *in vivo* conversion of brain-resident, PhMiG represents an attractive route toward clinical application. The first step towards this goal would be to achieve TF-mediated PhMiG-to-iNSC conversion *ex vivo*. A prerequisite would thus be the ability to efficiently isolate PhMiG from human brain tissue and to subsequently culture PhMiG *ex vivo* for a restricted time period. Although different protocols were published for the isolation of PhMiG, for example, from human immunodeficiency virus-infected patients' brains (Dick, A.D. *et al*., 1997), or *post mortem* human brain tissue (Mizee, M.R. *et al*., 2017), we here explored the use of an isolation protocol that is based on the 'Adult Brain Dissociation Kit, mouse and rat' kit from Miltenyi Biotec™ and had been implemented and kindly shared by the laboratory of Dr. Annette Halle (German center for neurodegenerative diseases, Bonn). By resorting to a commercial isolation kit, we expected to achieve a higher degree of standardization and, thus, more reliable, and reproducible results.

Therefore, human brain tissue was obtained from the neurosurgical department of the University Hospital Bonn, being donated by an epileptic patient undergoing neurosurgical resection, and processed using Miltenyi's 'Adult Brain Dissociation Kit, mouse and rat' kit. The resulting cell suspension was then FACSed for the microglial marker CD11b, yielding ~145,000 sorted events, which equaled to ~80,000 manually counted CD11b-positive cells (Figure 20A). Future experiments need to consolidate how this isolation efficiency relates to that of published protocols yielding around 450,000 and 145,000 CD11b-positive viable cells per gram of white and gray matter tissue, respectively (Mizee, M.R. *et al*., 2017), and whether the yield of our protocol can be increased, for instance, by limiting the amount of tissue input to a single grinding falcon tube.

After FACS, CD11b-positive cells were seeded in 96-well imaging plates and cultured for 7 days in PhMiG medium. On day 7 of *ex vivo* culture, iPSdMiG were seeded by Vanessa Frickel as controls for subsequent immunocytochemical analysis. Staining for the hematopoietic lineage and/or microglial markers CD14, CD45, IBA1 and PU.1 (for more information about the cell markers used, please see Attachment 6) revealed that isolated cells seemed to exhibit comparable expression of CD14, CD45 and PU.1 to iPSdMiG, while expression levels of IBA1 appeared to be lower in PhMiG than iPSdMiG (Figure

20B). Expression of the NSC markers SOX2 and NES was neither detected in iPSdMiG, nor PhMiG (data not shown). Altogether, these data preliminarily indicate that microglial cells were successfully isolated by the protocol employed, and viable even after 7 days of *ex vivo* culture, with no detectable contamination of NSCs. Since this experiment could not be repeated in the runtime of this thesis due to strike-dependent personnel shortage for elective surgeries, future projects will need to demonstrate data reproducibility and investigate, whether isolated PhMiG are amenable to SeV-mediated iNSC conversion *ex vivo*.

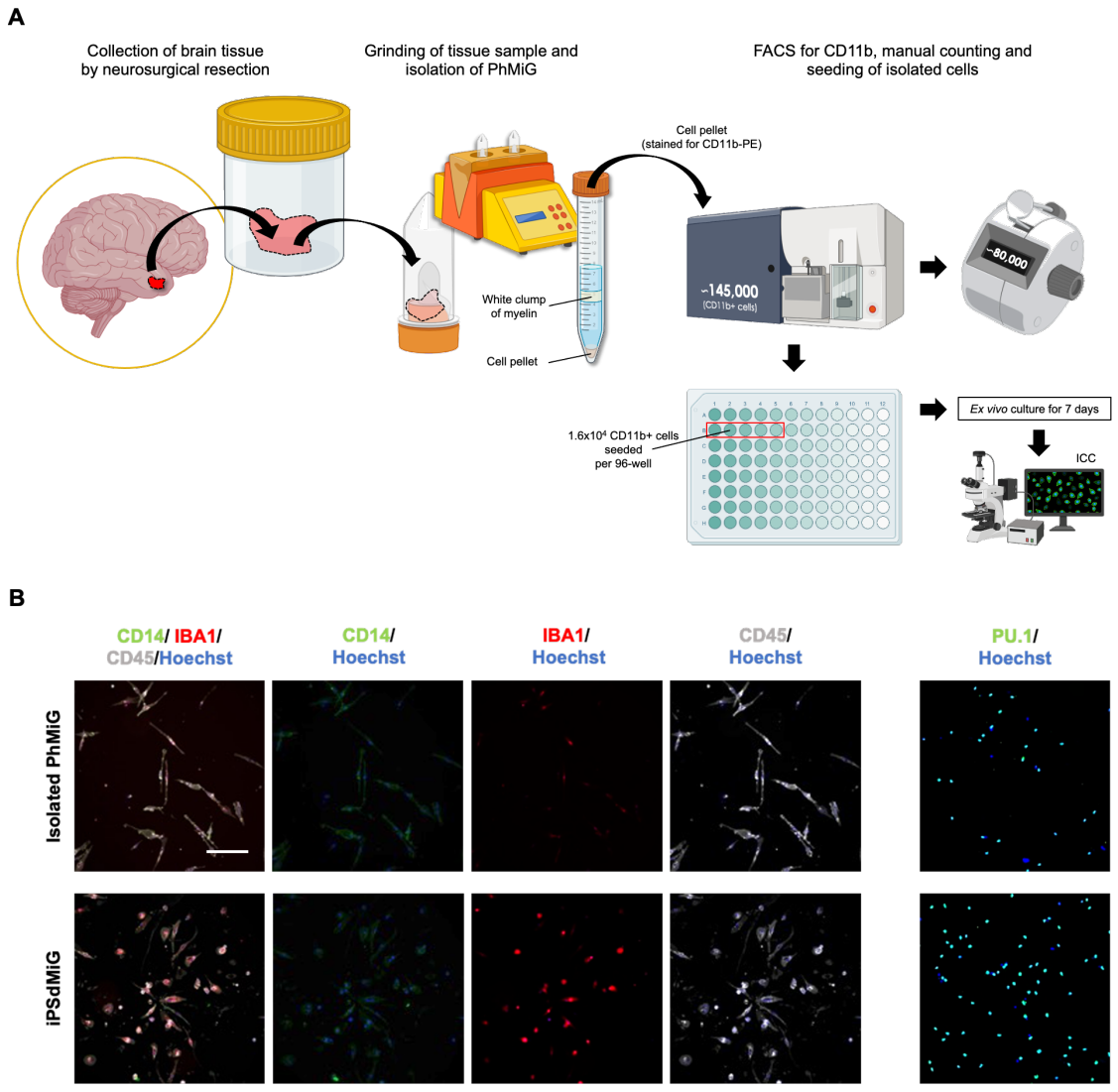

Figure 20 – Protocol devised for the isolation of primary mouse microglia suggests a successful isolation of CD11b-positive primary human microglia from a human brain tissue sample. A. Schematic illustration of the protocol employed for the isolation of PhMiG from a human brain tissue sample, which was donated by an epileptic patient undergoing neurosurgical resection at the neurosurgical department of the University Hospital Bonn. The brain tissue sample was dissociated and digested using the 'Adult Brain Dissociation Kit, mouse and rat' kit from Miltenyi Biotec™. Cells were prepared according to a protocol adapted by the group of Dr. Annette Halle, removing myelin, cell debris and erythrocytes. Subsequently, FACS was employed to derive a single cell suspension of CD11b-positive microglial cells, which were manually counted and then seeded in 96-well imaging plates for a 7 day-long *ex vivo* cultivation. Graphical elements were created with BioRender.com. **B.** Immunocytochemical analysis performed 7 days post seeding on isolated PhMiG and iPSdMiG. Cells were stained for the markers CD14, CD45, IBA1 and PU.1, and nuclei were counterstained with Hoechst. Scale bar = 100 µm.

5. Conclusion

In this project, we aimed to address different prerequisites to make microglia-to-iNSC fate conversion prospectively translatable to the clinics. First, we set out to faithfully trace the ontogeny of converted iNSCs across time by lineage tracing. We found that it was not possible to employ an AAVS1-targeting, ITGAM promoter-driven, EGFP-based genetic lineage tracing system, as although an EGFP sequence could be detected by PCR amplification, EGFP was not being efficiently transcribed and translated from the inserted construct. Yet, we successfully re-cloned this construct for lentiviral delivery, which should be further evaluated in the context of lineage tracing by infection of iPSdMiG and consequent induction of SeV-mediated conversion into iNSCs in a near future, as its appropriateness was emphasized by a potential positive correlation between GFP and CD11b expressions, despite the non-significant trend observed. In addition, TL594 marker-based cell tracking was explored, revealing a potential identification of iPSdMiG as founding cells of conversion-resulting iNSC colonies and demonstrating that iPSdMiG seem to start to be converted into iNSC-like cells from day 6 of conversion onwards. Although quite promising, follow-up experiments should still be performed to further optimize this system and to unequivocally demonstrate that iNSC colonies indeed arise from *ITGAM*/CD11b-expressing and/or TL594-positive microglial cells by continuously following them throughout the 14 days of conversion, now using a live cell imaging-based tracking system for that purpose.

Second, we investigated the feasibility to translate the currently employed SeV-mediated, SOX2- and cMYC-based conversion system to a DOX-inducible transgenic model, which would prospectively allow a timed conversion of SOX2/cMYC-equipped microglia into iNSCs *in situ*. Notably, we found that levels of transgenic SOX2 and cMYC induction substantially differed between iPSC clones as well as between cell types, namely in undifferentiated iPSCs and mature iPSdMiG. However, attempts to convert iPSdMiG by DOX addition similarly failed for two different clonal backgrounds, exhibiting comparably high and low induction levels. Specifically, iPSdMiG clones c2 and c7, in the presence of DOX, showed a significant decreased tendency in induction levels of specific microglial markers, but NSC makers were observed to have failed to be induced at all by the same drug. The inexistence of NSC-like cells was also then confirmed by immunocytochemical analysis that highlighted that this DOX system did not properly work out. Future studies should evaluate even further the applicability of this DOX-inducible system. However, if it proves ineffective in converting iPSdMiG into iNSCs, other genetic inducible systems can also be explored such as the widely used Cre/loxP recombinase system. On the other hand, if the current limitations are able to be surpassed, we should expect to reproducibly observe this transdifferentiation, and to further characterize the resultant cells for their tripotent differentiation capacity (into astrocytes, oligodendrocytes, and neurons). In addition, we should also expect to be able to proceed with transplanting SOX2/cMYC-engineered iPSdMiG into the CNS of adult immunodeficient mice, aiming at converting the transplanted iPSdMiG into iNSCs *in situ* via DOX application to the recipient's drinking water, and later evaluate within the brain tissue, the distribution and cellular phenotype of those grafted cells.

Third, we performed a preliminary experiment toward the principal possibility to convert PhMiG into iNSCs *in vivo*, in which we successfully isolated and *ex vivo*-cultivated microglial marker-expressing cells from human primary brain tissue. Although we were not yet able to test the amenability of the isolated PhMiG for iNSC conversion and compare it with the amenability of iPSdMiG, we believe that pursuing this route could hold great promises for future clinical translation. Given the increasing prevalence of human brain degeneration-related diseases, the need for viable therapeutics that cannot only resolve inflammation caused by degeneration of neuronal cells but also repopulate degenerated brain areas is undeniable. This research project thus set out to advance potentially suited technologies such as direct cell fate conversion toward translation, hoping that one day, they could revolutionize regenerative medicine.

6. References

A. D. International. Dementia statistics | Alzheimer's Disease International (ADI). (2020). [Online]. Available at: https://www.alzint.org/about/dementia-facts-figures/dementia-statistics/. Consulted on December 31st, 2021.

Adler, A. F., *et al.* Nonviral direct conversion of primary mouse embryonic fibroblasts to neuronal cells. (2012). *Mol. Ther. Nucleic Acids*, vol. 1, no. 7, pp. 1-10, doi: 10.1038/mtna.2012.25.

Adams, K. L., & Gallo, V. The diversity and disparity of the glial scar. (2018). *Nat. Neurosci.*, vol. 21, no. 1, pp. 9-15, doi: 10.1038/s41593-017-0033-9.

Albert, K., *et al.* Utilising induced pluripotent stem cells in neurodegenerative disease research: Focus on glia. (2021). *Int. J. Mol. Sci.*, vol. 22, no. 9, pp. 1-28, doi: 10.3390/ijms22094334.

Alzheimer's disease facts and figures, Alzheimers Dement. (2021). 2021 Alzheimer's disease facts and figures. *Alzheimers Dement*, no. 17, pp. 327-406. doi: 10.1002/alz.12328.

Ambasudhan, R., *et al.* Direct reprogramming of adult human fibroblasts to functional neurons under defined conditions. (2011). *Cell Stem Cell*, vol. 9, no. 2, pp. 113-118, doi: 10.1016/j.stem.2011.07.002.

Arvidsson, A., *et al.* Neuronal replacement from endogenous precursors in the adult brain after stroke. (2002). *Nat. Med.*, vol. 8, no. 9, pp. 96-970, doi: 10.1038/nm747.

Avilion, A. A., *et al*. Multipotent cell lineages in early mouse development depend on SOX2 function. (2003). *Genes and Development*, vol. 17, no. 1, pp. 126-140, doi: 10.1101/gad.224503.

Bachiller, S., *et al.* Microglia in neurological diseases: a road map to brain-disease dependent-inflammatory response. (2018). *Front. in Cellul. Neurosci.*, vol. 12, no. 488, pp. 1-17, doi: 10.3389/fncel.2018.00488.

Bar-Nur, O., *et al.* Lineage conversion induced by pluripotency factors involves transient passage through an iPSC stage. (2015). *Nat. Biotech.*, vol. 33, no. 7, pp. 761-768, doi: 10.1038/nbt.3247.

Barker, R. A. Continuing trials of GDNF in Parkinson's disease. (2006). *Lancet Neurol.*, vol. 5, no. 4, pp. 285-286, doi: 10.1016/S1474-4422(06)70386-6.

Barker, R. A., *et al.* Fetal dopaminergic transplantation trials and the future of neural grafting in Parkinson's disease. (2013a). *Lancet Neurol.*, vol. 12, no. 1, pp. 84-91, doi: 10.1016/S1474-4422(12)70295-8.

Barker, R. A., *et al*. The long-term safety and efficacy of bilateral transplantation of human fetal striatal tissue in patients with mild to moderate Huntington's disease. (2013b). *J. Neurol. Neuros. & Psyc.,* vol. 84, no. 6, pp. 657-665, doi: 10.1136/jnnp-2012-302441.

Barker, R. A., *et al*. Cell-based therapies for Parkinson disease-past insights and future potential. (2015). *Nat. Rev. Neurol*., vol. 11, no. 9, pp. 492-503, doi: 10.1038/nrneurol.2015.123.

Barker, R. A., *et al*. Human trials of stem cell-derived dopamine neurons for Parkinson's disease: Dawn of a new era. (2017). *Cell Stem Cell*, vol. 21, no. 5, pp. 569-573, doi: 10.1016/j.stem.2017.09.014.

Barker, R. A., *et al*. New approaches for brain repair - from rescue to reprogramming. (2018). *Nature,* vol. 557, no. 7705, pp. 329-334, doi: 10.1038/s41586-018-0087-1.

Bartus, R. T., & Johnson, E. M. (2017a). Clinical tests of neurotrophic factors for human neurodegenerative diseases, part 1: Where have we been and what have we learned? *Neurobiol. Dis.*, vol. 97, no. Pt. B, pp. 156-168, doi: 10.1016/j.nbd.2016.03.027.

Bartus, R. T., & Johnson, E. M. (2017b). Clinical tests of neurotrophic factors for human neurodegenerative diseases, part 2: Where do we stand and where must we go next? *Neurobiol. Dis.*, vol. 97, no. Pt B, pp. 169-178, doi: 10.1016/j.nbd.2016.03.026.

Bhagwan, J. R., *et al*. Variable expression and silencing of CRISPR-Cas9 targeted transgenes identifies the AAVS1 locus as not an entirely safe harbor. (2020). F1000Research, vol. 8, no. 1911, doi: 10.12688/f1000research.19894.2.

Bhat, R., *et al.* Astrocyte senescence as a component of Alzheimer's disease. (2012). *PLoS ONE*, vol. 7, no. 9, pp. 1-10, doi: 10.1371/journal.pone.0045069.

Bonneh-Barkay, D., & Wiley, C. A. Brain extracellular matrix in neurodegeneration. (2009). *Brain Pathology*, vol. 19, no. 4, pp. 573-585, doi: 10.1111/j.1750-3639.2008.00195.x.

Boyer, L. F., *et al.* Dopaminergic differentiation of human pluripotent cells. (2012). *Curr. Protoc. Stem Cell Biol.*, Chapter 1: Unit 1 H.6, doi: 10.1002/9780470151808.sc01h06s22.

Branda, C. S. & Dymecki, S. M. Talking about a revolution: the impact of site-specific recombinases on genetic analyses in mice. (2004). *Dev. Cell*, vol. 6, no. 1, pp. 7-28, doi: 10.1016/S1534-5807(03)00399-X.

Brawek, B., Olmedillas Del Moral, M., Garaschuk, O. In vivo visualization of microglia using tomato lectin. (2019). *Meth. Mol. Biol.*, vol. 2034, pp. 165-175, doi:10.1007/978-1-4939-9658-2_12.

Brennand, K. J., *et al*. Modelling schizophrenia using human induced pluripotent stem cells. (2011). *Nature*, vol. 473, no. 7346, pp. 221-225, doi: 10.1038/nature09915.

Brick, R. M., *et al*. Neurotrophically induced mesenchymal progenitor cells derived from induced pluripotent stem cells enhance neuritogenesis via neurotrophin and cytokine production. (2018). *Stem Cells Transl. Med*., vol. 7, no. 1, pp. 45-58, doi: 10.1002/sctm.17-0108.

Buffo, A., *et al.* Expression pattern of the transcription factor Olig2 in response to brain injuries: Implications for neuronal repair. (2005). *Proceedings of the National Academy of Sciences of the United States of America*, vol. 102, no. 50, pp. 18183-18188, doi: 10.1073/pnas.0506535102.

Burnside, E. R., & Bradbury, E. J. Manipulating the extracellular matrix and its role in brain and spinal cord plasticity and repair. (2014). *Neuropath. Appl. Neurobiol.*, vol. 40, no. 1, pp. 26-59, doi: 10.1111/nan.12114.

Button, E. B., *et al*. Microglial cell activation increases saturated and decreases monounsaturated fatty acid content, but both lipid species are proinflammatory. (2014). *Lipids*, vol. 49, no. 4, pp. 305-316, doi: 10.1007/s11745-014-3882-y.

Caiazzo, M., *et al*. Direct generation of functional dopaminergic neurons from mouse and human fibroblasts. (2011). *Nature*, vol. 476, no. 7359, pp. 224-227, doi: 10.1038/nature10284.

Carvey, P. M., *et al*. The blood-brain barrier in neurodegenerative disease: A rhetorical perspective. (2009). *J. Neurochem*., vol. 111, no. 2, pp. 291-314, doi: 10.1111/j.1471-4159.2009.06319.x.

Chambers, I., *et al.* Functional expression cloning of Nanog, a pluripotency sustaining factor in embryonic stem cells. (2003). *Cell*, vol. 113, no. 5, pp. 643-655, doi: 10.1016/S0092-8674(03)00392-1.

Chambers, S. M., *et al.* Highly efficient neural conversion of human ES and iPS cells by dual inhibition of SMAD signaling. (2009). *Nat. Biotech*., vol. 27, no. 3, pp. 275-280, doi: 10.1038/nbt.1529.

Chen, W., *et al*. Progress in dopaminergic cell replacement and regenerative strategies for parkinson's disease. (2019). *ACS Chem Neurosci*., vol. 10, no. 2, pp. 839-851, doi: 10.1021/acschemneuro.8b00389.

Chen, Y. C., *et al*. A NeuroD1 AAV-based gene therapy for functional brain repair after ischemic injury through in vivo astrocyte-to-neuron conversion. (2020). *Mol. Ther*., vol. 28, no. 1, pp. 217-234, doi: 10.1016/j.ymthe.2019.09.003.

Chen, Y., *et al*. A versatile polypharmacology platform promotes cytoprotection and viability of human pluripotent and differentiated cells. (2021). *Nat. Methods*, vol. 18, pp. 528-541, doi: 10.1038/s41592-021-01126-2.

Chieffi, S., *et al.* Neuroprotective effects of physical activity: Evidence from human and animal studies. (2017). *Front. Neurol.*, vol. 8, no. 188, pp. 1-7, doi: 10.3389/fneur.2017.00188.

Chinta, S. J., *et al*. Cellular senescence is induced by the environmental neurotoxin Paraquat and contributes to neuropathology linked to Parkinson's disease. (2018). *Cell Rep*., vol. 22, no. 4, pp. 930-940, doi: 10.1016/j.celrep.2017.12.092.

Cisbani, G., & Cicchetti, F. The fate of cell grafts for the treatment of Huntington's disease: The post-mortem evidence. (2014). *Neuropathol. Appl. Neurobiol*., vol. 40, no. 1, pp. 71-90, doi: 10.1111/nan.12104.

Corso, T. D., *et al*. Assessment of viral and non-viral gene transfer into adult rat brains using HSV-1, calcium phosphate and PEI-based methods. (2005). *Folia Morphol*., vol. 64, no. 3, pp. 130-144, PMID: 16228947.

Cowan, C. A., *et al*. Nuclear reprogramming of somatic cells after fusion with human embryonic stem cells. (2005). *Science*, vol. 309, no. 5739, pp. 1369-1373, doi: 10.1126/science.1116447.

Cox, D. B. T., *et al*. Therapeutic genome editing: Prospects and challenges. (2015). *Nat. Med*., vol. 21, no. 2, pp. 121-131, doi: 10.1038/nm.3793.

Cozene, B., *et al.* Mesenchymal stem cell-induced anti-neuroinflammation against traumatic brain injury. (2021). *Cell Transpl*., vol. 30, pp. 1-13, doi: 10.1177/09636897211035715.

Czapski, G. A., & Strosznajder, J. B. Glutamate and GABA in microglia-neuron crosstalk in alzheimer's disease. (2021). *Int. J. Mol. Sci*., vol. 22, no. 21, pp. 1-24, doi: 10.3390/ijms222111677.

Das, A. T., *et al*. Tet-On systems for doxycycline-inducible gene expression. (2016). *Curr. Gene Ther.,* vol. 16, no. 3, pp. 156-167, doi: 10.2174/1566523216666160524144041.

Davis, R. L., *et al*. Expression of a single transfected cDNA converts fibroblasts to myoblasts. (1987). *Cell*, vol. 51, no. 6, pp. 987-1000, doi: 10.1016/0092-8674(87)90585-X.

De Biase, L. M., *et al*. Local cues establish and maintain region-specific phenotypes of basal ganglia microglia. (2017). *Neuron*, vol. 95, no. 2, pp. 341-356, doi: 10.1016/j.neuron.2017.06.020.

Decressac, M., *et al.* α-synuclein-induced down-regulation of Nurr1 disrupts GDNF signaling in nigral dopamine neurons. (2012). *Sci. Transl. Med.*, vol. 4, no. 163, pp. 1-15, doi: 10.1126/scitranslmed.3004676.

Di Giorgio, F. P., *et al*. Human embryonic stem cell-derived motor neurons are sensitive to the toxic effect of glial cells carrying an ALS-causing mutation. (2008). *Cell Stem Cell*, vol. 3, no. 6, pp. 637-648, doi: 10.1016/j.stem.2008.09.017.

Dick, A. D., et al. Direct ex vivo flow cytometric analysis of human microglial cell CD4 expression: examination of central nervous system biopsy specimens from HIV-seropositive patients and patients with other neurological disease. (1997). *AIDS*, vol. 11, no. 14, pp. 1699-1708, doi: 10.1097/00002030-199714000-00006.

Dimos, J. T., *et al*. Induced pluripotent stem cells generated from patients with ALS can be differentiated into motor neurons. (2008). *Science*, vol. 321, no. 5893, pp. 1218-1221, doi: 10.1126/science.1158799.

Douvaras, P. & Fossati, V. Generation and isolation of oligodendrocyte progenitor cells from human pluripotent stem cells. (2015). *Nat. Protoc.*, vol. 10, no. 8, pp. 1143-1154, doi: 10.1038/nprot.2015.075.

Drake, S. A. & Yu, E. T. Using biomedical ethics model to explore use of postmortem specimens in tissue research. (2016). Open Med. J., vol. 3, no. 1, pp. 234-237, doi: 10.2174/1874220301603010234.

Elkabes, S., *et al*. Brain microglia/macrophages express neurotrophins that selectively regulate microglial proliferation and function. (1996). *J. Neurosci.*, vol. 16, no. 8, pp. 2508-2521, doi: 10.1523/jneurosci.16-08-02508.1996.

Elkabetz, Y., *et al*. Human ES cell-derived neural rosettes reveal a functionally distinct early neural stem cell stage. (2008). *Genes and Development*, vol. 22, no. 2, pp. 152-165, doi: 10.1101/gad.1616208.

Eme-Scolan, E. & Dando, S.J. (2020). Tools and approaches for studying microglia in vivo. *Front. Immunol.*, vol. 11, no. 583647, pp. 1-10, doi: 10.3389/fimmu.2020.583647.

Erickson, K. I., *et al*. Exercise training increases size of hippocampus and improves memory. (2011). *Proceedings of the National Academy of Sciences of the United States of America*, vol. 108, no. 7, pp. 3017-3022, doi: 10.1073/pnas.1015950108.

Evans, M. & Kaufman, M. Establishment in culture of pluripotential cells from mouse embryos. (1981). *Nature*, vol. 292, pp. 154-156, doi: 10.1038/292154a0.

Farkas, L. M. & Huttner, W. B. The cell biology of neural stem and progenitor cells and its significance for their proliferation versus differentiation during mammalian brain development. (2008). *Cell Biol*., vol. 20, no. 6, pp. 707-715, doi: 10.1016/j.ceb.2008.09.008.

Fawcett, J. W. The extracellular matrix in plasticity and regeneration after CNS injury and neurodegenerative disease. (2015). Prog Brain Res., vol. 218, pp. 213-226, doi: 10.1016/bs.pbr.2015.02.001.

Flitsch, L. J. & Brüstle, O. Evolving principles underlying neural lineage conversion and their relevance for biomedical translation. (2019). F1000Research, vol. 8, pp. 1-17, doi: 10.12688/f1000research.18926.1.

Ford, E., *et al.* Human pluripotent stem cells-based therapies for neurodegenerative diseases: Current status and challenges. (2020). *Cells*, vol. 9, no. 11, pp. 1-34, doi: 10.3390/cells9112517.

Fricker, R. A., *et al*. Site-specific migration and neuronal differentiation of human neural progenitor cells after transplantation in the adult rat brain. (1999). *J. Neurosci*., vol. 19, no. 14, pp. 5990-6005, doi: 10.1523/jneurosci.19-14-05990.1999.

Frisén, J. Neurogenesis and gliogenesis in nervous system plasticity and repair. (2016). *Annual Review of Cell and Developmental Biology*, vol. 32, pp. 127-141, doi: 10.1146/annurev-cellbio-111315-124953.

Gascón, S., *et al*. Identification and successful negotiation of a metabolic checkpoint in direct neuronal reprogramming. (2016). *Cell Stem Cell*, vol. 18, no. 3, pp. 396-409, doi: 10.1016/j.stem.2015.12.003.

Gascón, S., *et al.* Direct neuronal reprogramming: Achievements, hurdles, and new roads to success. (2017). *Cell Stem Cell*, vol. 21, no. 1, pp. 18-34, doi: 10.1016/j.stem.2017.06.011.

George, N. & Geller, H. M. Extracellular matrix and traumatic brain injury. (2018). *J. Neurosci. Res.*, vol. 96, no. 4, pp. 573-588, doi: 10.1002/jnr.24151.

German, D. C., *et al*. Midbrain dopaminergic cell loss in parkinson's disease: Computer visualization. (1989). *Annals of Neurology*, vol. 26, no. 4, pp. 507-514, doi: 10.1002/ana.410260403.

Ginhoux, F., *et al*. Fate mapping analysis reveals that adult microglia derive from primitive macrophages. (2010). *Science*, vol. 330, no. 6005, pp. 841-845, doi: 10.1126/science.1194637.

Gitler, A. D., *et al*. Neurodegenerative disease: Models, mechanisms, and a new hope. (2017). *DMM Disease Models and Mechanisms*, vol. 10, no. 5, pp. 499-502, doi: 10.1242/dmm.030205.

Gouvarchin Ghaleh, H. E., *et al.* Concise review on optimized methods in production and transduction of lentiviral vectors in order to facilitate immunotherapy and gene therapy. (2020). *Biomed. Pharmacother.*, vol. 128, no. 110276, pp. 1-11, doi:10.1016/j.biopha.2020.110276.

Graf, T. Historical origins of transdifferentiation and reprogramming. (2011). *Cell Stem Cell*, vol. 9, no. 6, pp. 504-516, doi: 10.1016/j.stem.2011.11.012.

Grande, A., *et al.* Environmental impact on direct neuronal reprogramming in vivo in the adult brain. (2013). *Nat. Com.*, vol. 4, no. 2373, pp. 1-12., doi: 10.1038/ncomms3373.

Grealish, S., *et al*. Human ESC-derived dopamine neurons show similar preclinical efficacy and potency to fetal neurons when grafted in a rat model of Parkinson's disease. (2014). *Cell Stem Cell*, vol. 15, no. 5, pp. 653-665, doi: 10.1016/j.stem.2014.09.017.

Grealish, S., *et al.* Monosynaptic tracing using modified rabies virus reveals early and extensive circuit integration of human embryonic stem cell-derived neurons. (2015). *Stem Cell Rep.*, vol. 4, no. 6, pp. 975-983, doi: 10.1016/j.stemcr.2015.04.011.

Griffin, É. W., *et al*. Aerobic exercise improves hippocampal function and increases BDNF in the serum of young adult males. (2011). *Phys. Beh.*, vol. 104, no. 5, pp. 934-941, doi: 10.1016/j.physbeh.2011.06.005

Guo, Z., *et al.* In vivo direct reprogramming of reactive glial cells into functional neurons after brain injury and in an Alzheimer's disease model. (2014). *Cell Stem Cell*, vol. 14, no. 2, pp. 188-202, doi: 10.1016/j.stem.2013.12.001.

Gurumoorthy, N., *et al*. Non-integrating lentiviral vectors in clinical applications: A glance through. (2022). *Biomed.*, vol. 10, no. 107, pp. 1-19, doi: 10.3390/biomedicines10010107.

Hargus, G., *et al.* Differentiated Parkinson patient-derived induced pluripotent stem cells grow in the adult rodent brain and reduce motor asymmetry in Parkinsonian rats. (2010). *Proceedings of the National Academy of Sciences of the United States of America*, vol. 107, no. 36, pp. 15921-15926, doi: 10.1073/pnas.1010209107.

Heins, N., *et al*. Glial cells generate neurons: The role of the transcription factor Pax6. (2002). *Nat. Neurosci.*, vol. 5, no. 4, pp. 308-315, doi: 10.1038/nn828.

Hickman, S. E., *et al*. The microglial sensome revealed by direct RNA sequencing. (2013). *Nat. Neurosci*., vol. 16, no. 12, pp. 1896-1905, doi: 10.1038/nn.3554.

Horisawa, K. & Suzuki, A. Direct cell-fate conversion of somatic cells: Toward regenerative medicine and industries. (2020). *Proceedings of the Japan Academy Series B: Physical and Biological Sciences* vol. 96, no. 4, pp. 131-158, doi: 10.2183/PJAB.96.012.

Hughes, A. N. & Appel, B. Microglia phagocytose myelin sheaths to modify developmental myelination. (2020). *Nat. Neurosci*., vol. 23, no. 9, pp. 1055-1066, doi: 10.1038/s41593-020-0654-2.

Ichida, J. K., *et al*. Comparative genomic analysis of embryonic, lineage-converted and stem cell-derived motor neurons. (2018). *Develop.*, vol. 145, no. 22, pp. 1-13, doi: 10.1242/dev.168617.

Israel, M. A., *et al.* Probing sporadic and familial Alzheimer's disease using induced pluripotent stem cells. (2012). *Nature*, vol. 482, no. 7384, pp. 216-220, doi: 10.1038/nature10821.

Karow, M., *et al*. Reprogramming of pericyte-derived cells of the adult human brain into induced neuronal cells. (2012). *Cell Stem Cell*, vol. 11, no. 4, pp. 471-476, doi: 10.1016/j.stem.2012.07.007.

Kefalopoulou, Z., *et al.* Long-term clinical outcome of fetal cell transplantation for parkinson disease: Two case reports. (2014). *JAMA Neurology*, vol. 71, no. 1, pp. 83-87, doi: 10.1001/jamaneurol.2013.4749.

Kim, J., *et al.* Direct reprogramming of mouse fibroblasts to neural progenitors. (2011). *Proceedings of the National Academy of Sciences of the United States of America*, vol. 108, no. 19, pp. 7838-7843, doi: 10.1073/pnas.1103113108.

Kim, J., *et al.* Human organoids: model systems for human biology and medicine. (2020). *Nat. Ver. Mol. Cell Biol.*, vol. 21, no. 10, pp. 571-584, doi: 10.1038/s41580-020-0259-3.

Klatt, D., *et al*. Differential transgene silencing of myeloid-specific promoters in the AAVS1 safe harbor locus of induced pluripotent stem cell-derived myeloid cells. (2020). *Hum. Gene Ther.*, vo. 31, no. 3-4, pp.199-210, doi: 10.1089/hum.2019.194.

Kordower, J. H., *et al.* Clinicopathological findings following intraventricular glial-derived neurotrophic factor treatment in a patient with Parkinson's disease. (1999). *Annals of Neurology*, vol. 46, no. 3, pp. 419-424, doi: 10.1002/1531-8249(199909)46:3<419::AID-ANA21>3.0.CO;2-Q.

Kosaka, N., *et al*. FGF-4 regulates neural progenitor cell proliferation and neuronal differentiation. (2006). *FASEB J.*, vol. 20, no. 9, pp. 1484-1485, doi: 10.1096/fj.05-5293fje.

Krencik, R., *et al*. Specification of transplantable astroglial subtypes from human pluripotent stem cells. (2011). *Nat. Biotech*., vol. 29, no. 6, pp. 528-534, doi: 10.1038/nbt.1877.

Kromer, L. F. Nerve growth factor treatment after brain injury prevents neuronal death. (1987). *Science*, vol. 235, no. 4785, pp. 214-216, doi: 10.1126/science.3798108.

Kronenberg, G., *et al*. Modulation of fate determinants olig2 and pax6 in resident glia evokes spiking neuroblasts in a model of mild brain ischemia. (2010). *Stroke*, vol. 41, no. 12, pp. 2944-2949, doi: 10.1161/STROKEAHA.110.583039.

Kucher, K., *et al*. First-in-man intrathecal application of neurite growth-promoting anti-Nogo- a antibodies in acute spinal cord injury. (2018). *Neurorehabilitation and Neural Repair*, vol. 32, no. 6-7, pp. 578-589, doi: 10.1177/1545968318776371.

Kwon, H. S. & Koh, S. H. Neuroinflammation in neurodegenerative disorders: the roles of microglia and astrocytes. (2020). *Transl. Neurodeg.*, vol. 9, no. 1, pp. 1-12, doi: 10.1186/s40035-020-00221-2.

Ladewig, J., *et al*. Auto-attraction of neural precursors and their neuronal progeny impairs neuronal migration. (2014). *Nat. Neurosci.*, vol. 17, no. 1, pp. 24-26, doi: 10.1038/nn.3583.

Lam, D., *et al*. Tissue-specific extracellular matrix accelerates the formation of neural networks and communities in a neuron-glia co-culture on a multi-electrode array. (2019). *Sci. Rep.*, vol. 9, no. 1, pp. 1-15, doi: 10.1038/s41598-019-40128-1.

Lang, A. E., *et al.* Randomized controlled trial of intraputamenal glial cell line-derived neurotrophic factor infusion in Parkinson disease. (2006). *Annals of Neurology*, vol. 59, no. 3, pp. 459-466, doi: 10.1002/ana.20737.

Larouche, J. & Aguilar, C. A. New technologies to enhance in vivo reprogramming for regenerative medicine. (2019). *Trends Biotechnol.*, vol. 37, no. 6, pp. 604-617, doi: 10.1016/j.tibtech.2018.11.003.

Lawson, L. J., *et al*. Heterogeneity in the distribution and morphology of microglia in the normal adult mouse brain. (1990). *Neurosci.*, vol. 39, no. 1, pp. 151-170, doi: 10.1016/0306-4522(90)90229-W.

Lawson, L. J., *et al*. Turnover of resident microglia in the normal adult mouse brain. (1992). *Neurosci.*, vol. 48, no. 2, pp. 405-415, doi: 10.1016/0306-4522(92)90500-2.

Lee, G., *et al*. Modelling pathogenesis and treatment of familial dysautonomia using patient-specific iPSCs. (2009). *Nature*, vol. 461, no. 7262, pp. 402-406, doi: 10.1038/nature08320.

Lei, W., *et al*. Non-engineered and engineered adult neurogenesis in mammalian brains. (2019). *Front. Neurosci.*, vol. 13, no. 131, pp. 1-13, doi: 10.3389/fnins.2019.00131.

Leong, C., *et al*. Microglia specific fluorescent probes for live cell imaging. (2014). *Chem. Commun.*, vol. 50, no. 9, pp. 1089-1091, doi:10.1039/c3cc45715j.

Lepore, A. C., *et al.* Focal transplantation-based astrocyte replacement is neuroprotective in a model of motor neuron disease. (2008). *Nat. Neurosci.*, vol. 11, no. 11, pp. 1294-1301, doi: 10.1038/nn.2210.

Levi-Montalcini, R. & Hamburger, V. Selective growth stimulating effects of mouse sarcoma on the sensory and sympathetic nervous system of the chick embryo. (1951). *J. Exp. Zool*., vol. 116, no. 2, pp. 321-361, doi: 10.1002/jez.1401160206.

Li, J. Y., *et al*. Lewy bodies in grafted neurons in subjects with Parkinson's disease suggest host-to-graft disease propagation. (2008). *Nat. Med*., vol. 14, no. 5, pp. 501-503, doi: 10.1038/nm1746.

Li, W., *et al.* Extensive graft-derived dopaminergic innervation is maintained 24 years after transplantation in the degenerating parkinsonian brain. (2016). *Proceedings of the National Academy of Sciences of the United States of America*, vol. 113, no. 23, pp. 6544-6549, doi: 10.1073/pnas.1605245113.

Liddelow, S. A., *et al*. Neurotoxic reactive astrocytes are induced by activated microglia. (2017). *Nature*, vol. 541, no. 7638, pp. 481-487, doi: 10.1038/nature21029.

Lindvall, O. Treatment of Parkinson's disease using cell transplantation. (2015). *Phil. Trans. R. Soc.* Series B, Biological sciences, vol. 370, no. 1680, pp. 1-7, doi: 10.1098/rstb.2014.0370.

Liu, H., *et al*. Neurotransmitter receptors on microglia. (2016). *Stroke and Vascular Neurology*, vol. 1, no. 2, pp. 52-58, doi: 10.1136/svn-2016-000012.

Liu, X., *et al.* The immunogenicity and immune tolerance of pluripotent stem cell derivatives. (2017). *Front. Immun*., vol. 8, no. 645, pp. 1-6, doi: 10.3389/fimmu.2017.00645.

Liu, Y. J., *et al.* Microglia elimination increases neural circuit connectivity and activity in adult mouse cortex. (2021). *J. Neurosci*., vol. 41, no. 6, pp. 1274-1287, doi: 10.1523/JNEUROSCI.2140-20.2020.

Livak, K. & Schmittgen, T. Analysis of relative gene expression data using real-time quantitative PCR and the $2^{-\Delta\Delta CT}$ method. (2001). *Methods*., no. 25, pp. 402-408, doi: https://doi.org/10.1006/meth.2001.1262

Lujan, E., *et al*. Direct conversion of mouse fibroblasts to self-renewing, tripotent neural precursor cells. (2012). *Proceedings of the National Academy of Sciences of the United States of America*, vol. 109, no. 7, pp. 2527-2532, doi: 10.1073/pnas.1121003109.

Maherali, N., *et al*. Directly reprogrammed fibroblasts show global epigenetic remodeling and widespread tissue contribution. (2007). *Cell Stem Cell*, vol. 1, no. 1, pp. 55-70, doi: 10.1016/j.stem.2007.05.014.

Majumdar, A., *et al*. Activation of microglia acidifies lysosomes and leads to degradation of Alzheimer amyloid fibrils. (2007). *Mol. Biol. Cell*, vol. 18, no. 4, pp. 1490-1496, doi: 10.1091/mbc.E06-10-0975.

Malikov, V., *et al*. FEZ1 phosphorylation regulates HSPA8 localization and interferon-stimulated gene expression. (2022). *Cell Rep.*, vol. 38, no. 7/110396, doi: 10.1016/j.celrep.2022.110396.

Marchetto, M. C. N., *et al*. A model for neural development and treatment of rett syndrome using human induced pluripotent stem cells. (2010). *Cell*, vol. 143, no. 4, pp. 527-539, doi: 10.1016/j.cell.2010.10.016.

Maroof, A. M., *et al*. Directed differentiation and functional maturation of cortical interneurons from human embryonic stem cells. (2013). *Cell Stem Cell*, vol. 12, no. 5, pp. 559-572, doi: 10.1016/j.stem.2013.04.008.

Martin, G. R. Isolation of a pluripotent cell line from early mouse embryos cultured in medium conditioned by teratocarcinoma stem cells. (1981). *Proceedings of the National Academy of Sciences*, vol. 78, no. 12, pp. 7634-7638, doi: 10.1073/PNAS.78.12.7634.

Martin, U. Therapeutic application of pluripotent stem cells: Challenges and risks. (2017). *Front. Med.*, vol. 4, no. 229, pp. 1-8, doi: 10.3389/fmed.2017.00229.

Mathews, M., Wißfeld, J., Flitsch, L.J. *et al*. Reenacting neuroectodermal exposure of hematopoietic progenitors enables scalable production of cryopreservable iPSC-derived human microglia. (2022). *Stem Cell Rev. and Rep.*, [published online ahead of print], doi: 10.1007/s12015-022-10433-w.

Matsuda, T., *et al*. Pioneer factor NeuroD1 rearranges transcriptional and epigenetic profiles to execute microglia-neuron conversion. (2019). *Neuron*, vol. 101, no. 3, pp. 472-485, doi: 10.1016/j.neuron.2018.12.010.

Mazzini, L., *et al*. Mesenchymal stem cell transplantation in amyotrophic lateral sclerosis: A Phase I clinical trial. (2010). *Exp. Neurol.*, vol. 223, no. 1, pp. 229-237, doi: 10.1016/j.expneurol.2009.08.007.

Mertens, J., *et al*. Directly reprogrammed human neurons retain aging-associated transcriptomic signatures and reveal age-related nucleocytoplasmic defects. (2015a). *Cell Stem Cell*, vol. 17, no. 6, pp. 705-718, doi: 10.1016/j.stem.2015.09.001.

Mertens, J., *et al*. Differential responses to lithium in hyperexcitable neurons from patients with bipolar disorder. (2015b). *Nature,* vol. 527, no. 7576, pp. 95-99, doi: 10.1038/nature15526.

Mertens, J., *et al*. Evaluating cell reprogramming, differentiation and conversion technologies in neuroscience. (2016). *Nat. Rev. Neurosci*., vol. 17, no. 7, pp. 424-437, doi: 10.1038/nrn.2016.46.

Mitsui, K., *et al.* The homeoprotein nanog is required for maintenance of pluripotency in mouse epiblast and ES cells. (2003). *Cell*, vol. 113, no. 5, pp. 631-642, doi: 10.1016/S0092-8674(03)00393-3.

Mitsumoto, H., *et al.* Arrest of motor neuron disease in wobbler mice cotreated with CNTF and BDNF. (1994). *Science*, vol. 265, no. 5175, pp. 1107-1110, doi: 10.1126/science.8066451.

Mizee, M. R., *et al.* Isolation of primary microglia from the human post-mortem brain: effects of ante- and post-mortem variables. (2017). *Acta Neuropathol. Commun.*, vol. 5, no. 1, p. 16, doi:10.1186/s40478-017-0418-8.

Murry, C. E., & Keller, G. Differentiation of embryonic stem cells to clinically relevant populations: Lessons from embryonic development. (2008). *Cell*, vol. 132, no. 4, pp. 661-680, doi: 10.1016/j.cell.2008.02.008.

Narantuya, D., *et al.* Human microglia transplanted in rat focal ischemia brain induce neuroprotection and behavioral improvement. (2010). *PLoS ONE*, vol. 5, no. 7, pp. 1-10, doi: 10.1371/journal.pone.0011746.

Nichols, J., *et al*. Formation of pluripotent stem cells in the mammalian embryo depends on the POU transcription factor Oct4. (1998). *Cell*, vol. 95, no. 3, pp. 379-391, doi: 10.1016/S0092-8674(00)81769-9.

Niwa, H., *et al.* Quantitative expression of Oct-3/4 defines differentiation, dedifferentiation or self-renewal of ES cells. (2000). *Nat. Genet.*, vol. 24, no. 4, pp. 372-376, doi: 10.1038/74199.

Nutt, J. G., *et al*. Randomized, double-blind trial of glial cell line-derived neurotrophic factor (GDNF) in PD. (2003). *Neurology*, vol. 60, no. 1, pp. 69-73, doi: 10.1212/WNL.60.1.69.

Oehme, I., *et al.* Agonists of an ecdysone-inducible mammalian expression system inhibit Fas Ligand- and TRAIL-induced apoptosis in the human colon carcinoma cell line RKO. (2006). *Cell Death Differ.*, vol. 13, no. 2, pp. 189-201, doi: 10.1038/sj.cdd.4401730.

Ogata, T. *et al*. Identification of an insulator in AAVS1, a preferred region for integration of adeno-associated virus DNA. (2003). J. Virol., vol. 77, no. 16, pp. 9000-9007, doi: 10.1128/jvi.77.16.9000-9007.2003.

Pajarskienė, J., *et al*. MicroRNA-124 acts as a positive regulator of IFN-β signaling in the lipopolysaccharide-stimulated human microglial cells. (2021). *Int. Immunopharmacol.*, vol. 101, no. Pt. A 108262, doi: 10.1016/j.intimp.2021.108262.

Pang, Z. P., *et al*. Induction of human neuronal cells by defined transcription factors. (2011). *Nature,* vol. 476, no. 7359, pp. 220-223, doi: 10.1038/nature10202.

Parkinsons.org. Statistics | Parkinson's Foundation. (2020). [Online]. Available at: https://www.parkinson.org/Understanding-Parkinsons/Statistics. Consulted on December 6th, 2021.

Peitz, M., *et al*. Protocol for the standardized generation of forward programmed cryopreservable excitatory and inhibitory forebrain neurons. (2020). *STAR Protoc.*, vol. 1, no. 1, pp. 1-15 (100038), doi: 10.1016/j.xpro.2020.100038.

Peschanski, M., *et al.* Rationale for intrastriatal grafting of striatal neuroblasts in patients with Huntington's disease. (1995). *Neurosci*., vol. 68, no. 2, pp. 273-285, doi: 10.1016/0306-4522(95)00162-C.

Pfisterer, U., *et al*. Efficient induction of functional neurons from adult human fibroblasts. (2011). *Cell Cycle*, vol. 10, no. 19, pp. 3311-3316, doi: 10.4161/cc.10.19.17584.

Politis, M., *et al*. Serotonergic neurons mediate dyskinesia side effects in Parkinson's patients with neural transplants. (2010). *Sci. Transl. Med*., vol. 2, no. 38, pp. 1-7, doi: 10.1126/scitranslmed.3000976.

Puri, M. C. & Nagy, A. Concise review: Embryonic stem cells versus induced pluripotent stem cells: The game is on. (2012). *Stem Cells*, vol. 30, no. 1, pp. 10-14, doi: 10.1002/stem.788.

Rando, T. A. & Chang, H. Y. Aging, rejuvenation, and epigenetic reprogramming: Resetting the aging clock. (2012). *Cell*, vol. 148, no. 1-2, pp. 46-57, doi: 10.1016/j.cell.2012.01.003.

Ransohoff, R. M. & Cardona, A. E. (2010). The myeloid cells of the central nervous system parenchyma. In Nature (Vol. 468, Issue 7321, pp. 253–262). Nature Publishing Group. https://doi.org/10.1038/nature09615.

Rao, Y., *et al*. NeuroD1 induces microglial apoptosis and cannot induce microglia-to-neuron cross-lineage reprogramming. (2021). *Neuron*, vol. 109, no. 24, pp. 4094-4108, doi: 10.1016/j.neuron.2021.11.008.

Ray Dorsey, E., *et al*. Global, regional, and national burden of Parkinson's disease, 1990-2016: a systematic analysis for the Global Burden of Disease Study 2016. (2018). *Lancet Neurol.*, vol. 17, no. 11, pp. 939-953, doi: 10.1016/S1474-4422(18)30295-3.

Reidling, J. C., *et al*. Human neural stem cell transplantation rescues functional deficits in R6/2 and Q140 Huntington's disease mice. (2018). *Stem Cell Rep.*, vol. 10, no. 1, pp. 58-72, doi: 10.1016/j.stemcr.2017.11.005.

Reinhardt, P., *et al*. Genetic correction of a lrrk2 mutation in human iPSCs links parkinsonian neurodegeneration to ERK-dependent changes in gene expression. (2013). *Cell Stem Cell*, vol. 12, no. 3, pp. 354-367, doi: 10.1016/j.stem.2013.01.008.

Ring, K. L., *et al*. Direct reprogramming of mouse and human fibroblasts into multipotent neural stem cells with a single factor. (2012). *Cell Stem Cell*, vol. 11, no. 1, pp. 100-109, doi: 10.1016/j.stem.2012.05.018.

Rivetti Di Val Cervo, P., *et al*. Induction of functional dopamine neurons from human astrocytes in vitro and mouse astrocytes in a Parkinson's disease model. (2017). *Nat. Biotech*., vol. 35, no. 5, pp. 444-452, doi: 10.1038/nbt.3835.

Roy, I., *et al*. Nonviral gene transfection nanoparticles: function and applications in the brain. (2008). *Nanomedicine: Nanotechnology, Biology, and Medicine*, vol. 4, no. 2, pp. 89-97, doi: 10.1016/j.nano.2008.01.002.

Samaco, R. C., *et al.* Epigenetic overlap in autism-spectrum neurodevelopmental disorders: MECP2 deficiency causes reduced expression of UBE3A and GABRB3. (2005). *Human Mol. Genet*., vol. 14, no. 4, pp. 483-492, doi: 10.1093/hmg/ddi045.

Schweitzer, J. S., *et al*. Personalized iPSC-derived dopamine progenitor cells for Parkinson's disease. (2020). *New England Journal of Medicine*, vol. 382, no. 20, pp. 1926-1932, doi: 10.1056/nejmoa1915872.

Shahbazi, E., *et al.* Conversion of human fibroblasts to stably self-renewing neural stem cells with a single zinc-finger transcription factor. (2016). *Stem Cell Rep.*, vol. 6, no. 4, pp. 539-551, doi: 10.1016/j.stemcr.2016.02.013.

Sheng, C., *et al.* A stably self-renewing adult blood-derived induced neural stem cell exhibiting patternability and epigenetic rejuvenation. (2018). *Nat. Com.*, vol. 9, no. 1, pp. 1-15, doi: 10.1038/s41467-018-06398-5.

Shi, Y., *et al.* Human cerebral cortex development from pluripotent stem cells to functional excitatory synapses. (2012). *Nat. Neurosci.*, vol. 15, no. 3, pp. 477-486, doi: 10.1038/nn.3041.

Siebert, J. R., *et al*. Chondroitin sulfate proteoglycans in the nervous system: inhibitors to repair. (2014). *Biomed. Res. Int.*, vol. 2014, no. 845323, pp. 1-15, doi: 10.1155/2014/845323.

Simpson, D. S. A. & Oliver, P. L. Ros generation in microglia: Understanding oxidative stress and inflammation in neurodegenerative disease. (2020). *Antioxidants*, vol. 9, no. 8, pp. 1-27, doi: 10.3390/antiox9080743.

Singh, A., *et al*. Oxidative stress: A key modulator in neurodegenerative diseases. (2019). *Molecules,* vol. 24, no. 8, pp. 1-20, doi: 10.3390/molecules24081583.

Soboleski, M. R., *et al*. Green fluorescent protein is a quantitative reporter of gene expression in individual eukaryotic cells. (2005). *FASEB J.*, vol. 19, no. 3, pp. 1-20, doi: 10.1096/fj.04-3180fje.

Song, I. & Dityatev, A. Crosstalk between glia, extracellular matrix and neurons. (2018). Br*ain Research Bulletin*, vol. 136, pp. 101-108, doi: 10.1016/j.brainresbull.2017.03.003.

Sui, Z., *et al*. Functional synergy between CD40 ligand and HIV-1 Tat contributes to inflammation: implications in HIV type 1 dementia. (2007). *J. Immunol.*, vol. 178, no. 5, pp. 3226-3236, doi: 10.4049/jimmunol.178.5.3226.

Stadtfeld, M. & Hochedlinger, K. Induced pluripotency: History, mechanisms, and applications. (2010). *Genes and Development*, vol. 24, no. 20, pp. 2239-2263, doi: 10.1101/gad.1963910.

Tada, M., *et al*. Nuclear reprogramming of somatic cells by in vitro hybridization with ES cells. (2001). *Curr. Biol*., vol. 11, no. 19, pp. 1553-1558, doi: 10.1016/S0960-9822(01)00459-6.

Takahashi, K. & Yamanaka, S. Induction of pluripotent stem cells from mouse embryonic and adult fibroblast cultures by defined factors. (2006). *Cell*, vol. 126, no. 4, pp. 663-676, doi: 10.1016/j.cell.2006.07.024.

Takahashi, K., *et al.* Induction of pluripotent stem cells from adult human fibroblasts by defined factors. (2007). *Cell*, vol. 131, no. 5, pp. 861-872, doi: 10.1016/j.cell.2007.11.019.

Tan, J. K. Y., *et al*. Non-viral nucleic acid delivery strategies to the central nervous system. (2016). *Front. Mol. Neurosci*., vol. 9, pp. 1-13, doi: 10.3389/fnmol.2016.00108.

Theka, I., *et al*. Rapid generation of functional dopaminergic neurons from human induced pluripotent stem cells through a single-step procedure using cell lineage transcription factors. (2013). *Stem Cells Transl. Med*., vol. 2, no. 6, pp. 473-479, doi: 10.5966/sctm.2012-0133.

Thier, M., *et al*. Direct conversion of fibroblasts into stably expandable neural stem cells. (2012). *Cell Stem Cell*, vol. 10, no. 4, pp. 473-479, doi: 10.1016/j.stem.2012.03.003.

Thompson, W. G. Successful brain grafting. (1890). *Science*, vol. 16, no. 392, pp. 78-79, doi: 10.1126/science.ns-16.392.78-a.

Thomson, J. A. Embryonic stem cell lines derived from human blastocysts. (1998). *Science*, vol. 282, no. 5391, pp. 1145-1147, doi: 10.1126/science.282.5391.1145.

Tian, C., *et al*. Direct conversion of dermal fibroblasts into neural progenitor cells by a novel cocktail of defined factors. (2012). *Curr. Mol. Med*., vol. 12, no. 2, pp. 126-137, doi: 10.2174/156652412798889018.

Torper, O., *et al.* Generation of induced neurons via direct conversion in vivo. (2013). *Proc. Natl. Acad. Sci. U.S.A.*, vol. 110, no. 17, pp. 7038-7043, doi: 10.1073/pnas.1303829110.

Torper, O., *et al.* In vivo reprogramming of striatal NG2 glia into functional neurons that integrate into local host circuitry. (2015). *Cell Rep*., vol. 12, no. 3, pp. 474-481, doi: 10.1016/j.celrep.2015.06.040.

Tropepe, V., *et al.* Distinct neural stem cells proliferate in response to EGF and FGF in the developing mouse telencephalon. (1999). *Develop. Biol*., vol. 208, no. 1, pp. 166-188, doi: 10.1006/dbio.1998.9192.

Tsuchiya, T., *et al.* Characterization of microglia induced from mouse embryonic stem cells and their migration into the brain parenchyma. (2005). *J. Neuroimmunol*., vol. 160, no. 1-2, pp. 210-218, doi: 10.1016/j.jneuroim.2004.10.025.

van Praag, H., *et al.* Running enhances neurogenesis, learning, and long-term potentiation in mice. (1999). *Proc. Natl. Acad. Sci. U.S.A.*, vol. 96, no. 23, pp. 13427-13431, doi: 10.1073/pnas.96.23.13427.

Vierbuchen, T., *et al.* Direct conversion of fibroblasts to functional neurons by defined factors. (2010). *Nature*, vol. 463, no. 7284, pp. 1035-1041, doi: 10.1038/nature08797.

Villacampa, N., *et al*. Tomato lectin histochemistry for microglial visualization. (2013). *Methods Mol. Bio.*, vol. 1041, pp. 261-279, doi: 10.1007/978-1-62703-520-0_23.

Villarreal, A., *et al*. Pathological neuroinflammatory conversion of reactive astrocytes is induced by microglia and involves chromatin remodeling. (2021). *Front. Pharmacol.*, vol. 12, no. 689346, doi: 10.3389/fphar.2021.689346.

Wang, C., *et al*. Microglia mediate forgetting via complement-dependent synaptic elimination. (2020). *Science*, vol. 367, no. 6478, pp. 688-694, doi: 10.1126/science.aaz2288.

Wang, K. C., *et al.* Oligodendrocyte-myelin glycoprotein is a Nogo receptor ligand that inhibits neurite outgrowth. (2002). *Nature*, vol. 417, no. 6892, pp. 941-944, doi: 10.1038/nature00867.

Wang, L. L., *et al*. Revisiting astrocyte to neuron conversion with lineage tracing *in vivo*. (2021). *Cell*, vol. 184, no. 21, pp. 5465-5481, doi: 10.1016/j.cell.2021.09.005.

Wang, L., *et al.* Generation of integration-free neural progenitor cells from cells in human urine. (2013). *Nature Methods*, vol. 10, no. 1, pp. 84-89, doi: 10.1038/nmeth.2283.

Wang, S. & Huang, R. Non-viral nucleic acid delivery to the central nervous system and brain tumors. (2019). *J. Gene Med*., vol. 21, no. 7, pp. 1-13, doi: 10.1002/jgm.3091.

Wang, S., *et al*. Autologous iPSC-derived dopamine neuron transplantation in a nonhuman primate Parkinson's disease model. (2015). *Cell Discovery*, vol. 1, no. 1, pp. 1-11, doi: 10.1038/celldisc.2015.12.

Wang, T., *et al.* Derivation of neural stem cells from human adult peripheral CD34+ cells for an autologous model of neuroinflammation. (2013). *PLoS ONE*, vol. 8, no. 11, pp. 1-18, doi: 10.1371/journal.pone.0081720.

Wang, Y., *et al*. In vivo direct conversion of astrocytes to neurons maybe a potential alternative strategy for neurodegenerative diseases. (2021). *Front. Aging Neurosci*., vol. 13, pp. 1-10, doi: 10.3389/fnagi.2021.689276.

Watanabe, K., *et al.* A ROCK inhibitor permits survival of dissociated human embryonic stem cells. (2007). *Nat. Biotechnol.*, vol. 25, no. 6, pp. 681-686, doi:10.1038/nbt1310.

Weissmiller, A. M. & Wu, C. Current advances in using neurotrophic factors to treat neurodegenerative disorders. (2012). *Transl. Neurodeg*., vol. 1, pp. 1-9, doi: 10.1186/2047-9158-1-14.

Wilmut, I., *et al.* Erratum: Viable offspring derived from fetal and adult mammalian cells. (1997). *Nature*, vol. 386, no. 6621, pp. 810-813, doi: 10.1038/386200a0.

Wu, Z., *et al*. Gene therapy conversion of striatal astrocytes into GABAergic neurons in mouse models of Huntington's disease. (2020). *Nat. Com*., vol. 11, no. 1, pp. 1-18, doi: 10.1038/s41467-020-14855-3.

Xiao, N. & Le, Q. T. Neurotrophic factors and their potential applications in tissue regeneration. (2016). *Archivum Immunologiae et Therapiae Experimentalis*, vol. 64, no. 2, pp. 89-99, doi: 10.1007/s00005-015-0376-4.

Yang, N., *et al*. Induced neuronal cells: How to make and define a neuron. (2011). *Cell Stem Cell*, vol. 9, no. 6, pp. 517-525, doi: 10.1016/j.stem.2011.11.015.

Yiu, G. & He, Z. Glial inhibition of CNS axon regeneration. (2006). *Nat. Rev. Neurosci*., vol. 7, no. 8, pp. 617-627, doi: 10.1038/nrn1956.

Zhang, P. W., *et al*. Generation of GFAP::GFP astrocyte reporter lines from human adult fibroblast-derived iPS cells using zinc-finger nuclease technology. (2016). *GLIA*, vol. 64, no. 1, pp. 63-75, doi: 10.1002/glia.22903.

Zhang, T., *et al.* The emerging role of exosomes in Alzheimer's disease. (2021). *Ageing Res. Rev*., vol. 68, doi: 10.1016/j.arr.2021.101321.

Zhang, X., *et al.* Commentary: In vivo neuroregeneration to treat ischemic stroke through NeuroD1 AAV-based gene therapy in adult non-human primates. (2021). *Front. Cell Develop. Biol*., vol. 9, no. 648020, pp. 1-3, doi: 10.3389/fcell.2021.648020.

Zou, Q., *et al*. Direct conversion of human fibroblasts into neuronal restricted progenitors. (2014). *J. Biol. Chem.*, vol. 289, no. 8, pp. 5250-5260, doi: 10.1074/jbc.M113.516.

7. Attachments

Cell lines	Abbreviation	Description
iPSdMiG c14bms11	WT iPSdMiG	WT line.
iPSC or iPSdMiG c14bms11 AAVS1-ITGAMp-EGFP	ITGAMp-EGFP iPSC or iPSdMiG	A lineage tracing reporter system based on the *ITGAM* gene promoter (gene encoding the characteristic microglial marker CD11b) driving EGFP expression.
iPSC or iPSdMiG c14bms11 AAVS1-TRE3G-SOX2-cMYC	SOX2/cMYC-transgenic iPSC or iPSdMiG	Expresses the TFs SOX2 and cMYC in a DOX-inducible manner.
iPSC c35mr1 NGN2	NGN2 iPSC	Expresses the TF NGN2 in a DOX-inducible manner.

Attachment 1 – Overview of cell lines used in this project.

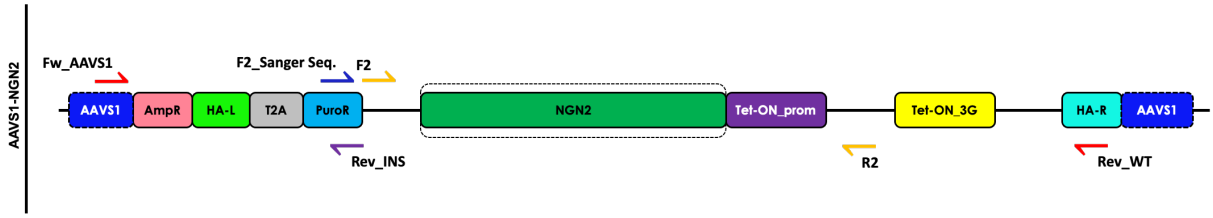

Attachment 2 – Schematic illustration of the AAVS1-NGN2 sequence and the respective binding sites of the different PCR primers employed for its characterization, quality control and/or amplification. Primers: F2/R2 (yellow arrows) – amplification of NGN2 sequence of interest in the scope of positive control sample for the study of and analysis to exclude occurrence of point mutations within AAVS1-ITGAMp-EGFP; F2_Sanger Seq. (blue arrow) – Sanger Sequencing primer to validate amplified sequence from the final Touchdown PCR; Fw_AAVS1(red arrow)/Rev_INS (purple arrow)/Rev_WT (red arrow) – genotyping-PCR to check presence of inserts within the AAVS1 safe harbor locus.

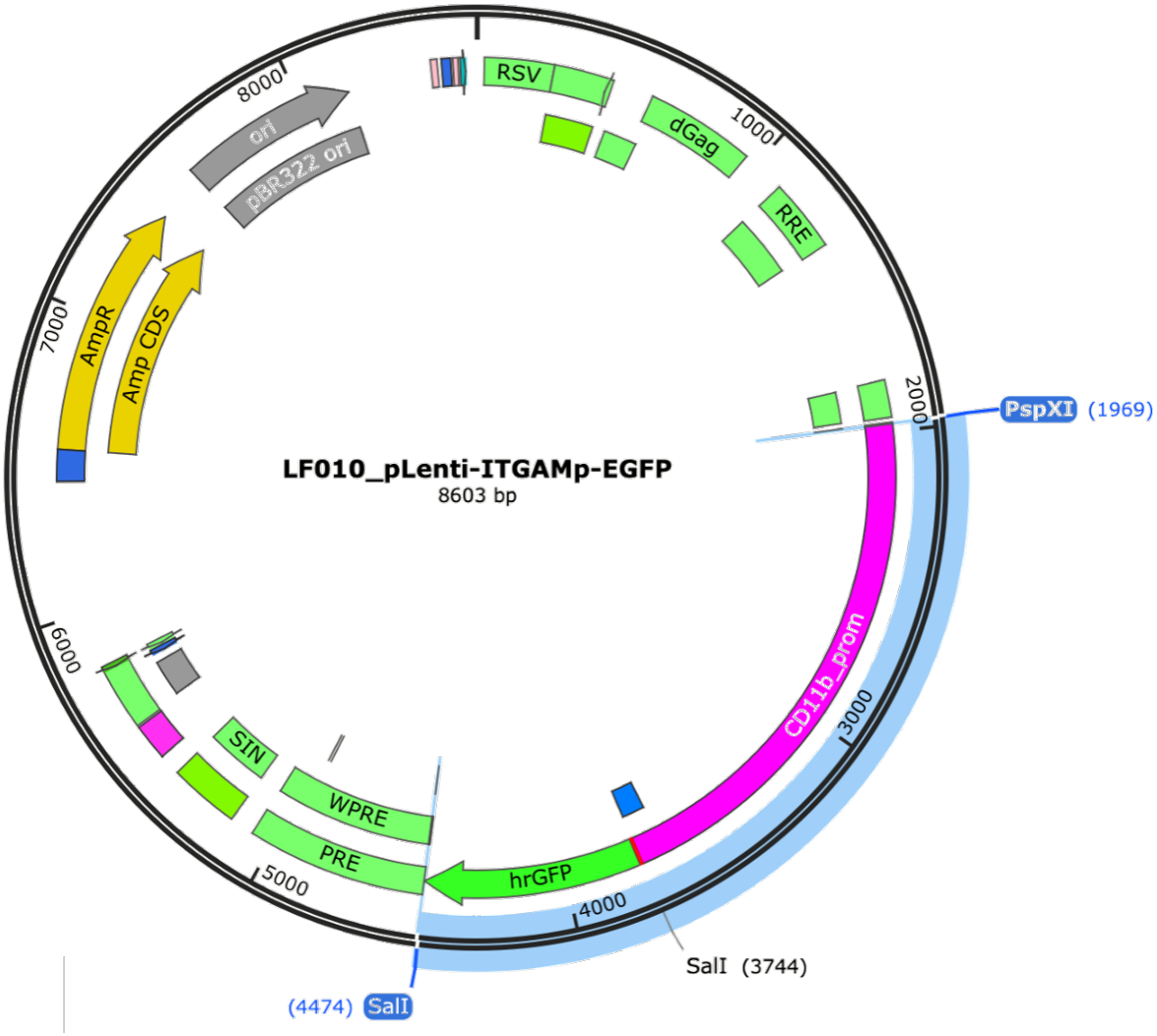

Attachment 3 – Plasmid map of the pLenti-ITGAMp-EGFP construct. The blue region, marking the ITGAMp-EGFP lineage tracing system, was extracted from the available AAVS1-ITGAMp-EGFP construct (provided by Lea Berg) using the REs PspXI and Sal1 for digestion. The rest of the plasmid corresponds to a lentiviral backbone that was kindly provided by Christina Au Yeung, Institute of Reconstructive Neurobiology.

Day 2

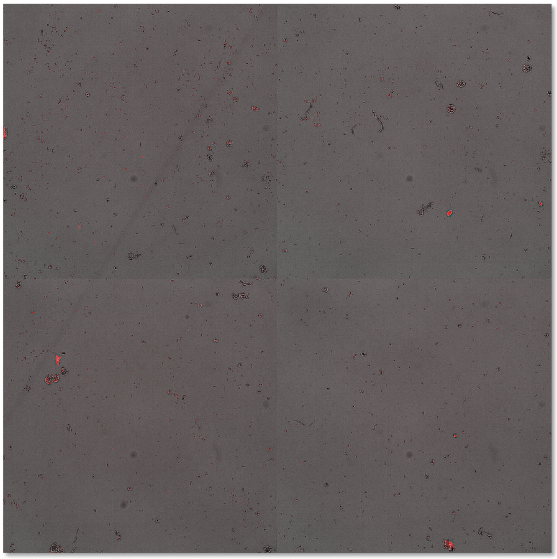

Day 2 (Cy3 channel – TL594)

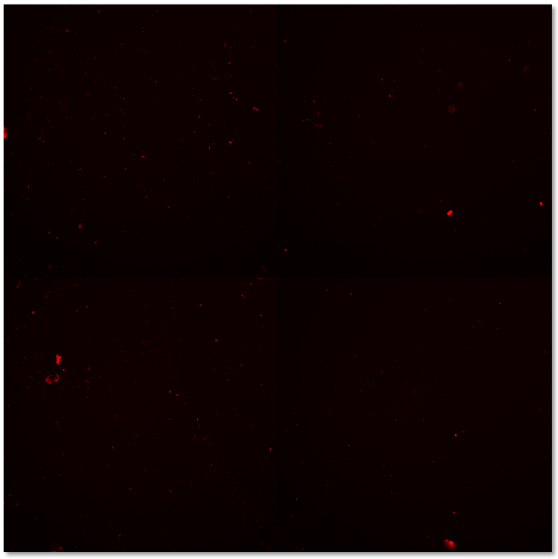

Day 3

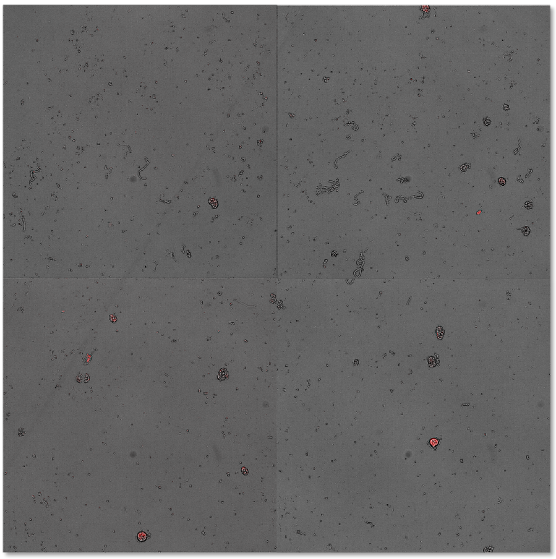

Day 4

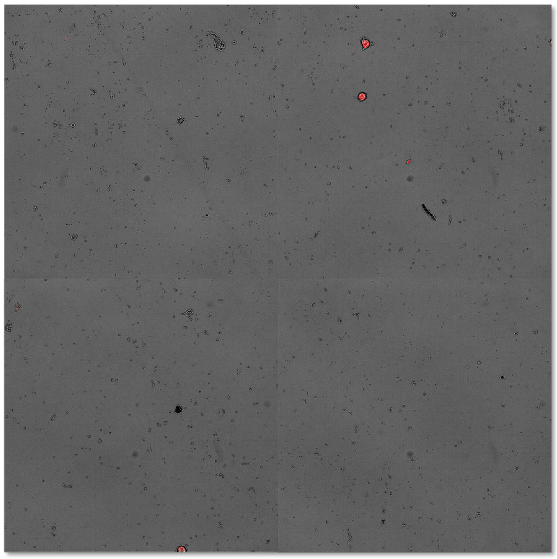

Day 5

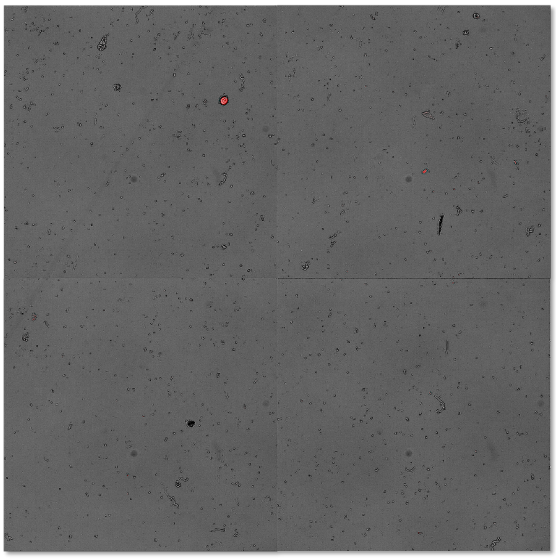

Day 6

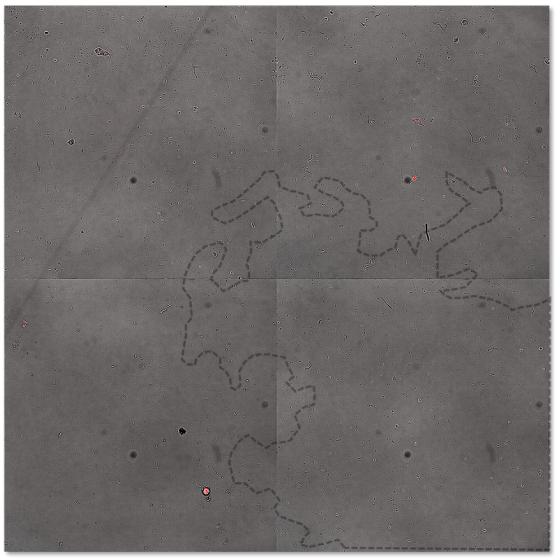

Day 7

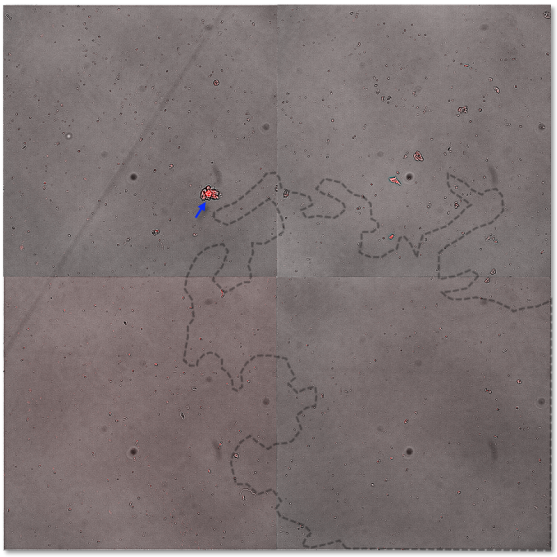

Day 8

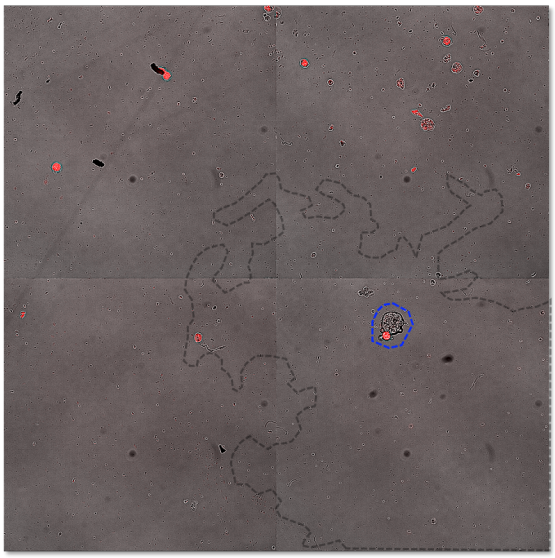

Day 9

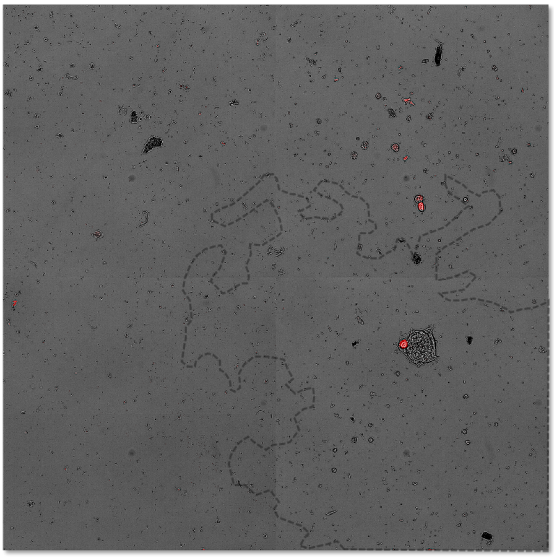

Day 10

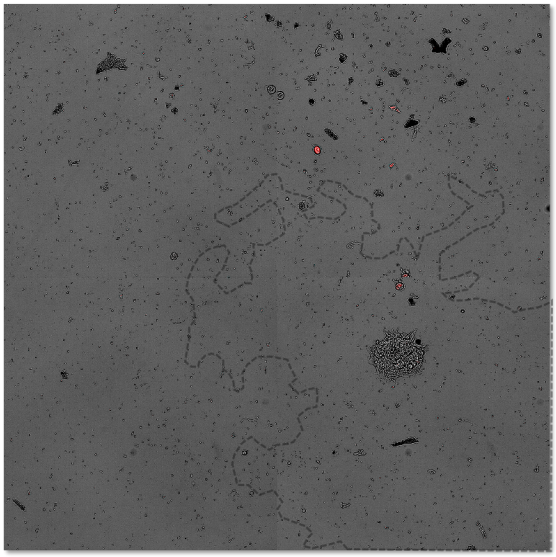

Day 11

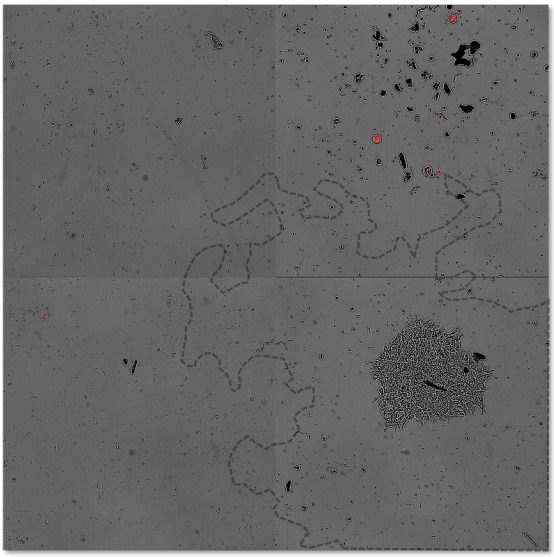

Day 12

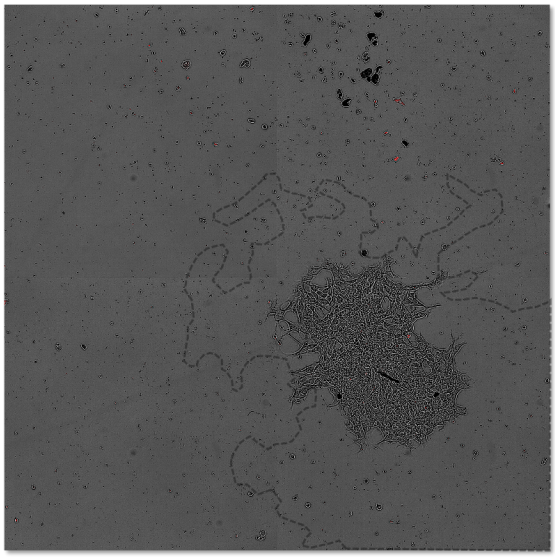

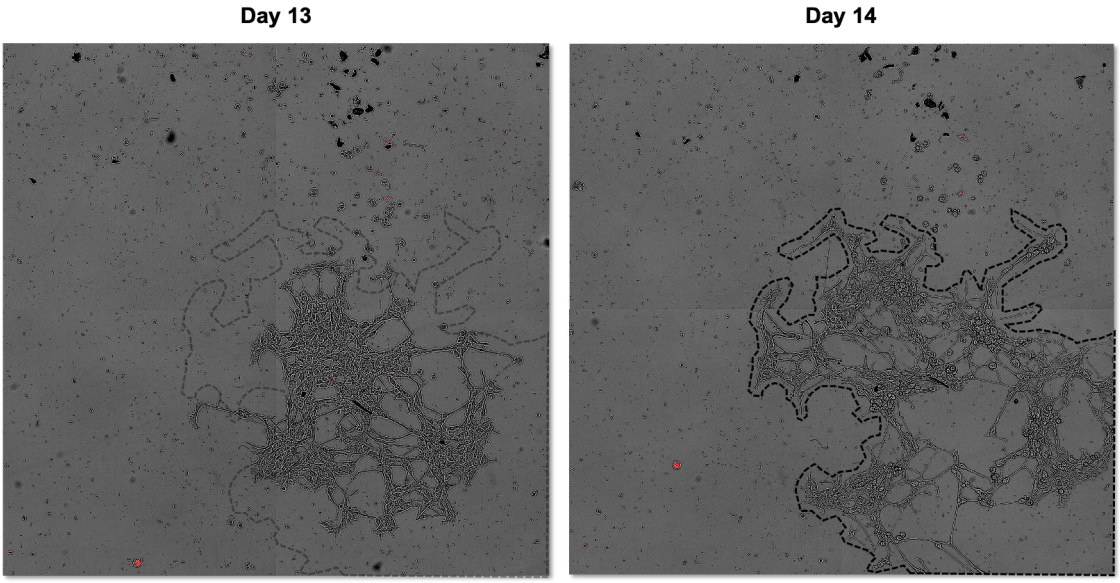

Attachment 4 – Complete timeline of iPSdMiG-to-iNSC conversion in 96-well imaging plates seeded with 10,714 iPSdMiG/cm^2 (relating to summary presented in Figure 14A). Merged 2x2 tiles of phase contrast and Cy3 channel INCell pictures (composed of fields 21, 22, 27 and 28). For day 2 of conversion, the Cy3 single channel image is displayed on the right of the overlayed image. Potential TL594-positive founding cells of a colony that was observed the following day are highlighted by a blue arrow (day 7) and outline (day 8), respectively.

Day 2

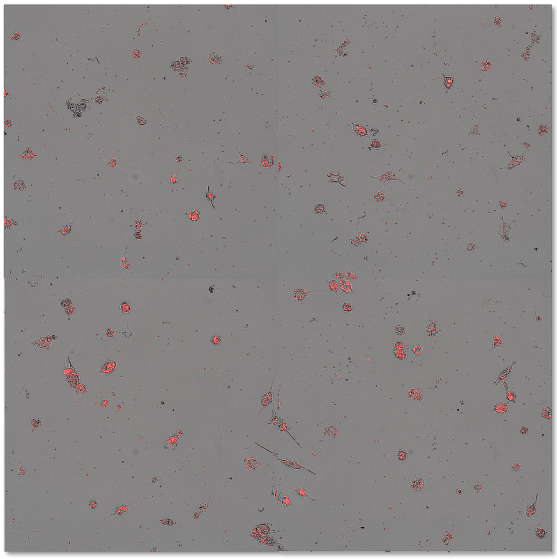

Day 2 (Cy3 channel – TL594)

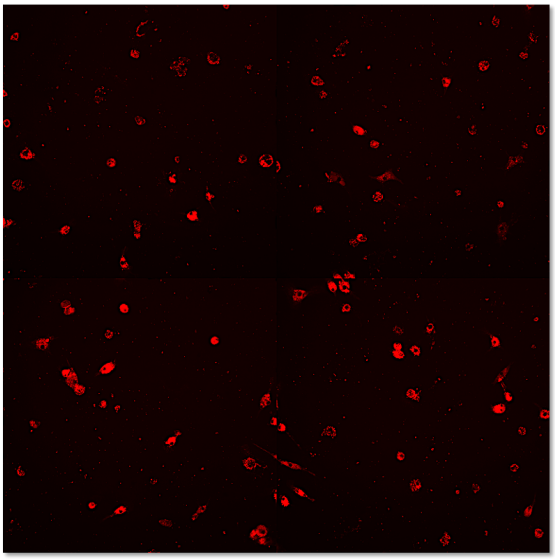

Day 3

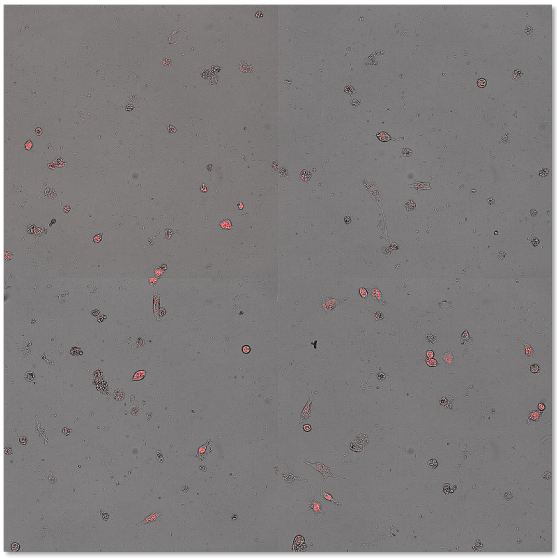

Day 4

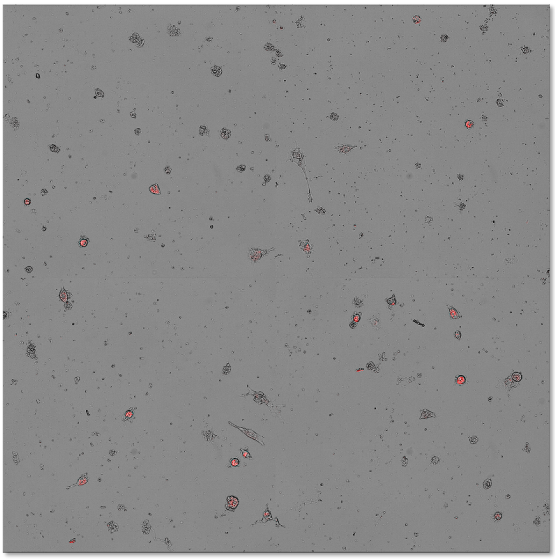

Day 5

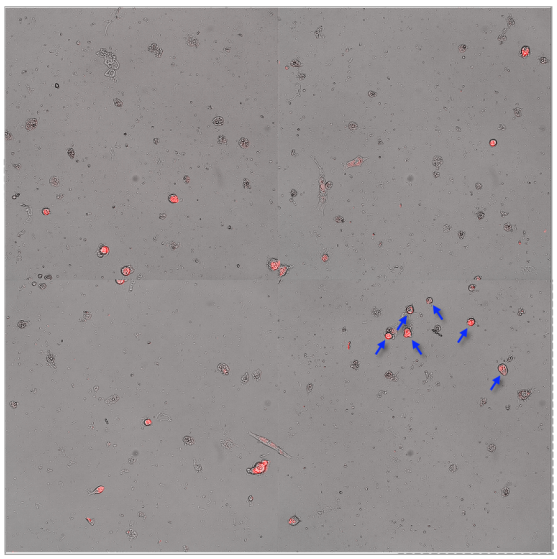

Day 6

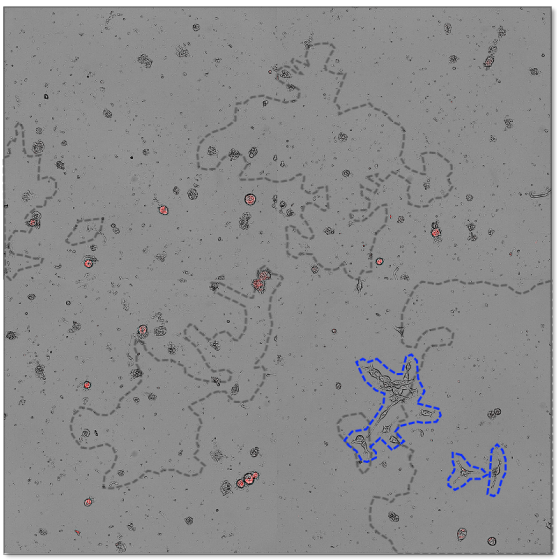

Day 7

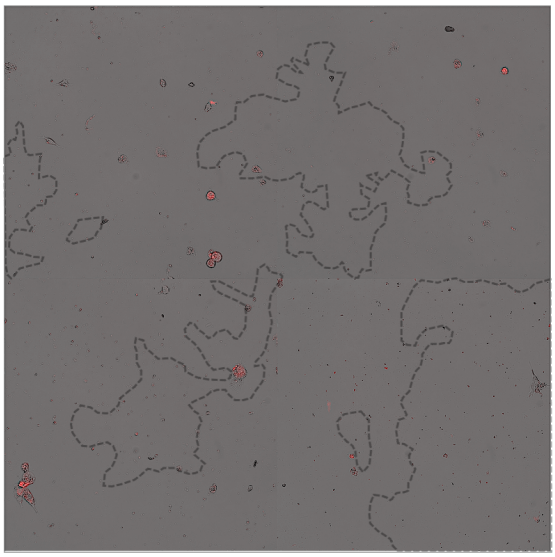

Day 8

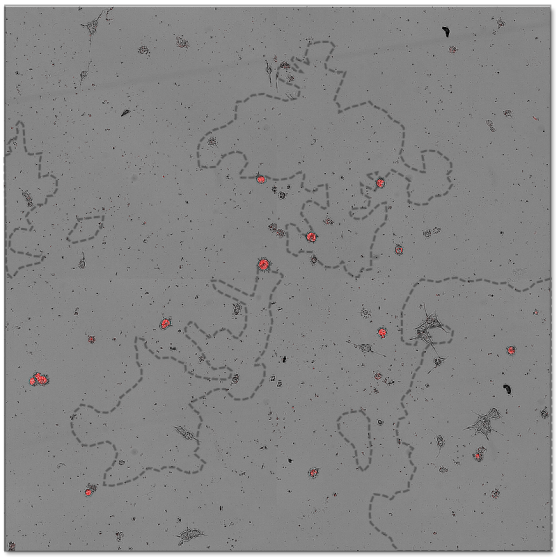

Day 9

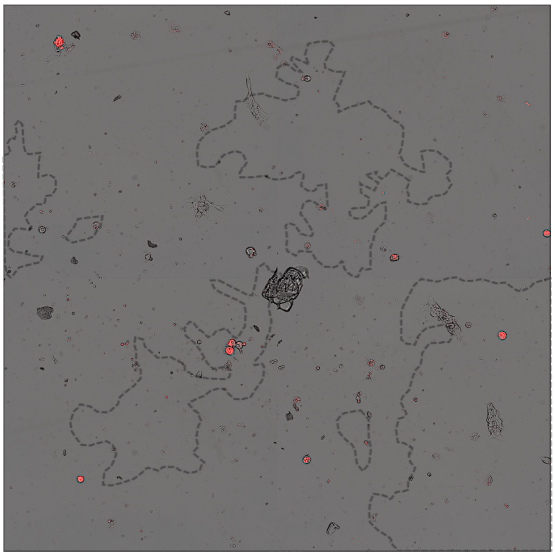

Day 10

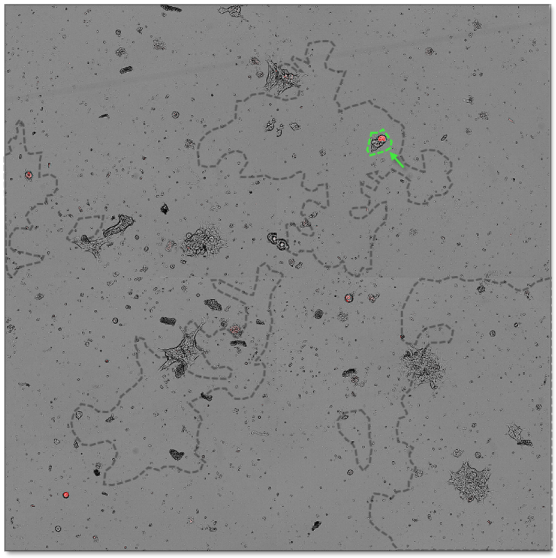

Day 11

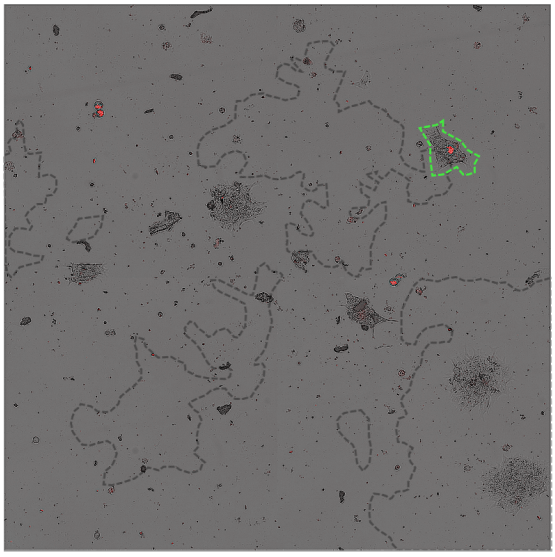

Day 12

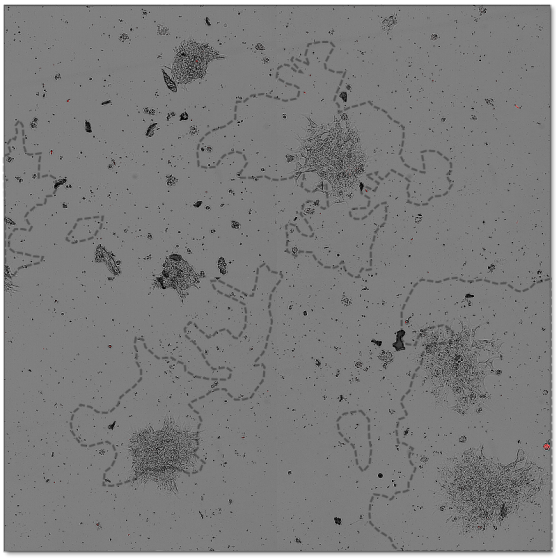

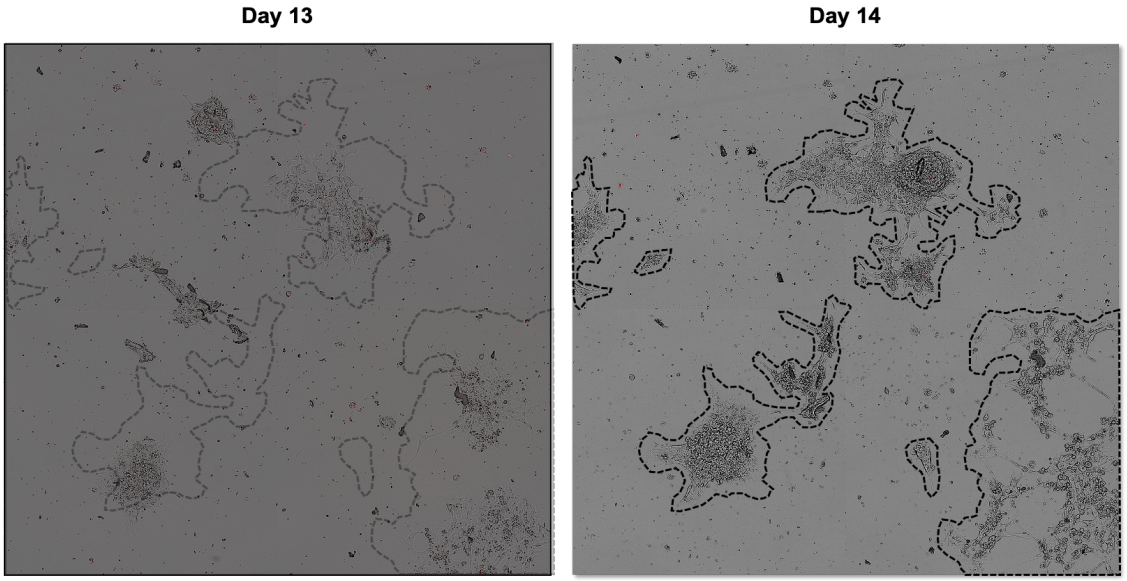

Attachment 5 – Complete timeline of iPSdMiG-to-iNSC conversion in 96-well imaging plates seeded with 21,429 iPSdMiG/cm^2 (relating to summary presented in Figure 14B). Merged 2x2 tiles of phase contrast and Cy3 channel INCell pictures (composed of fields 16, 17, 22 and 23). For day 2 of conversion, the Cy3 single channel image is displayed on the right of the overlayed image. Potential TL594-positive founding cells of a colony that was observed the following day are highlighted by a blue (day 5/6) or green (day 10/11) arrow and outline, respectively.

Cell Marker	Description	Reference
CD14	Expressed mainly in monocytic-like cells and interfollicular macrophages. Key organizer of microglial responses to CNS infection and injury.	Janova, H., *et al.* CD14 is a key organizer of microglial responses to CNS infection and injury. (2016). *Glia.*, vol. 64, no. 4, pp. 635-649, doi: 10.1002/glia.22955.
CD11b	Characteristic microglial cell marker encoded by the gene ITGAM (integrin alpha M) that mediates processes of inflammation and regular adhesion and migration properties.	Jurga, A.M., Paleczna, M. and Kuter, K.Z. Overview of general and discriminating markers of differential microglia phenotypes. (2020). *Front. Cell. Neurosci.*, vol. 14, no. 198, doi: 10.3389/fncel.2020.00198.
CD45	Leukocyte common antigen (LCA), expressed in all hematopoietic lineage-related cells.	Jurga, A.M., Paleczna, M. and Kuter, K.Z. Overview of general and discriminating markers of differential microglia phenotypes. (2020). *Front. Cell. Neurosci.*, vol. 14, no. 198, doi: 10.3389/fncel.2020.00198.
IBA1	Pan-microglial cell marker; responsible for cellular activation and inflammation processes.	Jurga, A.M., Paleczna, M. and Kuter, K.Z. Overview of general and discriminating markers of differential microglia phenotypes. (2020). *Front. Cell. Neurosci.*, vol. 14, no. 198, doi: 10.3389/fncel.2020.00198.
NES	Cytoskeletal intermediate filament characteristic of NSCs.	Lendahl, U., Zimmerman, L.B., McKay, R.D. CNS stem cells express a new class of intermediate filament protein. (1990). *Cell.*, vol. 60, no. 4, pp. 585-595, doi:10.1016/0092-8674(90)90662-x
PAX6	Transcription factor directly regulates cohorts of genes that promote neural stem cell self-renewal, basal progenitor cell genesis, and neurogenesis; expressed in early passage NSCs.	Sansom, S.N., *et al.* The level of the transcription factor Pax6 is essential for controlling the balance between neural stem cell self-renewal and neurogenesis. (2009). *PLoS Genet.*, vol. 5, no. 6, 1000511, doi:10.1371/journal.pgen.1000511.
PU.1	Transcription factor expressed during development of myeloid (*e.g.* microglia) and B-lymphoid cells.	Kierdorf, K. *et al.* Microglia emerge from erythromyeloid precursors via Pu.1- and Irf8-dependent pathways. (2013). *Nat. Neurosci.*, vol. 16, no. 3, pp. 273-280, doi: 10.1038/nn.3318.
P2RY12	Specific microglial protein marker, predominantly expressed in homeostatic microglia.	Kenkhuis, B., *et al.* Co-expression patterns of microglia markers Iba1, TMEM119 and P2RY12 in Alzheimer's disease. (2022). *Neurobiol. Dis.*, vol. 167, no. 105684, doi: 10.1016/j.nbd.2022.105684.
SOX2	Pan-neuronal cell marker; expressed in the majority of NSCs.	Ellis, P., *et al.* SOX2, a persistent marker for multipotential neural stem cells derived from embryonic stem cells, the embryo or the adult. (2004). *Dev. Neurosci., vol.* 26, no. 2-4, pp.148-165, doi: 10.1159/000082134.

Attachment 6 – Cell markers used in this project for RT-qPCR and/or immunocytochemical analysis.